Title
PROPERTIES OF TUNNEL JUNCTIONS WITH FLUOROCARBON DIELECTRIC BARRIERS

Author
Jack, Michael David.

Publication Date
1973-11-01

PROPERTIES OF TUNNEL JUNCTIONS WITH FLUOROCARBON DIELECTRIC BARRIERS

Michael David Jack
(Ph. D. thesis)

November 1973

Prepared for the U. S. Atomic Energy Commission
under Contract W-7405-ENG-48

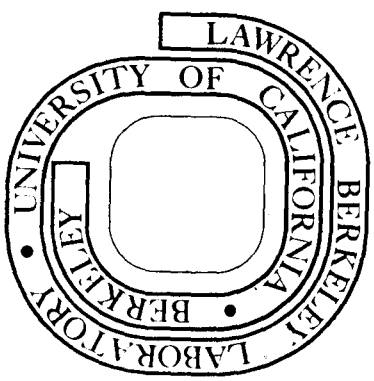

DISCLAIMER

Table of Contents

PROPERTIES OF TUNNEL JUNCTIONS WITH FLUOROCARBON DIELECTRIC BARRIERS

Michael David Jack

Inorganic Materials Research Division, Lawrence Berkeley Laboratory
and Department of Physics; University of California
Berkeley, California 94720

ABSTRACT

The electrical characteristics of In-I-In and In-I-Pb superconducting tunnel junctions have been studied in detail. Since In does not readily form pinhole free oxide layers, a thin insulating dielectric was formed on freshly deposited In film by passing an electric discharge through an atmosphere of fluorocarbon gas. Junctions were then completed by depositing a thin counter electrode of In or Pb. The same process was used to prepare high resistance junctions with Au as the base electrode; these were not however, studied in detail.

In-I-In and In-I-Pb junctions were produced with resistances in the range 0.01 ohms to 10^{10} ohms at liquid helium temperatures. Low resistance junctions exhibited non-linear electrical characteristics associated with good quality "oxide" superconducting junctions including (a) the D. C. Josephson effect, (b) quasiparticle tunneling characteristics, (c) phonon structure and (d) inelastic tunneling phenomena. The magnitude of the Josephson current for In-I-In junctions agreed to within a few percent of the value predicted by strong coupling theory. Current voltage (I-V) and first and second derivative curves for In-I-In and In-I-Pb were compared with curves for Al-I-In and Pb-I-Pb junctions. Discrepancies between the characteristics can be, for the most part, explained on the basis of existing theories of phonon mediated superconductivity using recent data from inelastic neutron scattering studies of In. Nonlinear

structure at voltages below the phonon spectrum was observed and is most likely associated with Kohn singularities. At higher voltages, second derivative curves exhibited resonances characteristic of CH and OH impurities in the barrier as well as a complex spectrum associated with the vibrational spectrum of the fluorocarbon dielectric. To better characterize this dielectric, a variety of surface analytic techniques were used to determine the complex index of refraction, the chemical composition and chemical homogeneity of the barrier. I-V curves for high resistance junctions were used to determine the potential at the metal-insulator interface.

I. INTRODUCTION

The increasing recognition of the versatility of superconducting tunnel junctions as sensitive detectors of magnetic flux, far infrared and microwave radiation and as accurate cryogenic thermometers has stimulated the search for a reliable method of producing stable, reproducible junctions.

Oxidation of the first metal electrode has historically been a very successful method of producing a pinhole free dielectric which is thin enough for tunneling to occur. Many nonconventional insulators have been tried as substitutes for oxide usually with poor to fair results. The development of a good nonconventional dielectric would be especially advantageous in the preparation of tunnel junctions from metals which do not readily form stable oxide junctions. One of the more interesting of these materials is the superconductor, Indium.

Although tunnel junctions containing In have been fabricated, the metal is usually deposited onto an oxidized Al or Mg metal film. Better resolution of nonlinear tunneling characteristics has been anticipated for In-I-In tunnel junctions. Several authors have reported the preparation of In-Oxide-In junctions which unfortunately proved unstable and for this reason we undertook the preparation of In tunnel junctions using a nonconventional insulator.

Section II deals with the theoretical models for nonlinear tunneling characteristics and the deviation of real junction behavior from theoretical predictions. Criteria are discussed for assessing junction quality and applied to various non-oxide junction reported in the literature. In section III the experimental properties of In-I-In and In-I-Pb fluorocarbon junctions are compared with theory and with the experimental behavior of Al-I-In and Pb-I-Pb oxide junctions. In general good agreement is obtained between

theory and experiment. For example the D. C. Josephson current for In-I-In junctions is within a few percent of the strong coupling theoretical prediction and excess current in the quasiparticle characteristics of In-I-Pb junctions is less than 0.1% of the normal state current. "Phonon structure" in the tunneling conductance derivative curves for In-I-In and In-I-Pb junctions agrees qualitatively with the line shape and location of similar structure observed for Al-I-In and Pb-I-Pb junctions respectively. Different amplitudes for these structures can be explained by the different amplitudes of the theoretical density of states singularity predicted for the different superconducting electrodes. Additional structure resolved in the In tunneling characteristic agfees with critical points in the In phonon spectrum determined by recent inelastic neutron scattering experiments. Nonlinearities seen just above the gap edge in In-I-In and In-I-Pb are tentatively attributed to Kohn anomalies.

Above 20 mV inelastic tunneling structure was observed for both In-I-In and In-I-Pb junctions. This structure was complex and with few exceptions (such as CH stretch modes) could not be assigned to simple diatomic or triatomic species in the dielectric.

In order to more precisely determine the chemical nature of the dielectric, a variety of surface analytic techniques were used and the results are reported in section IV. The dielectric constant, complex index of refraction chemical stochiometry and chemical homogeneity of the barrier were determined. The asymmetric barrier height was calculated using high voltage tunneling characteristics of high resistance junctions. All data was consistent with the assignment of stochiometry of $(CF_2)_n$ to the barrier. The structure is believed to be that of amorphous polytetrafluoroethylene.

Noble metal junctions, i.e. Au-I-In, Au-I-Pb, and Au-I-Au junctions were produced using identical techniques and their properties are briefly discussed in section IV.D. Section V deals with experimental methods of junction characterization and preparation, and section VI summarizes these results.

II. TUNNELING IN SUPERCONDUCTORS

A. B.C.S. Characteristics

Bardeen, Cooper and Schrieffer (B.C.S.)[1] predicted using a microscopic reduced Hamiltonian model that the excited states of a superconductor would be separated by a minimum energy 2Δ from the ground state. In contrast the excited states of a normal metal form a continuum with the ground state. Both sets of excitations may be placed in 1:1 correspondence using a crystal momentum k as the transfer index. In accordance with the theory of Landau this approach is valid for $\underset{\sim}{k}$ near the Fermi momentum, and those excited states so represented are designated quasiparticles. This model is not strictly valid especially in the case of strong coupling superconductors (as discussed in Section II-D) but will be adopted in the following sections since it is conceptially convenient to consider an excited superconducting state as a single particle (quasiparticle) which partakes of the superconducting interaction.

Giaever and co-workers[2] used thermally oxidized tunnel junctions with one or more superconducting electrodes to unambiguously corroborate the existence of this energy gap in the excitation spectrum of a superconductor. Making the reasonable assumption (rigorously justified by Cohen, Falicov and Phillips[3]) that the tunneling current through a junction at a given voltage V and temperature T depends on the density of states in the left (L) and right (R) electrodes as

$$I = C_{NN} \int_{-\infty}^{\infty} N_L(E) N_R(E+V) \, [f(E) - f(E+V)] \, dE \qquad (1)$$

Giaever was able to fit his experimental I-V curves using the B.C.S. density of states:

$$N(E) = \left\{ \begin{array}{ll} 0 & E < \Delta \\ \dfrac{|E|}{(E^2-\Delta^2)^{1/2}} & E > \Delta \end{array} \right\} \qquad (2)$$

where f(E) is the Fermi-Dirac occupation probability $[\exp(E/k_BT)+1]^{-1}$, E is the quasiparticle energy $E = [\epsilon^2 + \Delta^2]^{1/2}$, and ϵ is the free electron energy referred to the Fermi energy μ_F.

Equation (1) predicts qualitatively different characteristics for junctions composed of: one normal metal and one superconductor (S-I-N), two identical superconductors (S-I-S), or two different superconductors (S_1-I-S_2).

The density of states of a superconductor can be determined from the differential conductance G(V) of an S-I-N junction at temperatures approaching T = 0°K. This can be seen from Eq. (1) with $N_R(E+V) = 1$, i.e., the right electrode assumed normal. Since

$$f(E) - f(E+V) \underset{T=0°K}{\longrightarrow} [\Theta(-E) - \Theta(-(E+V))] \quad \left\{ \begin{array}{ll} \Theta(x) = 1 & x > 0 \\ = 0 & x \leq 0 \end{array} \right\} \qquad (3)$$

we have

$$G_{SN}(V) \equiv \frac{dI_{SN}}{dV} = \frac{d}{dV} C_{NN} \int_0^V N_L(E)dE \cong C_{NN}\, N_L(V) \qquad (4)$$

If both electrodes are normal $G_{NN}(V) = C_{NN}$ which is approximately independent of voltage for V of the order of Δ. Thus to good approximation

$$\frac{G_{SN}(V)}{G_{NN}(V)} = \frac{|V|}{\sqrt{V^2-\Delta^2}} \qquad |V| > \Delta$$

$$= \quad 0 \qquad\qquad |V| < \Delta \qquad (5)$$

Taylor et al.[4] have computed I_{ss} for S-I-S junctions and Shapiro et al.[5] have solved Eq. (1) numerically for the case of nonidentical superconductors. Table I compares the major features in the current vs voltage (I-V) characteristics as calculated for all three cases. Junctions composed of two superconductors exhibit a discontinuous rise at half the sum of the energy gaps $\Delta_1 + \Delta_2$ and a negative resistance region well below this energy, whereas junctions with only one superconductor exhibit a rapid but not discontinuous rise (except at 0°K) at half the energy gap. A logarithmic singularity is predicted for junctions composed of two distinct superconductors at half the difference in energy gaps $\Delta_1 - \Delta_2$ ($\Delta_1 > \Delta_2$).

The close agreement obtained between experiment and theory provides convincing evidence for the validity of the B.C.S. theory and for the expression for the tunneling current, (Eq. 1). Small deviations from theory have also been vigorously investigated with the aid of derivative techniques. Four major classes of irregularities in experimental characteristics have been found: (1) broadening of sharp structure predicted by the B.C.S. theory (2) excess currents below the gap, (3) additional structure in G(V) and G'(V) associated with phonons in the electrodes, and (4) structure in G'(V) associated with inelastic

Table I. Characteristic Features of Superconducting Tunnel Junctions

S-I-N		S-I-S		S_1-I-S_2	
Temp./Voltage	Tunnel Current	Temp./Voltage	Tunnel Current	Temp./Voltage	Tunnel Current
$T\to 0$ $V\to 0$	$\frac{I_{SN}}{I_{NN}} = \exp\frac{-\Delta}{k_B T}$	$2\Delta > k_B T > V$	$I_{SS} \propto \exp^{-\Delta/k_B T} \frac{V}{2k_B T} \ln[\frac{4k_B T}{V}]$	$V < \lvert\Delta_1-\Delta_2\rvert$	No Accurate Approximation
			$[\frac{d^2V}{dI^2} > 0]$	$T > 0$	$[\frac{d^2V}{dI^2} < 0]$
$k_B T \ll eV < \Delta$	$I_{SN} \propto \exp(\frac{eV}{k_B T})$	$k_B T \lesssim .3\Delta$	$I_{SS} \propto (\frac{\pi k_B T}{V})^{1/2} + \ldots$	$T > 0$	$I_{12} \sim \ln\lvert V-(\Delta_1-\Delta_2)\rvert$
				$V \sim \pm\lvert\Delta_1-\Delta_2\rvert$	CUSP
		$V < 2\Delta$	$[\frac{dV}{dI} < 0]$	$\lvert\Delta_1-\Delta_2\rvert < V < \Delta_1+\Delta_2$	$[\frac{dV}{dI} < 0]$
		Small Negative Resistance Region		$T > 0$	Negative Resistance Region
$V\to\Delta+0^+$	$\frac{I_{SN}}{I_{NN}} = \sqrt{1-(\frac{\Delta}{V})^2}$	$V \to 2\Delta$	$\Delta I_{SS} = \frac{\pi\Delta}{2R_N} B(T)$	$V \to \Delta_1+\Delta_2$	$\Delta I_{\perp 12} = \frac{\pi\sqrt{\Delta_1\Delta_2}}{2R_N} B(T)$
$T=0$		$T \geqslant 0$	Jump Discontinuity	$T \geqslant 0$	Jump Discontinuity

processes in the barrier. Sections B-E summarize these observations, and discuss them in terms of extending the original simple B.C.S. treatment.

B. Broadening of the Density of States

Those characteristics (enumerated in Table I) associated with the square root singularity in the B.C.S. density of states at Δ, most notably the discontinuous current rise at half the sum of the energy gaps and the logarithmic singularity at half the difference, are always broadened in real junctions. A variety of mechanisms have been proposed to explain this effective smearing of the energy gap. Residual electron-phonon interactions not accounted for in the B.C.S. Hamiltonian lead to a finite lifetime for the quasiparticle and an energy dependent complex valued gap function. Calculations by Scalapino and Taylor[6] have demonstrated that broadening obtained from the mechanism is small compared to gap anisotropy and spatial inhomogeneity discussed below.

The anisotropy of the energy gap has been estimated from the variation in the apparent gap with cleavage plane in tunneling from single crystals to thin films. The spread of the energy gap W_g divided by 2Δ has been determined from tunneling into bulk single crystals. Sn,[7] Pb,[8] and Ga[9] have values of $\delta \equiv W_g/2\Delta$ of 0.5, 0.16 and 0.05 respectively. These can be compared to values of gap spread estimated from the width of the current rise for thin film junctions. Typical Sn-I-Sn,[10] Pb-I-Pb,[11] and In-I-In[12] junctions had δ's of 0.1, 0.04 and 0.2 respectively. The effective gap width for films is comparable or smaller in the case of Sn and Pb than the measured anisotropy for the bulk crystals. This is often

attributed to the preferential orientation of thin film crystallites grown on room temperature substrates.[13]

Inhomogeneities due to strain or impurity gradients may, if large compared with the superconducting coherence length, cause a spatial variation in energy gap across the junction and a consequent smearing of the effective tunneling density of states.

C. Excess Currents and Multiparticle Tunneling

The tunnel current at voltages well below the current rise (associated with the energy gap) should decrease with temperature as exp $- \Delta/k_B T$. Real junctions however exhibit a residual current even when cooled to very low temperatures. This excess current varies from one junction to another and can be used as a measure of junction quality. Giaever[14] and Rowell[15] have found that for their best Pb-I-Pb junctions at 1°K excess currents at low voltages are of the order of 10^{-5} of the normal state current I_{NN} as compared to the theoretical prediction of 10^{-7} I_{NN}. It is extremely easy to make junctions with excess currents larger than this. Conductance and the first derivative of conductance vs voltage curves, are often presented in the literature without any reference to junction quality; consequently, one must be very careful in interpreting the data. A rough quality factor, Q, can be constructed from an I-V curve by taking the ratio of the resistance of the junction at voltages well below the current rise at Δ or $\Delta_1+\Delta_2$ to the resistance above the rise.

Anomalous structure often occurs at submultiples of the energy gap, i.e., $\frac{2\Delta}{n}$ n $\geqslant$ 2 for S-I-S junctions and $\frac{\Delta_1}{n}$ and $\frac{\Delta_2}{n}$ n $\geqslant$ 1 for S_1-I-S_2 junctions. Rowell and Feldmann[16] have noted that for junctions with a Q ~ 1000 large increase in current is observed at Δ, Δ_1 or Δ_2 which is similar in appearance to the rise at 2Δ but several orders of magnitude smaller. This they attribute to multiparticles tunneling, i.e., simultaneous tunneling of two or more quasiparticles. Junctions with Q ~ 1 exhibit small current decreases at the same voltages which Rowell and Feldmann attribute to interactions of shorts with the quasiparticles. Examples of multiparticle tunneling can be seen in Fig. 1 for an In-I-Pb junction at 0.9°K with Q ~ 10^3. We notice a large current rise at $\Delta_{In} \cong 0.55$ mV and $\Delta_{Pb} \cong 1.44$ mV. The decrease in conductance in the region 0.8 - 1.0 mV is a broadened version of the B.C.S. logarithmic singularity expected at the difference in the energy gaps $\Delta_{Pb}-\Delta_{In} \sim 0.85$ mV. This structure becomes more pronounced at higher temperatures, as can be seen in Fig. 2; note the negative resistance region. Figure 3 shows similar behavior for an In-I-In junction with Q = 10; a large current rise at $\Delta_{In} = 0.55$ mV is seen.

It is important to note that some characteristics of junctions change only slightly when the quality factor changes drastically. For example, in many cases the author has observed little correlation between excess current and width of the current rise. Gap width may remain virtually unchanged from junction to junction while the quality factor may vary over an order of magnitude or more. A similar phenomena was observed by Rowell and Feldmann[16] for the "phonon structure" of Pb-O-Pb junctions. After accidentally decreasing the Q of a junction

from 10^5 to 30, they re-measured the differential conductance plot (as will be discussed in Section D) and found approximately 10% change in the magnitude of the structure but virtually no change in position or relative heights of the peaks.

Thus, "phonon data" may be interpreted using the model of a low $Q \simeq 10\text{-}50$ junction as a simple low resistance in parallel with an ideal junction, an assumption which is reinforced by the ohmic behavior of excess currents observed by Giaever.[17]

D. Phonon Density of States from Tunneling Measurements

Deviations from the B.C.S. theory occur at voltages in the range 5-30 mV above the energy gap. These were first observed by Giaever, Hart and Megerle[18] in the I-V characteristic for Pb-I-Pb and could be clearly resolved in conductivity vs voltage plots for Mg-I-Pb junctions. Instead of the smooth

$$\frac{V}{\sqrt{V^2 - \Delta^2}}$$

approach to the normal state conductivity, Giaever et al. observed wiggles about the B.C.S. curve amounting to ~ 5% of the B.C.S. value which they attributed to an energy dependent gap. A physical interpretation of this phenomena was provided by Schrieffer, Scalapino and Wilkins.[19] They attribute structure in the conductivity to decay processes whereby an excited quasiparticle of energy E may emit a phonon of energy $\hbar\omega$ and obtain a final state energy $\Delta = E - \hbar\omega$ at the gap edge thus sampling the final state singularity. Thus, while the singularity at the gap remains, a quasiparticle in an eigenstate of the B.C.S.

Hamiltonian will decay with a finite lifetime, τ, determined by the density of final phonon states. For superconductors such as Pb and Hg with very strong electron-phonon interactions the Landau quasiparticle picture is no longer valid since the energy of the excitation is comparable to the breadth ($\hbar/\tau$) of the state. Utilizing a Green's function formalism for superconductivity developed by Nambu,[20] Gorkov[21] and Eliashberg,[22] Schrieffer, et al.[19] obtained a quantitative fit to the tunneling conductivity measure ments of Rowell, Thomas and Anderson[23] on Al-I-Pb and Pb-I-Pb junctions by replacing the B.C.S. density of states

$$N(E)_{BCS} = \frac{|E|}{\sqrt{E^2 - \Delta^2}} \tag{6}$$

with the strong coupling density of states.

$$N(E)_{SC} = \text{Re}\left\{\frac{|E|}{\sqrt{E^2 - \Delta^2(E)}}\right\} \quad \text{in Eq. 1} \tag{7}$$

where the energy gap parameter is now a complex function of energy

$$\Delta(E) = \Delta_1(E) + i\Delta_2(E) \tag{8}$$

The imaginary component is associated with the lifetime of the quasiparticle.[24] (E) can be determined self-consistently by solving a set of integral equations similar to those derived by Eliashberg.[22] They involve an integral of the form

$$\Delta(E) = Z(E)^{-1}\int dE' \mathrm{Re}\left\{\frac{\Delta(E')}{[E'^2-\Delta^2(E')]^{1/2}}\right\}\int d\omega_q\ \alpha^2(\omega_q)F(\omega_q)\left\{\frac{1}{(E'+E+\omega_q)-i\delta}\right.$$

$$\left. + \frac{1}{E'-E+\omega_q-i\delta}\right\} \qquad (9)$$

Here $\alpha^2(\omega_q)$ is an effective electron-phonon interaction typically chosen as an adjustable parameter independent of the phonon energy ω_q, and $F(\omega_q)$ is the normalized phonon density of states. $Z(E)$ is a normalization factor which must be determined by simultaneously solving a similar expression. Scalapino et al.[19] used a simple form of the phonon density of states consisting of transverse and longitudinal Lorentzian peaks. The peak locations and widths were chosen to match neutron data for Pb; then by successive iteration the coupled equations were solved for $\Delta(E)$ and the renormalization factor $Z(E)$. The electron phonon coupling constant has been shown by Scalapino[25] to be slowly varying on the scale of the phonon density of states and is chosen as a constant for each phonon peak to yield the correct experimental value of the energy gap.

$$\Delta_1(\Delta_0) = \Delta_0 \qquad (10)$$

McMillan and Rowell inverted this procedure using experimental values of I, $\frac{dI}{dV}$ and $\frac{d^2I}{dV^2}$ as a function of V to deconvolute Eq. (1) thus numerically obtaining an experimental $N(E)$. By choosing a model $F(\omega)$, calculating a first order $N^{Ex}(\omega)$, comparing this to the tunneling density N^{Th} and changing $F(\omega)$ so as to obtain convergence, McMillan and Rowell[26] were able to obtain approximate phonon spectrum for a great variety of metal and alloys.

In addition to the general features of the phonon spectrum the second derivative curves ($\frac{d^2I}{dV^2}$ vs V) for Pb were shown by Rowell, Thomas and Anderson[23] to contain structure which could be associated with discontinuities in the derivative of the phonon density of states $F'(\omega)$. Van Hove[27] and Phillips[28] have analyzed these discontinuities. Infinite discontinuities can be produced by singular points in the phonon dispersion i.e., $\nabla_q \omega(q) = 0$ at maxima, minima and saddle points.

Scalapino and Anderson[29] calculated the lineshape and amplitude of the resulting conductance derivative structures expected from these singularities and compared their results with experimental values from Rowell et al. Good agreement was obtained for several isolated singularities in Sn-I-Sn Pb-I-Pb junctions. Similar data for In-I-In junctions will be discussed in detail in Chapter III.

E. Inelastic Tunneling Processes

At voltages past the phonon spectrum in the metal smooth B.C.S. behavior is still not seen. Kinks in the derivative of the conductivity for a Pb-O-Pb junction in the range 30-60 mV were interpreted by Rowell et al.[30] as due to inelastic tunneling processes whereby an electron excites an optical phonon in the PbO_x barrier region. At still higher energies Jaklevic and Lambe[31] investigated peaks in the conductance derivative of Al-I-Pb junctions in the region 50-500 mV. This structure was attributed to impurity assisted inelastic tunneling. The electron scatters from an impurity during the tunneling exciting a molecular species (C-H, O-H, etc.) to a higher vibrational or rotational level and loses energy. This increase in the number of

final states into which an electron may tunnel, i.e., the sum of the final states arrived at by elastic + inelastic processes produces a step increase in the conductivity and consequently a peak in G'(V) at

$$\left.\begin{array}{lll} V = \Delta_1+\Delta_2 + \hbar\omega & (S_1\text{-I-}S_2) & \\ V = 2\Delta \quad + \hbar\omega & (S\text{-I-}S) & \\ V = \Delta + \hbar\omega \ . & (S\text{-I-}N) & \\ V = \hbar\omega & (N\text{-I-}N) & \end{array}\right\}$$

where $\hbar\omega$ is the energy of the excitation. Recent experiments have reported the observation of inelastic tunneling via magnon excitation[32] and resonant scattering from magnetic impurities.[33] "Infra-red spectra" of high molecular weight adsorbed organic molecules have been studied,[34] and Leger and Klein[35] have observed what is believed to be inelastic excitation of the low energy electronic levels (at the incredibly high voltage of 1V) of an organic impurity dopant.

Since the observed structure often resembles the infrared spectrum of the dopant one hopes to utilize a quantitative theory of lineshapes in conjunction with experimental plots of G'(V) to identify materials adsorbed on surfaces by their characteristic tunneling spectrum.

F. Josephson Current

An additional contribution to the tunneling current in S-I-S and S_1-I-S_2 junctions was predicted by B.D. Josephson in 1962.[36] This current may be viewed as the tunneling of pairs of electrons bound by an attractive phonon mediated interaction. Phenomena predicted by Josephson and subsequently verified by experiment include: (a) existence of a D.C.

pair current which flows without the development of voltage across the junction, (b) an A.C. supercurrent oscillating at a frequency proportional to the voltage developed across the junction ($\omega = \frac{2\ eV}{h}$) which is generated when the D.C. current through the junction exceeds a critical value I_c, and (c) nonlinear harmonic generation and frequency mixing effects. Several extensive reviews[37] of the subject have been given and in the following section only concepts pertinent for subsequent experimental analysis will be discussed.

A tunnel junction may be considered as an intermediate state between the two extremes of placing two pieces of superconductor infinitely far apart and fusing them together. In the latter case the phases of the superconductors are totally independent; in the former the phases are locked due to the pairing interaction which makes it energetically favorable for electrons to be "bound" in time reversed pairs. These are product states of the form $\psi(x,t)T\psi(x,t)$ where T is the time reversal operator and $T\psi(x,t) = \psi^*(x-t)$. To maximize the attractive superconducting interaction the center of mass phase θ is the same for electron pairs whose center of mass lies within a sphere of radius $\xi \equiv$ coherence length. In the absence of fields this phase is normally preserved throughout the superconductor.

In a weakly coupled superconductor such as a tunnel junction it is also energetically favorable for the phase to be locked but this coupling energy is much smaller. Anderson[38] has shown that the coupling energy at T = 0°K depends on the relative phase $\phi = \theta_1 - \theta_2$ of the two superconducting pieces as

$$E = E_o - E_T \cos\phi \tag{11}$$

where

$$E_T = \frac{\hbar}{2e}\left[\frac{4\pi\Delta_1\Delta_2}{\Delta_1+\Delta_2} K\left(\frac{|\Delta_1-\Delta_2|}{|\Delta_1+\Delta_2|}\right) \frac{1}{R_{NN}}\right] \tag{12a}$$

K is a complete elliptic integral. An approximate expression for comparable gaps is

$$E_T = \frac{\hbar}{2e}\left[\frac{2\pi^2}{R_{NN}} \frac{\Delta_1\Delta_2}{\Delta_1+\Delta_2}\right] \tag{12b}$$

For a typical junction of resistance 1Ω, this energy is approximately 10^{-11} eV/atom whereas the coherence energy in a bulk superconductor is of the order of 10^{-7}eV/atom. It is reasonable to expect and indeed is true that bulk superconductor parameters such as the London penetration depth critical field, critical current and plasma frequency exist for such a weak link but are scaled down by a factor of $\sim 10^{-4}$. From the form of Eq. (11) equilibrium will be established when $\phi=0$. If a small current is passed through the junction ϕ will be non-zero, and Josephson[36] has shown that to first order the current phase relationship can be expressed as

$$j = j_c \sin\phi \tag{13}$$

This can be verified by noting that the number of superconducting pairs n and the phase are conjugate variables hence

$$\frac{J}{2e} = \dot{n} = \frac{1}{\hbar}\frac{\partial E}{\partial \phi}$$

$$J = \frac{2e}{\hbar} E_T \sin\phi$$

using Eq. (12b) we obtain

$$j_c \cong \frac{\pi}{AR_{NN}} \frac{\Delta_1\Delta_2}{\Delta_1+\Delta_2} \tag{14}$$

Ambegaokar and Baratoff[39] have evaluated j_c for non-zero temperatures and find

$$(S\text{-}I\text{-}S)\ j_c^{AB} = \frac{\pi\Delta_s(T)}{2R_{NN}A} \tanh\left[\frac{\Delta_s(T)}{2k_BT}\right] \qquad (\Delta_1 = \Delta_2) \tag{15a}$$

$$(S_1\text{-}I\text{-}S_2)\ j_c^{AB} = \frac{\pi\Delta_1(T)\Delta_2(T)(k_BT)}{R_{NN}A} \sum_{\ell=0,\pm1\pm\ldots} \left[\left\{\omega_\ell^2+\Delta_1^2(T)\right\}\left\{\omega_\ell^2+\Delta_2^2(t)\right\}\right]^{-1/2} \tag{15b}$$

$$\omega_\ell \equiv \pi(2\ell+1)k_BT \qquad (\Delta_1 \neq \Delta_2)$$

Fulton and McCumber[40] predict a reduced maximum Josephson current for S-I-S junctions when strong coupling effects are taken into account. They obtained the expression

$$J_c^{F.M.} = \frac{\pi\Delta_o(T)}{2R_{NN}A}\left[\tanh\frac{\left[\frac{\Delta_o(T)}{2k_BT}\right]}{[1-\Delta_1'(\Delta_o(T))]} - \frac{1}{AR_{NN}}\int_{\Delta_o}^{\infty} dE\ \tanh\left(\frac{E}{2k_BT}\right) \mathrm{Im}\left\{\frac{\Delta^2(E)}{E^2-\Delta^2(E)}\right\}\right] \tag{16}$$

which evaluated at T=0°K yields reduced critical currents of .788 J_c^{AB} and .911 J_c^{AB} for Pb and Sn respectively. $\Delta(E)$ is the complex energy dependent gap parameter.

In the presence of electromagnetic fields the simple relationship $j = j_c \sin\phi$ is modified in two ways: 1) ϕ depends linearly on externally applied fields 2) there is nonlinearity due to enhancement of the external fields by the self field of the junction.

In the linear region the self fields of the junction are considered small. For simplicity let us assume a planar junction with its normal along the z axis. The phase is modified by the presence of external fields. The presence of a magnetic field causes a spatial variation of the relative phase as

$$\phi(x) = \Theta_1(x,z_1) - \Theta_2(x,x_2) \tag{17}$$

$$= \phi_o - \frac{2e}{\hbar c} \int_{z_1}^{z_2} A(z,x)\, d_z$$

For simplicity the magnetic field B = curl A is assumed to have only a y component. This is clearly the variation of the phase of the center of mass wavefunction of the electron pair integrated from a point z_1 on one side of the barrier to point z_2 on the other side. Because of the finite penetration of the magnetic field into a superconductor, the limits of integration must extend roughly a distance λ (typically a few hundred Å) into each electrode before A = 0.

In the presence of an electric field which may vary in time the phase varies as

$$\phi(t) = \Theta_1(z_1 t) - \Theta_2(z,t) = \mu_1 - \mu_2 \tag{18}$$

$$= \frac{2e}{\hbar} \int^{t} \int_{z_1}^{z_2} E(z,t)\, dzdt$$

Here the electric field is rigorously excluded from the superconducting electrodes, thus the limits of integration are points just on either side of the insulator of thickness s. For slowly varying fields we can combine Eq. (17) and Eq. (18) to give

$$\phi(x,t) = \phi_o + \frac{2ed}{\hbar c} B_y x + \frac{2 eV}{\hbar}^{\dagger}$$
$$d \equiv 2\lambda + s \tag{19}$$

In the static limit $V = E_s$ and

$$j = j_c \sin (\phi_o + (\frac{2ed}{\hbar c}) B_y x) \tag{20}$$

Integrating from $x = -\frac{L}{2}$ to $x = \frac{L}{2}$ the total Josephson current becomes

$$I = I_o \sin\phi_o \frac{\sin \pi\Phi/\Phi_o}{\pi\Phi/\Phi_o} \tag{21}$$

$\Phi = B_y d L$ is the flux through the junction

$\Phi_o = \frac{hc}{2e}$ is the quantum of flux (2.07×10^{-7} gauss-cm^2)

In the limit of small self fields the D.C. supercurrent oscillates as the enclosed flux increase, going to zero with the inclusion of an integral number of flux quanta. For junctions of area of the order 10^{-4} cm^2 the first null is a few gauss.

If a finite voltage is developed across the junction, and B = 0 $j = j_c \sin\left(\phi_o + \frac{2 eVt}{\hbar}\right)$. A more exact solution[41] yields an amplitude that is a slowly varying function of the D.C. component of the voltage, except in the region around $V = 2\Delta_o$ where a logarithmic singularity

(Riedel singularity) is predicted. This has recently been observed by Buckner et al.[13]

Up to this point we have assumed all fields in question were external to the junction. If the self field of the junction becomes appreciable the parameters in the equation $j_s = j_c \sin(\phi_o + kx - \omega t)$ $k = \frac{2edB_y}{hc}$ and $\omega = \frac{2\ eV}{\hbar}$ contain the sum of the self and external fields. In this case the coupled set of Maxwell-Josephson equations must be used. In two dimensional form they are

$$\frac{\partial H_x}{\partial y} - \frac{\partial H_y}{\partial x} = \frac{4\pi}{c} j_z + \frac{1}{c} \varepsilon \frac{\partial E_z}{\partial t} \tag{22}$$

$$j_z = j_c \sin(\phi(x,t)) + j_{QP}$$

$$\phi(x,t) = \frac{2ed(H_y x - H_x y)}{hc} + \frac{2eV}{\hbar} + \phi_o$$

The term j_{QP} normally neglected for simplicity is the parallel quasiparticle current. These three equations may be combined to yield a differential equation for ϕ. Solving for ϕ

$$\nabla^2\phi - \frac{1}{\bar{c}^2}\ddot{\phi} = \frac{\sin\phi}{\lambda_J^{\,2}} \tag{23}$$

$$\bar{c} = \left(\frac{s}{\varepsilon_s d}\right)^{1/2} c$$

$$\lambda_j = \left[\frac{\hbar c^2}{8\pi \varepsilon d\ J_c}\right]^{1/2}$$

Where $\bar{c}$ is the phase velocity of the electromagnetic radiation in the junction cavity (typically $\frac{c}{20}$) and λ_J is the Josephson penetration depth. The meaning of this last term is clarified if a linear approximation is made for the $\sin\phi$ term. From Eq. (23) we have

$$k^2 = \frac{\omega^2}{(\bar{c})^2} - \frac{1}{\lambda_J^2} \quad . \tag{24}$$

In the static limit $k^2 = -1/\lambda_J^2$. In this limit a junction exhibits a Meissner effect with the screening length λ_J typically 1 mm. Owen and Scalapino[42] have made a study of the full non-linear equation

$$\nabla^2\phi = \frac{\sin\phi}{\lambda_J^2} \tag{25}$$

The periodicity of ϕ allows solutions $\phi = \phi + 2\pi n$ representing the inclusion of vortices. The screening currents, unlike bulk superconductors, are zero at the very edge rising to a maximum a distance λ_J into the junction. For $\lambda_J > s$ the magnetic field penetrates more or less uniformly and the Fraunhoffer diffraction expression (21) is valid. For $\lambda_J < s$ self field limiting occurs and the maximum Josephson current is reduced by its internal magnetic field.

Neglecting the $\sin\phi$ term in Eq. (23) the solution for ϕ is that of a propagating wave with phase velocity $\bar{c}$. If the junction is rectangular with lengths L_x and L_y and if boundary conditions $\phi = 0$ are applied at the junction edges the allowed stationary modes have frequencies

$$\omega_{nm} = \frac{n\pi\bar{c}}{L_x} + \frac{m\pi\bar{c}}{L_y} \quad , \quad n,m = (0,1,2 \ . \ . \ .) \tag{26}$$

For values of V such that the frequency of the Josephson oscillation coincides with one of these modes i.e.,

$$V_n = \frac{\hbar n\pi\bar{c}}{2eL} \ ,$$

the driving term $\sin\phi$ in Eq. (23) synchronously feeds the electromagnetic fields. The increased contribution to E_x is in turn fed back to ϕ. Coon and Fiske[43] found peaks in the D.C. current due to this zero beating at $V = V_n$. The amplitude but not the position of these peaks can be modified by the magnetic field and the width is dependent on the width of the junction cavity resonance. If the junction is driven by a constant current source, these peaks take the form of current steps called Fiske steps.

G. Search for Non-Oxide Tunneling Barriers

The tremendous growth of the field of tunneling in superconductors as documented in the preceeding sections has depended to a great extent on the tenacity and self healing properties of thermally grown metallic oxide films. Oxide films are by no means a panacea and various workers have searched for insulators which could be grown on any metal surface in layers thick and uniform enough to prevent shorting but thin enough

to allow tunneling. The advantages of such a wonder material are threefold. (1) Though most metals form a stable oxide in many cases this oxide is not suitable for tunneling. In some cases (Au, Ir, Pt) the oxide will decompose under high vacuum; in other cases the oxide is either a small band gap semiconductor (Cu_2O) or is stochiometrically impure (InO, SnO_2) thus heavily doped and a poor insulator. Occasionally a thick layer of an elemental semiconductor such as C or Ge can provide a reasonable tunneling barrier,[44] however as we shall see there is often a broadening of the I - V characteristics possibly associated with inelastic mechanisms in the insulator. (2) Even when a good oxide junction has been grown using a particular metal, reproducibility of junctions even within a laboratory is often poor and may be much worse from laboratory to laboratory. This is no doubt due to the complicated dependence of oxide growth on variables such as temperature, moisture, residual gases, surface properties of the substrate, and purity of the metals. Any insulator less dependent on any of these parameters could aid in standardizing tunnel junction technology. (3) The technology of planar Si integrated circuits is based for the most part on thermally grown SiO_2 as an insulator and capacitor dielectric. The use of a low defect non oxide insulator which could be grown in thin layers would allow alternate materials such as GaAs to be used.

Tables II, III and IV are a condensation of published characteristics of artificial barrier junctions. This is not meant to be an exhaustive list and apologies must be extended to those authors whose data is insufficiently represented. Errors of perhaps a factor of two have been made in the determination of excess currents and gap width from

Table II. Dielectric Barriers-Tunneling Verified by Superconducting Electrode Test

Insulator	Electrode	Method of Preparation	Q**	$W_g^{\dagger}$(mV)	d(Å)	Reference
PbO	Pb/Pb	Thermal Oxidation	5×10^4	0.2	10-20	(a)
Al_2O_3	In(bulk)/Pb	Thin Aluminum layer deposited on In and thermally oxidized	$\gtrsim 10^2$	0.3	10-30	(b)
C	Sn/Pb	Sublimation	$\gtrsim 15$	1.	140	(c)
Ge	Al/Pb	Deposition from Alumina Crucible	$\gtrsim 10$	0.5	40	(d)
Formar	Pb/Pb	Spin Coating	$\gtrsim 40$	1.	30	(e)
$(CF_2)_n$	In/Pb	Glow Discharge in Fluorocarbon Gas	10^3	0.2	10-20	Author
"	In/In	"	$10-10^2$	.2	10-20	Author
"	Au/Pb	"	1	1.	10-20	Author

** Q is the estimated resistance ratio $\frac{R(V \ll \Delta g)}{R(V > \Delta g)}$ from published data No better than a factor of 2 accuracy.

† Wg is the estimated width of the current rise.

(a) J. M. Rowell and W. L. Feldmann, P. R. V. 172 #2, p.393 (68).

(b) R. F. Averill, L. S. Straus, and W. D. Gregory, Appl. Phys. Lett. V. 20 #2, p.55 (72), W. D. Gregory, private communication

(c) M. L. A. MacVicar, S. M. Freake, and C. J. Adkins, J. of Vac. Sci. & Tech. V.6 #4, p. 717 (69).

(d) B. Konig, Physics Letters, V. 39A #3, p.117

(e) G. Faraci, G. Giaquinta and N. A. Mancini, Phys. Lett. 30A #7, p. 400 (69)

poorly reproduced or inaccurately scaled I-V prints.

The most stringent test of junction quality consists of observing the approximate B.C.S. characteristics enumerated in Table I when one of the electrodes is a superconductor. Table II lists primarily those junctions which (a) had an exclusively non-oxide insulator and (b) were tested with one or more electrodes superconducting. We have included a comparison with typical best thermal oxide junctions of Pb-PbO_x-Pb (cf Table II Ref. a) and data from an In-Al_2O_3-Pb junction with a thin deposited Aluminum layer subsequently oxidized as the barrier (cf Table II Ref. b). The quality Q and gap width W_g are defined in Section II-B. Note that broad characteristics occur for thick small gap semiconductors such as C (140Å). The author has listed several types of junctions including In-I-In, In-I-Pb, and Au-I-In produced with a fluorocarbon insulator. Their properties are discussed in Section III in detail. The production of Au junctions which exhibited small but significant gap characteristics appears to be definitive evidence that oxide barriers are not involved. In Section IV we discuss surface characterization of the dielectric which substantiates this claim. Fluorocarbon In-I-Pb junctions appear to have excess current comparable to the best thermally grown oxides.

Table III lists those junction for which (a) oxide was used to fill in the pinholes in an otherwise artificial dielectric barrier, and (b) the superconducting test was also applied. Pinhole filling was first reported by Giaever et al.[45] in the study of light sensitive CdS junctions. In his experiments the bulk of the tunnel current is assumed to pass through the non-oxide. One may thus logically assume

Table III. Dielectric Barriers + Oxygen Tunneling Verified by Superconducting Electrode Test.

Insulator	Electrodes Bottom/Top	Method of Preparation	Q W_g(mV) approximate	d(Å)	Reference
BaStearate	Sn/Pb	Monolayer transfer from aqueous solution to film	> 10 ~ .2	monolayer (~24)	f
Cyanine-Stearate	Al/Pb	"	> 10 ~ .5	22	g
Te+PbTe	Pb/Pb	Vacuum deposition	> 2 ~ .5	100-200	h
CdS	Sn/Sn	Vacuum deposition	> 1000 ~ .1	50	i

(f) J. L. Miles and H. O McMahon, J. Appl. Phys. 32 (61)

(g) A. Leger, J. Klein, M. Belin, and D. Defourneau, Thin Solid Films, 8(71) R 51-54

(h) Ph. Cardinne, M. Marti, and M. Renard, Revue do Physique Appliquee V.6 (71) p. 547

(i) I. Giaever and H. R. Zeller, J. Vac. Sci, & Tech. V. 6 #4 p.502 (69).

Table IV. Dielectric Barriers-Tunneling Verified by Theoretical Fit to High Voltage Data.

Insulator	Electrodes Bottom/Top	Method of Preparation	R(V)/V approx.	d(Å)	Reference
BN	Au/Au	Vapor reaction at 900°C BCl_3+NH_3	10^5/4	120	j
Cd salts of $CH_3(CH_2)_{n-2}COOH$	Al/Hg,Pb,Al	Monolayer deposition from aqueous solution	10^7/.5	28	k
Polymerized Silicone Pump Oil	Al/Al	Electron beam initiated Polymerization	10^6/1	80	l
Mica	Al/Au	Cleaving	10^6/1	40	m
EuS(Se)	Au/Au	Vacuum Deposition without breaking vacuum	10^6/.8	300	n
$(C_2F_4)_n$	In/Ag	Glow Discharge in C_2F_4	10^8/1	40	author

(j) Wolfgang M. Feist, "Cold Cathode Emitters" pp. 1-59 in Electron Beam and Laser Beam Technology, L. Marton and A. B. El-Kareh Ed., Academic Press 1968
(k) Bernhard Mann and Hans Kuhn, J. of Appl. Phys. V. 42, #11, p. 4398 (1971)
(l) C. W. Wilmsen and W. H. Hartwig, Univ. of Texas Tech. Rept. 25 (1967).
(m) Malcolm McColl and C. A. Mead, Trans. of Met. Soc. AIME 233, 502 (65)
(n) L. Esaki, P. J. Stiles, and S. von Molnar, P.R.L. V. 19, #15 p. 852

that the oxide may be thicker or have a higher barrier height than the non-oxide material.

Table IV lists representative high impedance junctions (of the order of 10^5-10^8 ohms at a volt). These junctions only weakly exhibit, did not exhibit, or were not tested for low voltage superconducting characteristics. Tunneling was determined by fitting to an approximate analytic expression for the tunneling probability D(E) at high voltages usually of the form:

$$D(E) = \exp\left[-2 \int_o^s k_E(x)\, dx\right] \tag{27a}$$

For a rectangular barrier of thickness s, $k_E(x)$ is approximately

$$k_E(x) = \int_o^{s_{eff}} \sqrt{2m/\hbar^2}\, [\phi_o(1 - \frac{x}{s_{eff}})]^{1/2} dx \tag{27b}$$

$$s_{eff} \equiv \frac{\phi_o s}{V}$$

$$= \sqrt{2m/\hbar^2}\ \phi_o^{3/2}\ \frac{s}{V} \quad .$$

This is known as the Fowler-Nordheim model[46] and is accurate at voltages large compared to the barrier height. Table IV includes an In-I-Ag junction exhibiting very high impedance and dielectric strength. High voltage data for this junction has fit the Fowler-Nordheim model up to 7 volts (Section IV).

III. EXPERIMENTAL RESULTS

A. Josephson Junctions

In this section the experimental data on the D.C. Josephson effect in In-I-In junctions is compared with the theoretical value in the weak coupling (Ambegaokar and Baratoff)[39] and the strong coupling (Fulton and McCumber)[40] models.

Many In-I-In junctions with resistance less than 10 ohms exhibited a substantial D.C. Josephson current. Those with parallel shorts which were evident from the poor diffraction pattern[48] (Eq. (21)) obtained were discarded. We note in Fig. 4 the I-V characteristic of one of the better In-I-In junctions. A plot of the critical current vs magnetic field is shown in Fig. 5. The ratio of the minimum critical current at the first zero to the maximum critical current is 1:100. The other minima are less than ambient noise in the circuit i.e., less than .3% of the peak. This suggests strongly that the current step at zero voltage is entirely due to pair tunneling. The junction of Fig. 4 (#99A) was recyled to temperatures above 73°K by removing it from the dewar while cold, and subsequently replacing it. The magnitude and zeros of the pattern were repeatable to better than 1%. The junction dimensions 0.011 cm×0.016 cm were considerably smaller than the Josephson penetration depth given by

$$\lambda_J = \left[\frac{\hbar c^2}{16\pi\epsilon\lambda_{In}^2 J_c}\right]^{1/2} \cong .4 \text{ cm} \qquad (28)$$

Here λ_{In} is taken as 350Å as measured by Toxen.[49] This implies that the current distribution in the junction is only weakly affected by the self field, and consequently assuming the tunneling probability is uniform across the junction area, the current is uniformly distributed assuming H=0.

TABLE V

Experimental and Theoretical Values for I_o

Sample	$I_o^{Exp.}$	R_n	$\frac{I_o^{A\&B}}{I_o^{Exp}}$	$\frac{I_o^{F\&M}}{I_o^{Exp}}$	$I_o^{F\&M} = .90\ I_o^{A\&B}$
45E	1.6 mA	.432Ω	.80	.89	
66C	.475 mA	1.54 Ω	.886	.98	
99A	.357 mA	2.15 Ω	.89	.99	

Since the junction is not self field limited, the full critical current, j_c, should be developed (neglecting noise rounding of the characteristics). Table V is a comparison of several of the critical currents of three junctions with the predicted values of Ambegaokar and Baratoff, (AB) and Fulton and McCumber (FM). We assume in both cases the T = 0°K formula. The error incurred with this assumption at 1°K is negligible. From Section II-F we have, making the assumption of uniform distribution of current across the junction

$$I^{AB} = \frac{\pi\Delta^{o}_{In}}{2R_{NN}} \tag{29}$$

$$I^{FM} = I^{AB}\left[\frac{1}{1-\Delta'(\Delta^{\circ})} - \frac{2}{\pi\Delta^{\circ}}\int_{\Delta^{\circ}+}^{\infty} dE\ \mathrm{Im}\left(\frac{\Delta^{2}(E)}{[E^{2}-\Delta(E)^{2}]^{1/2}}\right)\right] \tag{30}$$

This last expression was evaluated for In-I-In using the complex energy gap parameters obtained by R. Dynes.[50] The primary error appears in the determination of the derivative of the gap function at the gap edge, $\Delta'(\Delta^{\circ})$, due to the difficulty of obtaining accurate characteristics close to the gap edge.[51]

We obtain the value $I_c^{FM} = (.90 \pm .02)I_c^{AB}$ for Indium, using the gap value $\Delta^{\circ}_{In} = .541$. As seen from Table IV consistent underestimates are obtained using AB theory, whereas the I^{FM} value agrees well with experiment to within a few percent. The agreement is somewhat poorer for junction with high critical current.

Josephson currents have also been observed for In-I-Pb junctions. The junctions of this type had fairly large resistances of about 20 ohms; consequently, noise tended to decouple the junction and reduce the value of the critical current. Figure 7 shows a 20 ohm junction with a critical current of approximately 20 μA. Evaluating the T=0°K expression obtained by Anderson, Eq. (14), for S_1-I-S_2 junctions with $\Delta^\circ_{In} = .54$, $\Delta^\circ_{Pb} = 1.4$ yields $I \cong 50$ μA. If strong coupling effects are taken into account this value is expected to be reduced. Although an accurate calculation of the magnitude of this effect has not been attempted, as an estimate one might expect the same reduction from strong coupling effects as is observed for Pb-I-Pb junctions. This yields a predicted Josephson current reduced by a factor of .788 (I = 40 μA), still a factor of 2 too big. The discrepancy is most likely due to room temperature noise $k_B T = .025$ eV which propagates down the unfiltered leads to the 20Ω junction whose total coupling energy is only

$$E_T \cong I_c \frac{h}{2e} = .1 \text{ eV} \tag{31}$$

and causes the transition to the resistive state at lower values of critical current.

Nonlinear coupling of the A.C. Josephson current at finite voltage with the cavity modes of the junction results in well defined Fiske steps. In Fig. 6 these are shown for an In-I-In junction with the magnetic field applied to maximize the first step. If a dielectric constant of 2.0 is assumed the expression for the spacing of the first step

$$V_1 = \frac{\hbar n \pi \bar{c}}{2eL} \qquad \bar{c} = c\left(\frac{s}{\varepsilon(2\lambda+s)}\right)^{1/2} \tag{32}$$

gives a value of the dielectric thickness of 8.4 Å., which seems a somewhat small but not unreasonable estimate.

B. Phonon Critical Points in Tunneling Characteristics

In this section the differential resistance, R(V), and its first derivative, $\frac{dR(V)}{dV}$, obtained from four terminal measurements of In-I-In and In-I-Pb junctions are analyzed. The agreement of the observed "phonon structure" with tunneling characteristics obtained by Dynes[50] for Al-I-In and by Rowell and McMillan[50] for Pb-I-Pb is suprisingly good. Differences in the magnitude of these observed structures are found to be consistent with strong coupling tunneling theory. Sharp structure in the second derivative has been tentatively correlated with Van Hove[27] and Phillips[28] critical points or Kohn[51] anomalies seen in In and Pb phonon dispersion curves. The theory of Scalapino and Anderson[29] is applied to junctions comprised of dissimilar superconductors to estimate these singularities. Comparison with experimental magnitudes allows the relative electron-phonon coupling constants of the two metals to be determined.

In Fig. 8 the 2nd harmonic $\left(\frac{dR(V)}{dV}\right)$ of an In-I-In junction at .9°K (taken by the author) is compared to the equivalent characteristic for an Al-I-In junction at .3°K (taken by R. C. Dynes).[50] The similarity is somewhat fortuitous, stemming from the fact that Aluminum is a weak coupling superconductor which which exhibits very little phonon

structure in its density of states. Consequently, according to strong coupling theory both curves are a convoluted representation of the phonon density of states of Indium with a square root energy gap singularity and should be nearly identical. Care was taken to reproduce the In-I-In derivative to eliminate noise or junction variance as possible sources of the small differences between the traces. Three other In-I-In junctions produced identical curves. Adler and Rogers,[52] and Rowell and Kopf[53] obtained identical Al-I-In derivatives at higher temperatures. Thus the explanation for any differences must lie in the nature of the Indium phonon spectrum and the mathematical complexities of the tunneling integral.

The Indium lattice is face centered tetragonal (fct), obtained from an approximately 10% compression of an fcc lattice along the (001) axis. (a=4.58, c=4.94). The In phonon density of states approximates a two peaked structure similar to neighboring fcc metals such as Pb and Al. This is clearly exhibited in Fig. 9. The upper curve is the product of the effective electron-phonon coupling constant $\alpha^2(\omega)$ and the normalized phonon density of states $F(\omega)$ and was obtained by Dynes by inverting the Eliashberg equations using his tunneling data from Al-I-In junctions as explained in detail by McMillan and Rowell.[26] The lower curve is an approximate density of states obtained by Smith and Reichardt[54] using the Born von Karman (BvK) model[55] to fit phonon dispersion measurements along the symmetry directions (x00), (00x), (xx0), (x0x), and is obtained by inelastic neutron scattering. The agreement between the curves is quite good despite the lack of success of the

BvK model for other materials. At all but a few singular points (Kohn anomalies) $\alpha^2(\omega)$ varies slowly on the scale of $F(\omega)$; consequently the upper curve is essentially proportional to $F(\omega)$. Several discontinuities in the slope of $F(\omega)$ can be observed at approximately 5 mV, 6.5 mV, 9 mV and 13.5 mV. Discontinuities in $F(\omega)$ are due to (a) singular points in the $\omega_\lambda(q)$ vs q phonon curves at which $\nabla_q \omega_\lambda(q) = 0$ (Van Hove singularities), or (b) points of sharp contact between phonon branches at which one component of the gradient is discontinuous and the other components are zero (Phillips singularities).

Singularities can be more clearly resolved in the raw derivative of the conductivity (resistivity) than in the tunneling density of states. Scalapino and Anderson[29] have analyzed in detail the effect of these critical points on the derivative of the conductance for S-I-S junctions. At points of infinite discontinuity in $\frac{dF}{d\omega}$ for which $F(\omega) \sim |\omega_c - \omega|^{1/2}$ the result is a square root singularity:

$$G'_{ss}(V) \sim \frac{c^{ss}_{<}}{|V'-\omega_c|^{1/2}} \quad |V'| < |\omega_c|$$

$$G'_{ss}(V) \sim \frac{c^{ss}_{>}}{|V'-\omega_c|^{1/2}} \quad |V'| > |\omega_c| \tag{33}$$

$$V' \equiv V - 2\Delta$$

The constants $c_>$ and $c_<$ depend on the type of singularity (maximum, minimum, saddle point) and vary inversely as the square of the critical phonon frequency. Finite discontinuities in $\frac{dF}{d\omega}$ for which $F(\omega) \sim |\omega - \omega_c|$

produce a logarithmic singularity and a jump discontinuity.

$$G'_{ss}(V) \sim D_1^{ss} \ln|V'-\omega_c| + D_2^{ss}\,\Theta(V'-\omega_c) \qquad (34)$$

In Appendix II we show that the same discontinuities occur in a S_1-I-S_2 junction; however, the amplitudes are different. The singular terms in $G'(V)_{s_1s_2}$ are the singularities that would occur in $G'_{s_1s_1}(V)$ plus those that would occur in $G'_{ss}(V)$; the zero of energy is chosen in each case as $\Delta_1+\Delta_2$ or 2Δ.

Tentative identification of sharp structure in G'(V) for In-I-In and Al-I-In (see Fig. 8) with singularities in the In phonon spectrum has been made by fitting with logarithmic or inverse square root curves. The results are given in Table VI. To identify the singularities in Table VI with the structure in Fig. 9 a voltage of 1.05 mV must be subtracted from the In-I-In trace and .72 mV must be subtracted from the In-I-Al trace. Due to the apparently higher resolution obtainable with In-I-In junctions, singular points which do not appear in Al-I-In curves have been resolved. These include the square root singularity at 6.7 mV corresponding to a maximum in the lower transverse phonon branch, T_2, at x = .82 along (x0x); the sharp dip at 9 mV which corresponds to the discontinuity in slope of the BvK determination of $F(\omega)$ at 9 mV (Fig. 9) (this does not correspond to any singularity along the measured symmetry directions but may be due to a branch contact or other singularity in an off symmetry direction); and the split peak resolution of the longitudinal maxima at 13.45 mV (xx0) and 14.5 mV (00x). The end of the spectrum at 14.85 seems to be associated with an infinite change in slope in G'(V).

TABLE VI.

Critical Points in the Tunneling Characteristics of In-I-In Junctions

Energy (mV)	Singular Behavior	Possible Neutron Assignment	Energy (mV)	Type of Singularity
14.9±.2	discontinuity in slope	LA, x00 LA, x0x	14.85 14.85	maximum, x=1 end of spectrum
14.37±.2	$+\lvert V - V_c \rvert^{-1/2}$	LA, 00x LA, xx0	14.5 14.5	maxima, x=1
13.66±.2	$+\lvert V - V_c \rvert^{-1/2}$	LA, xx0		maximum, x=.55
9.0±.2	sharp dip	? Discontinuity in BvK model of $F(\omega)$		sharp branch contact
6.7±.2	$+\lvert V - V_c \rvert^{-1/2}$	TA_2, x0x	6.72	maximum x=.82
6.4±.1	jump discontinuity	$LA-TA_1$, xx0 degeneracy	6.2	branch contact x=1
		TA_2, x00 TA_2, 00x	6.2 6.3	maximum, x=1 maximum, x=1
5.6±.2	$+\lvert V - V_c \rvert^{-1/2}$	TA_2, x0x	5.7	non analytic minimum, x=1
		TA_2, x00	5.3	kink in curve x=.7 (Kohn anomaly)?
4.1±.2	$-\lvert V - V_c \rvert^{-1/2}$	TA_2, x0x	4.1±.5	kink in curve x=.4 (Kohn anomaly)?
3.1±.2	Dip	TA_2, 00x	3.3±.5	kink in curve x=.4 (Kohn anomaly)?

Peaks are also observed in the very low energy region, 2.7-4.0 mV (Fig. 11). It is likely that they do not correspond to a Van Hove or Phillips critical point in the In phonon spectrum even in an off-symmetry direction. Similar low voltage structure has been observed by Rowell, Anderson and Phillips[56] in Pb-I-Pb characteristics and has been seen by the author in In-I-Pb characteristics at 1.6 mV and 3.0 mV. Rowell et al., identified the peak at 3.0 mV with a kink in the neutron data of Brockhouse and coworkers[57] for Pb. Both Brockhouse and Rowell suggest that the kink (peak) is caused by a Kohn type anomaly. This can be explained as follows: a sharp increase (decrease) in the effective screening of the inter-ionic potential by electrons occurs for the phonon momentum greater than (less than) a critical value q_G which satisfies the criterion $q_G = |\underset{\sim}{k}_2 - \underset{\sim}{k}_1 - \underset{\sim}{G}|$ with k_2 and k_1 lying on high density of states region of the Fermi surface and G a reciprocal lattice vector. For momenta greater than (less than) q_c screening processes involving scattering of the electron from one side of the Fermi surface to the other can (cannot) occur. The rapid change in screening causes a corresponding step increase or decrease in the phonon frequency at q_c i.e. an infinite discontinuity in $\nabla_\lambda \omega(q_c)$. These singularities also occur in $\alpha^2_\lambda(\omega_c)$ (infinite discontinuities in slope) and consequently sharp rises are expected in the second derivative characteristic $G'(V)$ at $V = \Delta_1 + \Delta_2 + \omega_c$.

The derivative structure at 1.6 mV was not however observed in Brockhouse's neutron data. Recently Stedman, Almqvist, Nilsson, and Raunio[58] have extended the work of Brockhouse to lower phonon energies.

The phonon dispersion curves indicate not only the kink in the T(111) curve at q = .55 corresponding to the 3.0 mV anomalous peak but a small departure from linearity in the T_2(220) branch at q = .35 - .4 centered on a frequency of 1.8 ± .2 mV. This small effect well within the quoted resolution of ± .04 mV has not to my knowledge been discussed in the literature.

The Indium phonon dispersion curves taken by Smith and Reichardt also reveals low energy kinks most likely Kohn anomalies at 2.4 mV, 2.9 mV, 3.3 mV and 4.1 mV along various transverse modes. The author has resolved these only to an accuracy of ± .5 mV. We note that the kink at 4.1 mV agrees with the approximate square root singularity at 4.1 mV in G'(V). The other singularities lie close to the low energy structure though no fit has been made. It is likely that accurate dispersion relations of other materials will indeed reveal 1:1 correlation between structure in the dispersion curves and in G'(V) and may prove useful for experimental analysis of the fine structure in the Fermi surface.

C. Magnitude of Phonon Structure in Tunneling Characteristics

In addition to locating the critical points, we have compared the relative magnitudes of the phonon structures of In-I-In, In-I-Pb, Al-I-In, and Pb-I-Pb junctions. In the vicinity of a large phonon peak or critical point at ω the conductivity of an S_1-I-S_2 junction may be written (see Appendix I)

$$G_{S_1S_2}(V) \cong F_{S_1S_2}(V) + \frac{\alpha_1^2}{(\omega+\Delta^\circ_{S_2})^2}\sqrt{\Delta^\circ_{S_1}}\; I'(V'+\Delta_{S_2},F_2(\omega)) \qquad (35)$$

$$+ \frac{\alpha_2^2}{(\omega+\Delta^\circ_{S_1})^2}\sqrt{\Delta^\circ_{S_2}}\; I'(V'+\Delta_{S_1},F_1(\omega))$$

$$\omega = V' \equiv V - \Delta_{S_1} - \Delta_{S_2}$$

α^2 is assumed constant for each material. I' is a function of the phonon spectrum of the superconductor designated by the subscripts in its argument and is independent of the other superconductor. In the vicinity of a phonon peak or critical point I' or I'' changes rapidly whereas the background conductance $F(V) \sim C_{NN}$ is slowly varying for $V \gg \Delta_1 + \Delta_2$. Since in general phonon structure for different materials does not occur at the same energies, it is often possible to distinquish the separate contributions to the conductance from the two superconductors. For example, the Al phonon spectrum consists of a transverse structure at 15 mV and a sharp longitudinal peak at 34 mV.[59] Thus since most other superconductors have a phonon spectrum at lower energies (i.e. less than 15 mV), the phonon conductance characteristic of an Al-I-S junction below 15 mV is due solely to the "S" electrode. However, because the coefficient of I' falls off as $1/\omega^2$, Al will exhibit much smaller peaks even in the 15-30 mV range, ($<$ 1/20 the size of Pb peaks) despite the fact that the electron-phonon coupling constant for Al is only a factor of 2 smaller than that for Pb.[60]

Thus, in the case of an Al-I-In junction, for example,

$$G'_{InAl}(V) \cong F'_{InAl} + \frac{\alpha^2_{In}}{(\omega-\Delta^\circ_{In})^2} \sqrt{\Delta_{Al}} \; I'(V'+\Delta_{In}, F_{In}(\omega)) \qquad (36a)$$

whereas for a two superconductor junction such as In-I-In

$$G'_{InIn} = F'_{InIn} + \frac{(2)\alpha^2_{In}}{(\omega-\Delta^\circ_{In})^2} \sqrt{\Delta_{In}} \; I'(V'+\Delta_{In}, F_{In}(\omega)) \qquad (36b)$$

the factor of "2" coming from the identical contribution at both limits of the integral (AI, Eq. (2)). The background conductance derivative should be small as long as the voltage is much less than the barrier height of the tunnel junction. Hence the relative magnitude of this structure in In-I-In in comparison to Al-I-In junctions is approximately

$$\frac{G'_{InIn}}{G'_{InAl}} = 2\sqrt{\Delta_{In}/\Delta_{Al}} \sim 3.6 \qquad (37)$$

Since the vertical scale of both graphs in Fig. 8 is arbitrary there is no certain way of verifying this value. However, the signal to noise ratio for Al-I-In is roughly a factor of 3-4 worse than for In-I-In. The difference undoubtedly is due to the difference in the junctions rather than experimental techniques, and provides the explanation for the increased resolution of the critical points in the In-I-In characteristic.

A more quantitative comparison can be made using the conductance curves of In-I-Pb and Pb-I-Pb junctions shown in Fig. 10. Since the conductance background is large but slowly varying we subtract it off near phonon peaks by forming the expression

$$\overline{g'(V)}\Delta V \equiv 2\left[\frac{G(V_1) - G(V_2)}{G(V_1) + G(V_2)}\right] = 2\left[\frac{R(V_2) - R(V_1)}{R(V_2) + R(V_1)}\right] \equiv \overline{r'(V)}\ \Delta V \qquad (38)$$

An error of at most 5% is incurred in equating $\overline{g'(V)}$ with $\frac{G'(V)}{G_o(V)}$ at the two phonon peaks. G_o is the normal state conductance. Since the latter normalized conductance derivative is independent of junction resistance, $\overline{g'(V)}$ and $\overline{r'(V)}$ are also approximately independent of junction resistance. At the longitudinal phonon peak of Pb at 8.5 mV

$$\frac{\overline{g'(V)}^{L}_{Pb-Pb}}{\overline{g'(V)}^{L}_{In-Pb}} = \frac{.259}{.0778} = 3.32$$

This compares favorably with the prediction of $2\sqrt{\Delta^\circ_{Pb}/\Delta^\circ_{In}}$ = $2\sqrt{1.395/.541}$ = 3.21[61]

For the transverse peak at 4.4 mV the ratio

$$\frac{\overline{g'(V)}^{T}_{Pb-Pb}}{\overline{g'(V)}^{T}_{In-Pb}} = 2.3 \ .$$

The disagreement in this case stems from the failure of approximations made in the derivation of Eq. (13) based on the assumption that the

phonon frequency was much larger than the sum of the energy gaps. This is clearly not true since

$$\frac{\omega_{ph}^{T}}{2\Delta_{Pb}} \cong 1.5$$

for the transverse case.

In the preceeding discussion the implicit assumption was made that very little conductance structure was due to the Indium in In-I-Pb junctions. This appeared justified considering the close similarity of the two curves in Fig. 10. A more rigorous check may be made by comparing the conductance derivatives of In-I-Pb and Pb-I-Pb junctions as in Fig. 12. Here again the similarity is striking, however, some small deviations are noted in the vicinity of the arrows in Fig. 12a which occur at the large In phonon peaks of Fig. 8 suitably corrected for the difference in the sum of the energy gaps in the two cases. A rough estimate indicates In structure is of the order of 1/10 th that of Pb. However a more precise determination may be made by comparing isolated singularities stemming from analogous critical points in the phonon spectrum of the two materials. The theory of Scalapino and Anderson predicts the shape and amplitude of these singularities for S-I-S junctions and is easily extended in Appendix II to S_1-I-S_2 junctions. The conductance derivative in the vicinity of a Van Hove singularity can be written as:

$$G'_{S_1S_2}(V) = C\alpha_j^2 \sqrt{\frac{\Delta^\circ_{S_1}\,\Delta^\circ_{S_2}}{(\omega_j+\Delta^\circ_{S_j})^2}} \begin{pmatrix} \pm\ \beta_j \\ \pm\ \gamma_j \end{pmatrix} \frac{V_j}{(a)^{3/2}} \left[\frac{1}{(V-\Delta^\circ_1-\Delta^\circ_2-\omega_i \pm \delta)^{1/2}}\right] \qquad (39)$$

$$V \to \omega_j + \Delta^\circ_1 + \Delta^\circ_2 \pm \delta$$

$j = S_1$ or S_2; $i = S_2$ or S_1

$\omega_j \equiv$ the critical point

$V_j \equiv$ volume/unit cell

$z \equiv$ # atoms/unit cell

$a \equiv$ curvature of the dispersion relations near ω_j

$$\gamma \equiv \mathrm{Im}\left[\frac{\Delta(\omega_j)}{Z(\omega_j)}\right]$$

$$\beta \equiv \mathrm{Re}\left[\frac{\Delta(\omega_j)}{Z(\omega_j)}\right]$$

The expression $\begin{pmatrix} \pm\ \beta_j \\ \pm\ \gamma_j \end{pmatrix}$ is shorthand for the fact that the coefficient of the square root singularity in (41) has either $\pm\ \beta$ or $\pm\ \gamma$ as a factor. If the coefficient contains β as V approaches $V_c \equiv \omega_i+\Delta^\circ_{S_1}+\Delta^\circ_{S_2}$ from below, it contains γ as V approaches V_c from above. For example, at a maximum the factor is $+\beta$ below V_c and $+\gamma$ above. The corresponding coefficients for a minimum are $-\gamma$ and $-\beta$ (see Appendix II (21)). In general $\gamma > \beta$ at a critical point. Near the maximum in the longitudinal phonon branch for In and Pb we have:

$$\gamma_{Pb} \cong .73 \quad \beta_{Pb} \cong .22$$

and

$$\gamma_{In} \cong .81 \quad \beta_{In} \cong .47$$

Since the BCS singularity at the energy gap is smeared for real junctions, the predicted singularities are inevitably rounded. Nevertheless, it is possible to fit the behavior of a peak such as in Fig. 12 to the form

$$\frac{A}{(V-V_c)^{1/2}}$$

for V well above V_c. We have done this for the peak corresponding to the longitudinal phonon maximum of Pb at 8.85 mV (Fig. 12a $V = \Delta^\circ_{In} + \Delta^\circ_{Pb} + 8.85$ mV) and for the peak corresponding to the longitudinal phonon maximum of In at 14.5 mV (Fig. 12a $V = \Delta^\circ_{In} + \Delta^\circ_{Pb} + 14.5$). From (14) the ratio of the coefficients of these square root singularities is should be

$$\frac{A_{Pb}}{A_{In}} = \frac{\alpha^2_{Pb}}{\alpha^2_{In}} \frac{(14.5 + .54)^2}{(8.85 + 1.4)^2} f$$

where

$$f = \frac{\gamma_{Pb}}{\gamma_{In}} \left(\frac{a_{In}}{a_{Pb}}\right)^{3/2} \frac{V_{Pb}}{V_{In}}$$

Experimentally we find $\frac{A_{Pb}}{A_{In}} \cong 3.3$. If the curvatures, a_{In} and a_{Pb}, are estimated from the neutron dispersion curves and $\hat{\gamma}$ evaluated using the Δ and Z the values given in the McMillan, Rowell and Dynes tabulation,[50] f becomes .85 and the ratio of the coupling constants between electrons and longitudinal phonons in In and Pb is

$$\frac{\alpha^2_{Pb}}{\alpha^2_{In}} \cong 1.7$$

Using the value $\alpha^2_{Pb} = 1.2$ determined by Rowell and McMillan[26] as the best fit for their observed tunneling characteristics we have

$$\alpha^2_{In} \cong .70$$

The parameter

$$\bar{A}^2 = \int_0^\infty \sum_\lambda \alpha_\lambda{}^2(\omega_\lambda F_\lambda(\omega)\ d\omega$$

has been evaluated[50] by summing the values of $\alpha^2(\omega)F(\omega) \equiv \sum_\lambda \alpha_\lambda(\omega)F_\lambda(\omega)$ obtained point by point by inverting Al-I-In tunneling data.

$$\bar{A}^2 = 2.7$$

Assuming an approximately constant value of $\alpha_\lambda{}^2$ for each phonon polarization we have

$$\bar{A}^2 = \sum_\lambda \alpha_\lambda{}^2 \int_0^\infty F_\lambda(\omega)d\omega = \sum\alpha_\lambda{}^2 = 2.7$$

If equal coupling constants for all polarizations are assumed $\alpha^2_{Longitudinal} = .9$. If the longitudinal constant is twice the transverse constant (as is assumed for Pb) $\alpha^2_L = 1.4$. The value of $\alpha^2_L = .7$ obtained through the singularity fit appears to indicate that equal coupling constants are a better approximation. This type of analysis in conjunction with conductance derivative measurements of greater sensitivity could be used to determine for a variety of superconductors the electron phonon coupling constant α_λ as a function of the phonon polarization λ.

IV. EXPERIMENT - NATURE OF THE BARRIER

We have determined the stochiometry, dielectric constant, and barrier height of the fluorocarbon dielectric. X-ray photoemission[63] and Auger spectroscopy[64] have provided quantitative or semiquantitative analyses of the the chemical constituents of the dielectric and the variation in chemical environment. Ellipsometry measurements[65] allow determination of the real and imaginary parts of the index of refraction. High voltage I-V plots have been used to determine the asymmetric barrier heights. The "tunneling spectra" of In-I-S junctions yields information on the constituent molecular species of the barrier. These measurements are discussed in the following section, as well as some preliminary data from Au-I-In(Pb,Au) junctions.

A. Chemical Composition and Environment

The chemical composition of junction dielectric layers of total mass approximately 10^{-5} micrograms may be analyzed using the sensitive techniques of inelastic electron or X-ray scattering from the surface. Inelastic techniques including Auger electron spectroscopy (AES) and X-ray photoemission spectroscopy (XPS) involve the analysis of the energy distribution of scattered electrons emanating from a target bombarded by a monochromatic beam of X-rays, electrons, or light ions. Depending on the depth of surface that is to be studied various incident energies and particles may be used. For AES the incident beam is of the order of 1-5 kV electrons (or X-rays). The sampling depth from which electrons are ejected from the sample by normal inelastic scattering and Auger processes is a few monolayers. An

Auger electron is ejected in a three part process whereby (1) an electron is removed from an inner level, (2) another electron fills the vacancy transferring the energy to (3) a third electron which is ejected. Auger processes have a smaller cross section than that of normal inelastic processes but have the advantage that low energy electrons are emitted which have definite energies characteristic of the atomic level spacing thus allowing chemical element identification. These low energy electrons can only reach the surface from shallow depths of about 10Å. XPS involves an incident Kα beam of about 25 kV. Core electrons, i.e., 1S, 2S, 2P are ionized. The ionization energy, equals the difference in energy of the emitted and incident beams and is dependent on the particular atomic potential and the perturbation due to the chemical environment of the atom. Resolution of approximately 2eV is possible the limitation being the energy spread of the incident beam. The excited core electrons will penetrate from a maximum depth of about 50Å.

Both XPS and AES have been used to analyze the dielectric. In both cases two samples were used; one with the fluorocarbon layer, the other an In substrate as a control without the insulating layer. This was done to determine the extent of unavoidable contamination by atmospheric molecules. Figure 13 shows the Auger structure (actually the second derivative of the particle flux as a function of energy) of an In sample. The top curve indicates the approximate composition of the In sample surface after reaction with fluorocarbon vapor and exposure to atmosphere. The middle is the same surface after Ar ion bombardment, and the bottom curve is the control (a fresh In surface just exposed to atmosphere).

All three traces indicate the presence of In triplet peaks, from 300-400 V, C at 275 V and O at 500 V. A F peak at 650 V is shown in the bottom two traces. Sulfur was present in the analyzer as an unavoidable contaminant. Quantitative determination is difficult, however three features should be noted: (1) The top two traces have a F peak which increases after ion bombardment whereas the O peak decreases drastically. (2) Similarly the C peak decreases somewhat whereas the In peak increases dramatically. (3) Peak area scales roughly as inverse energy. We can infer first that both C (either from diffusion pump oil or atmospheric CO_2) and O_2 are unavoidable contaminants which may be removed by ion bombardment; second, that F and some C are present as a tenacious layer which is thick enough together with an atmospheric monolayer to obscur the In peak somewhat; finally a rough estimate yields the C/F ratio after bombardment, approximately 3:1. This last figure should be taken as an order of magnitude estimate due to some recontamination with C during the bombardment and inaccuracies in the cross section estimate used for this dielectric, and the fact that only the first monolayer approximately is sampled.

A more quantitative determination is possible using XPS. A somewhat thicker sample fluorocarbon layer was used for this analysis. Figures 14 and 15 show the C(1s) and F(1s) peaks respectively for the In plus dielectric sample with the control carbon peak superimposed for comparison. The full graph (not shown here) indicates that oxygen appears in the control, but no detectable oxygen appears in the sample. The lack of

oxygen adhering to the sample surface despite atmospheric contamination is virtually unique to this material. The thickness of the layer can be inferred from the fact that the In peak is severely obscured (i.e., $\gtrsim$50Å). The four distinct carbon peaks in Fig. 14 correspond to sites with varying number of fluorine atoms in the vicinity. The highly electro-negative fluorine increases the C(1s) ionization energy by stripping away the outer carbon electrons, thus shifting the fluorocarbon peaks below the control peak. A comparison with the XPS data for fluoromethanes obtained by Thomas, Davis and Shirley[66] is shown in Table VII. There is a rough 1:1 correspondence in the energy shifts observed in both cases. However, the binding energy is less in the polymer than in the gaseous fluorocarbons. Strong evidence that the fluorocarbon layer is a very disordered form of poly-tetrafluoroethylene is provided by the measurements of Clark and Kilcast[67] on the C(1s) and valence levels of a pressed film of PTFE. They obtained a C(1s) binding energy of 292.4 eV with a spread of 1.5 eV. This corresponds identically with the binding energy of the largest peak in the C(1s) band. Quantitative determination of the C/F area ratios was made after averaging consecutive channels to eliminate asymmetric clocking errors. Using the measured relative cross sections determined from CF_4 gaseous phase analysis[68] the actual C/F ratio of 1/1.98 was obtained corresponding to a stochiometry of $(CF_2)_n$. Conclusions drawn are: (1) a dielectric insulator with the same stochiometry as poly-tetrafluoroethylene (PTE) is formed, (2) this insulator sheds oxygen, and (3) the chemical environment of the carbon atoms is inhomogeneous corresponding to various numbers of surrounding fluorine atoms.

Table VII.

Fluorocarbon Layer		Fluoromethane	
C(1s) Energy	Energy Shift Relative to Control (-285.2eV)	C(1s) Energy	Energy Shift Relative to CH_4 (-290.8eV)
-288.6	3.4	-293.6	2.58 (CH_3F)
-290.4	5.2	-296.4	5.55 (CH_2F_2)
-292.4	7.2	-299.1	8.3 (CHF_3)
-294.2	9.0	-301.8	11.0 (CF_4)

Measurements of the change in polarization of elliptically polarized light incident on a sample can measure thicknesses of minute surface layers on a material of known refractive index (theoretically fractions of Å's i.e. submonolayer averages) as well as both the real and imaginary index of refraction $(n + i\kappa)$.[65] Measurements on a Au + dielectric sample using elliptically polarized light yield values of s, n and κ of 250Å ± 5Å; 1.39 ± .005, and <.01, respectively. Assuming that ionic and dipole polarizabilities are not large, (a good assumption for common polymers) the optical dielectric constant $\varepsilon(\omega) = n^2 = 1.935 \pm .01$ is approximately $\varepsilon(0)$ the static dielectric constant. This value is close to but distinct from the dielectric constant of bulk semicrystalline PTE. $\varepsilon = 2.10$, $n = 1.35$

B. "High Voltage" I-V Characteristics and the Barrier Height

At biases in the vicinity of the barrier height the tunneling characteristic of both normal and superconducting junctions becomes very non-linear. Several approximate expressions have been developed for tunneling in this region. The validity of these approximations has been reviewed by Duke.[69] Using a stationary state formalism (i.e., constructing appropriate single particle wavefunctions localized on one side of the barrier, calculating the transmission coefficient, and summing over all states weighted with Fermi-Dirac occupation number) he obtains the formal expression

$$j = \frac{2e}{h} \int dE[f(E)-f(E+eV)] \int \frac{d^2k_{\parallel}}{(2\pi)^2} D(E,k_{\parallel}) \qquad (40)$$

The transmission probability $D(E, k_{\parallel})$ evaluated using the W.K.B. approximation with $k_{\parallel}$ assumed to be zero is

$$D(E) = \exp - 2J(E) \tag{41}$$

$$J(E) = \int_{x_1}^{x_2} \left\{\frac{2m}{\hbar^2} [V_B(x) - E]\right\}^{1/2} dx$$

"x_1" and "x_2" are the classical turning points of the motion. V(x) is generally taken to be a smooth analytic shape corresponding to an effective barrier height. Of course on a 10Å scale with an amorphous insulator this should not be a good approximation and detailed calculation of short range scattering in a random potential array would be required. This is an intractable problem, however, and the average barrier technique will quite often give agreement with experiment for ordered insulators with no impurities. The most common approximation for V(x) is a trapezoidal barrier which can be written

$$V(x) = V_{B1} + (V_{B2} - V_{B_1}) \frac{x}{S} \tag{42}$$

When V is larger than $\text{Max}(V_{B1} \text{ or } V_{B2})$ the turning point becomes smaller than x_2. The voltage dependent effective thickness is then

$$s_{eff1} = \left[\frac{V_{B1}}{|V| + V_{B1} - V_{B2}}\right] s$$

or

$$s_{eff2} = \left[\frac{V_{B2}}{|V| + V_{B2} - V_{B1}}\right] s \qquad (43)$$

corresponding to a negative V applied to side (1) or (2) respectively. Intergrating over the triangular barrier region we have

$$D(E_x)1 \cong \exp\left[-2\sqrt{\frac{2m}{\hbar^2}}\ \frac{V_{B1}^{3/2}\, s}{V + V_{B1} - V_{B2}}\right] \qquad (44)$$

$$D(E_x)2 \cong \exp\left[-2\sqrt{\frac{2m}{\hbar^2}}\ \frac{V_{B2}^{3/2}\, s}{V + V_{B2} - V_{B1}}\right]$$

At $T \cong 0°K$

$$I_{21} \sim V^2 \exp -\left[2\sqrt{\frac{2m}{\hbar^2}}\ \frac{V_{B2}^{3/2}\, s}{V + V_{B2} - V_{B1}}\right]$$

$$I_{12} \sim V^2 \exp -2\sqrt{\frac{2m}{\hbar^2}}\ \left[\frac{V_{B1}^{3/2}}{V + V_{B1} - V_{B2}}\right] s$$

Consequently a plot of $FN \equiv \ln \frac{(I_{12})}{V^2}$ vs. V^{-1} yields for $V_{B1} - V_{B2}$ small compared to V has an approximate slope

$$\frac{FN}{V^{-1}} \sim V_{B1}^{3/2}\left[1 - \frac{V_{B1} - V_{B2}}{V}\right] s \qquad V \gg V_{B_1} - V_{B_2}$$

In the region of validity of the approximation the slope of the plot is $V_{B1}^{3/2}$ s. A similar plot of $\ln(I_{21}/V^2)$ vs V^{-1} yields $V_{B2}^{3/2}$s. This linear behavior can be clearly seen in Fig. (16) for an In-I-Ag junction at 73°K. Using the thickness of the dielectric as determined by the D.C. capacitance (44Å), we obtain values of V_{B1} = 370 mV (In^+) and V_{B2} = 210 mV (In^-). These values are probably underestimates as shown by Hansma, McBride and Rochlin,[70] due to the inequivalent determination of the dielectric thickness by resistance and capacitance measurements. This discrepancy occurs because a thin dielectric has a distribution $F(S_i)$ of low spots which, in comparison to a uniform barrier, will generate a much larger effective increase in

$$R \propto \sum_i \exp\left[-\frac{V_B^{3/2}}{V}[S_i]\right] F(S_i) \qquad (45)$$

than in

$$C \propto \sum_i \frac{F(S_i)}{S_i}\ \varepsilon$$

C. Tunnel Spectrum of the Insulator

At voltages above the phonon energies, infrared vibrations of the molecular species of the barrier can be observed in the G'(V) characteristic. This can be seen as a series of peaks roughly centered on characteristic vibrational frequencies. The strongest of these peaks are associated with light dimers i.e. C-H, O-H and the like. Various theories[71-76] have attempted to explain the line shape of the peaks. The general conclusions

are: (1) the amplitude depends on the location of the vibrator following a cosh $(x-x_o)$ dependence with x_o the end on the far side of the tunneling electron. This is due to the more rapid decay of the electron after losing some energy to the vibrator. (2) The line shape is not a simple resonant structure in general and the density of states of the electrodes play a part in determining the shape. (3) Interference effects occur between the normal elastic channel and the inelastic channel. The theoretical picture appears to be somewhat murky at this time so that accurate interpretation of the line shape of the resonant peaks is difficult for more complicated barrier species. Figure 17 is the conductance tunnel spectrum of the barrier for an In-I-In junction and Fig. 18 is the tunneling spectrum for an In-I-Pb junction. The arrows (Fig. 18) refer to known vibration or rotational energies of gaseous CF_4 and solid PTE. No clear correlation exists between G'(V) and either spectrum. This result is not suprising since the amorphous structure of the insulator and the distribution of potential sites (shown in the XPS study) does not correspond well with the structure of either CF_4 or semicrystalline PTE.

D. Gold Junctions

An additional indication that no oxygen is incorporated in the barrier is the production of Gold based junctions, i.e., Au-I-Au, Au-I-Pb, and Au-I-In. The latter two have demonstrated clearly defined current rises at the energy gap when the Pb and In were superconducting although the quality of the junctions was considerably poorer than for In. Figure 19 shows a the I-V and R(V) vs V characteristics of

a Au-I-In junction. The second derivative exhibits considerable structure as is seen in Fig. 20 which corresponds approximately to the low phonon peaks for In. At higher energies the structure is washed out. High resistance gold (10^{10} Ω) junctions have been made in CF_4. Considering the the resistance of Au to oxidation it is extremely unlikely that substantial oxygen is present in the insulating layer of any of these Au junctions.

E. Surface Structure

The Scanning Electron Microscope was used to determine the homogeneity of the indium plus polymer surface. Figure 21 shows a comparison of a pure indium surface (upper photograph) and the indium surface after reaction in the fluorocarbon discharge. The polymer surface (lower photograph) has a grainy appearance. The magnification is X10,000. Light specks are thick insulating particles.

V. EXPERIMENTAL METHODS

A. Fluorocarbon Junction Preparation

Junction preparation involved the following new technique. An indium or gold film was deposited onto a standard glass substrate 3 " × 1 " in a vacuum of 10^{-5}-10^{-6} Torr. Better surface properties of indium were obtained when the substrate was maintained at 73°K and this procedure was generally used. After deposition the chamber was valved off and the sample allowed to equilibrate to room temperature. Indium was often annealed for one to five days at room temperature. The film was then placed in a reaction chamber (Fig. 22) consisting of a standard 3 in. high vacuum high voltage 2 electrode feedthrough bolted onto a copper pipe to which was attached a gas bleeding line and a liquid nitrogen trap backed by a mechanical pump. Fluorocarbon vapor is pumped through the chamber while a D.C. plasma discharge is maintained at pressures from 300-750μ for periods of 5 sec to a few minutes. Several fluorocarbon compounds have been used with similar results. These are "Fluorinert" 77 (3M trademark), CF_4 and C_2F_4. High resistance junctions were made by exposing the film directly to the discharge approximately 2 " from the electrodes. Low resistance junctions were shielded by turning the film away from the electrodes facing the grounded copper tube. Most of the discharge occurred in the localized region between the electrodes which were 1/4 " diameter on 3/4 " centers. Junctions were left in the reaction chamber to cool generally from 15 minutes to overnight. Some outgassing of the

walls did occur. About one torr accumulated in a 24 hour period. This procedure does not appear to produce oxygen contamination since the fluorocarbon layer actually is not "wet" by atmospheric oxygen as determined by XPS results of the previous section, but is probably necessary as a re-annealing finally counter electrodes of In, Pb or Au were deposited process.

A few general remarks are in order concerning the relative merits of the different fluorocarbons. Fluorinert appears to yield the best results for low resistance junctions; however, most of the junctions made with the lighter gases were deliberately high resistance. The most probable chemical reaction is the fragmentation of the molecule followed by polymerization of the low molecular weight radicals. Fluorinert yields a large portion of higher molecular weight components which act to dilute the critical monomers such as C_2F_4. This may result in a smoother, slower reaction process yielding more homogeneous films. All of the fluorocarbons produced high resistance junctions quite easily.

B. Cryogenics

Measurements were performed in a standard glass double-walled nitrogen-jacketed liquid helium cryostat (Fig. 23). Temperature was regulated by an A.C. bridge regulator[77] with one arm, a 1/8 watt Allen Bradley resistor and the offset signal fed through a manganin wire heater. A cylindrical solenoid with output up to 20G was used to make Josephson diffraction patterns. Samples were measured at room temperature, liquid nitrogen, and 4.2°K to .9°K.

C. Electronics

Four terminal I-V measurements were made in three ways. Josephson junctions were current swept by a Wavetek oscillator with a triangle wave of 10-100 Hz applied to a current limiting resistor R_I in series with a smaller current monitoring resistor R_s and the junction. The voltage across R_I was applied directly to the y-axis of a Hewlett Packard 7000A x-y recorder while the voltage across the junction was amplified by a Sanborn differential amplifier and applied to the x-axis. Higher resistance junctions were swept by a motorized helipot drive applied through a low pass filter to the same circuit. Junctions of 1 Megohm or greater were swept by the helipot acting as a voltage source. The current across the junction was monitored by the voltage across R_s amplified by a PAR 113 differential amplifier (1000 Meg input impedance) and applied to the y axis of the recorder while the junction voltage was buffered by a Keithley 602 electrometer (10^{14} ohms input impedance) and applied to the x-axis.

The first and second derivatives were determined using a standard phase sensitive lock-in derivative technique. A PAR HR-8 lock-in amplifier monitored the A.C. voltage signal (either the fundamental or the first harmonic frequency) across the junction produced by an A.C. current source obtained by applying a low noise voltage through a transformer across a very large R_M in series with the junction. Modulation signal levels of 10-50μV p-p were used in first derivative

traces; 100-500μV p-p were used in second derivative measurements. The most critical phonon measurements were made at several levels to determine if the line shape was modulation dependent. This was not the case for levels of 200μV p-p or less at 1°K.

VI. CONCLUSIONS

We have shown that, by means of glow discharge induced polymerization of gaseous fluorocarbon species, thin tencious insulating layers can be formed on inert metals. Results for In and Au indicate that non-shorting tunnel junctions can be formed with this insulator.

We have studied the properties of junctions made with the base electrodes either In or Au which have low temperature normal state resistances in the range $0.01\text{-}10^{10}$ ohms. Particular attention has been paid to In-I-In, and In-I-Pb junctions in the low resistance range.

Sensitive four terminal derivative studies on In-I-In and In-I-Pb junctions have been instrumental in tentatively identifying energies of the critical points in the In phonon spectrum as well as the Kohn anomalies associated with the In Fermi surface. The relative amplitude of the more prominent of these singular structures for In-I-Pb and Pb-I-Pb junctions agrees with the extended theory of Anderson and Scalapino. This agreement has been utilized to estimate the electron phonon coupling constant of the transverse In phonon branch as $\alpha^2_{In} = 0.7$. In principle the simple scaling law

$$\frac{\alpha^2_{S1}}{\alpha^2_{S2}} = \frac{A_{S_1}}{A_{S_2}} \left(\frac{V_1}{V_2}\right)^2 \cdot f$$

discussed in Section III-C (where A and V are the amplitude and voltage of a particular phonon singularity observed in the second harmonic and f is factorizable into contributions from each superconductor and is of the order of unity) can be applied to any S_1-I-S_2 junction. The

self consistency of this method can be checked by studying all possible heterogeneous junctions formed by combinations of three superconductors.

The magnitude of the Josephson current exhibited by low resistance In-I-In system has been compared to the theoretical calculations of Ambegaokar and Baratoff[39] Fulton and McCumber.[40] The strong coupling theory yields considerably better agreement (1%) with experiment.

Preliminary observations on Au-I-In and Au-I-Pb junctions include (a) gap structure in the I-V curves and (b) phonon structure (due to the superconducting counter-electrodes) in the second derivative curves. Further study on these junctions as well as Au-I-Au is indicated.

The nature of the insulating layer has been studied with the aid of various surface analysis techniques (i.e., Auger and X-ray electron spectroscopy, and ellipsometry) as well as through the junction characteristics. To very high confidence the insulator stochiometry is $(CF_2)_n$, an amorphous form of poly-tetrafluoroethylene. The contact potential of this dielectric has been estimated by fitting high voltage (i.e., between 1 and 7 volts) characteristics to the Fowler Nordheim approximation. Values of 210 mV with In and 370 mV with Ag were obtained. The inhomogeneity, thickness and dielectric strength of the insulator vary with the particular fluorocarbon utilized in the discharge reaction.

It is hoped that this discovery will be used to extend the investigation of metals by metal-insulator-metal tunneling using junctions which heretofore have proved intractable to fabricate by traditional

techniques. The study of superconductors such as Rh, Ru, Tc and Os as well as non-superconducting noble metals would be of considerable interest.

ACKNOWLEDGEMENTS

It would be nearly impossible to enumerate all those whose support, encouragement or insight aided me during my graduate studies. However, I would like to particularly thank my adviser Professor G. I. Rochlin whose insight, experimental expertise and steadfast backing was instrumental in completion of this project, my colleagues Dr. James Sweet, Dr. Paul Hansma, Dr. Yeong de Song and Dr. Duncan McBride and many others whose assistance and spirited conversations made research very pleasant.

Many researchers at Lawrence Berkeley Laboratories provided invaluable assistance in surface analysis. I would like to especially thank Dr. G. Somorjai and Dr. F. Szalkowski for their aid in performing the Auger analysis, Dr. D. Shirley and his colleagues for their cooperation in taking the XPS curves, and Dr. Jorg Mathieu for help in performing the ellipsometry measurements.

Dr. H. G. Smith is due special thanks for sending to me his neutron data before publication. I would like to acknowledge several helpful conversations pertaining to various aspects of this project with Dr. J. M. Rowell, Dr. C. C. Pimentel and Dr. W. D. Gregory. I would also like to express my gratitude to Alice Ramirez for her excellent job of typing this thesis.

Most especially I would like to thank my parents who encouraged me to begin my graduate studies, my wife Betty Ann who warmly supported me during many trying years of graduate research, and my daughter Rachel who encouraged me to conclude this project.

This work was done under the auspices of the U. S. Atomic Energy Commission.

APPENDIX I

Decomposition of G'(V) for S_1-I-S_2 Junctions

The current through an S_1-I-S_2 junction at T=0°K can be written

$$I = C_{NN} \int_o^V dE N_L(E) N_R(E-V) \qquad (1)$$

C_{NN} is the normal state conductivity assumed to be a slowly varying function for V in the range of interest (0-30 mV) and will be set equal to 1 in the remainder of the calculation. N(E) is the density of excited states of the superconductor of energy E as measured from the Fermi surface of the left (L) electrode, and by convention a positive bias V has been applied to the left electrode. Substituting the strong coupling density of states

$$N(E) = \mathrm{Re}\left\{\frac{|E|}{[E^2-\Delta^2(E)]}\right\}^{1/2} \Theta(|E|-\Delta(\Delta_o))$$

$$\Delta = \Delta_1 + i\Delta_2 \qquad \Delta(\Delta_o) \equiv \Delta^\circ$$

We have

$$I = \int_{\Delta_L^\circ}^{V-\Delta_R^\circ} E\, d\,\mathrm{Re}\left\{\frac{E}{[E^2-\Delta_L{}^2(E)^{1/2}}\right\} \mathrm{Re}\left\{\frac{V-E}{[(V-E)^2 - \Delta_R{}^2(V-E)]^{1/2}}\right\} \qquad (2)$$

For $\Delta_1^\circ + \Delta_2^\circ \ll V \ll \chi_{L,R}$ (χ is the work function of the metal) the integral may be approximated by contributions from the singularities

at the upper and lower limits

a) Lower limit

$$V \gg E + \Delta_R$$

$$E \sim \Delta_L$$

$$\mathrm{Re}\left\{\frac{V-E}{[(V-E)^2 - \Delta_R^2(V-E)]^{1/2}}\right\} \simeq 1 + \frac{\mathrm{Re}\left[\Delta_R^2(V-E)\right]}{2(V-E)^2} + \cdots$$

$$\simeq 1 + \frac{\Delta_{R_1}^2(V-E) - \Delta_{R_2}^2(V-E)}{2(V-E)^2} \qquad (3)$$

and

$$\mathrm{Re}\ \frac{E}{\sqrt{E^2-\Delta_L^2(E)}} \cong \sqrt{\frac{\Delta_L^o}{2}}\ \frac{1}{(E-\Delta_L^o)^{1/2}}$$

This is quite a good approximation for E well below the first phonon peak at $\omega_{ph} + \Delta_L^o$. Since the imaginary part of the gap goes to zero and the real part of the gap is approximately constant even for very strong coupling materials such as Pb.

b) Upper limit:

$$E \sim V - \Delta_R^o$$

$$V \gg \Delta_R^o + \Delta_L^o$$

$$\mathrm{Re}\left[\frac{(V-E)}{[(V-E)^2 - \Delta_R^{\,2}(V-E)]^{1/2}}\right] \simeq \sqrt{\frac{\Delta_R^{\,o}}{2}}\ \frac{1}{(V-E-\Delta_R^{\,o})^{1/2}}$$

and (4)

$$\mathrm{Re}\left[\frac{E}{\sqrt{E^2 - \Delta_L^{\,2}(E)}}\right] \simeq 1 + \frac{\Delta_{L_1}^2(E) - \Delta_{L_2}^2(E)}{2E^2} + \ldots$$

Substituting in (2)

$$I \cong \int_{\Delta_L^o}^{a+\Delta_L^o} \sqrt{\frac{\Delta_L^o}{2}}\ \frac{1}{(E-\Delta_L^{\,o})^{1/2}}\left[1 + \frac{\Delta_{R_1}^2(V-E) - \Delta_{R_2}^2(V-E)}{(V-E)^2} + \ldots\right] dE \tag{5}$$

$$+ \int_{V-\Delta_R^o-a'}^{V-\Delta_R^o} \sqrt{\frac{\Delta_R^o}{2}}\ \frac{1}{(V-E-\Delta_R^o)^{1/2}}\left[1 + \frac{\Delta_{L_1}^2(E) - \Delta_{L_2}^2(E)}{E^2} + \ldots\right] dE$$

$$+ \int_{\Delta_L^o+a}^{(V-\Delta_R^{\,o})-a'} N_L(E)\, N_R(E-V)\, dE$$

Making the variable changes

$$V' = V - \Delta_R^o - \Delta_L^o$$

and

$$\varepsilon = E - \Delta_L^o$$

in the first integral and

$$\varepsilon = V - E - \Delta_R^o$$

in the second integral

$$I(V) \cong \sqrt{\Delta_L^o} \int_o^a d\varepsilon \frac{\Delta_{R_1}^2 (V'+\Delta_R^o-\varepsilon) - \Delta_{R_2}^2 (V'+\Delta_R^o-\varepsilon)}{\sqrt{2}\ (\varepsilon)^{1/2}(V'+\Delta_R^o-\varepsilon)^2} \tag{6}$$

$$+ \sqrt{\Delta_R^o} \int_o^{a'} \frac{\Delta_{L_1}^2 (V'+\Delta_L^o-\varepsilon) - \Delta_{L_2}^2 (V'+\Delta_L^o-\varepsilon)}{\sqrt{2}\ (\varepsilon)^{1/2}\ (V'+\Delta_L^o-\varepsilon)^2}$$

$$+ I_o(V)$$

$$I^o(V) = \sqrt{\frac{\Delta_L^o}{2}} \int_o^a \frac{d\varepsilon}{\varepsilon^{1/2}} + \sqrt{\frac{\Delta_R^o}{2}} \int_o^{a'} \frac{d\varepsilon}{\varepsilon^{1/2}} + \int_{\Delta_L^o+a}^{(V-\Delta_R^o-a')} N_L(E)N_R(E-V)dE \tag{7}$$

If

$$V \gg a' \geqslant \Delta_R^o$$

$$V \gg a \geqslant \Delta_L^o$$

Then $$N_L(E) \sim N_R(E-V) \simeq 1$$

in the range of the last integral and

$$I^o(V) = V-\Delta_R^o-\Delta_L^o-a'-a+2\sqrt{\frac{\Delta_L^o}{2}}\ a^{1/2}+2\sqrt{\frac{\Delta_R^o}{2}}\ (a')^{1/2} \simeq V$$

The complex energy gap is given by[24]

$$\Delta(E) = \frac{1}{Z(E)} \int \mathrm{Re}\left[\frac{\Delta(E')}{[E'^2 - \Delta^2(E')]^{1/2}}\right] [K(E\,E') - V_c]dE' \tag{8}$$

$$K(EE') = \int d\omega\alpha^2(\omega)\ F(\omega) \left[\frac{1}{E'+E-\omega-i\delta} + \frac{1}{E'+E+\omega-i\delta}\right]$$

If V_c, the coulomb pseudopotential, is zero and α^2 is a constant then

$$\Delta(E) = \frac{\alpha^2}{Z(E)} \int \mathrm{Re}\left[\frac{\Delta(E')}{[E'^2-\Delta^2(E')]^{1/2}}\right] \int d\omega F(\omega)\left[\frac{1}{E'+E-\omega-i\delta} + \frac{1}{E'+E+\omega-i\delta}\right] \qquad (9)$$

Thus writing $\omega \equiv V'$ and substituting (9) into (6) we obtain the desired expression,

$$\frac{I(V)}{C_{NN}} \cong I^o(V) + \frac{\sqrt{\Delta_L{}^o\ \alpha_L{}^2}}{(\omega+\Delta_L{}^o)^2}\ I_1(V' + \Delta_L{}^o,\ F_L(\omega)) \qquad (10)$$

$$+ \frac{\sqrt{\Delta_R{}^o\ \alpha_R{}^2}}{(\omega+\Delta_R{}^o)^2}\ [I_1(V'+\Delta_R{}^o,\ F_R(\omega)]$$

The squared term in the denominator has been assumed approximately constant in the range of integration compared to the contribution from the other terms. Defining

$$\omega \equiv V' + \Delta_L^o\ ,\quad I_1(V'+\Delta_L^o,\ F_L(\omega))$$

becomes

$$I_1(\omega, F(\omega_o)) = \int \frac{d\varepsilon}{\sqrt{2\varepsilon}}$$

$$\left\{\mathrm{Re}\left[\frac{1}{Z'(\varepsilon+\omega)} \int d\omega' \mathrm{Re}\left[\frac{\Delta(\omega')}{[\omega'^2-\Delta_L^2]^{1/2}}\right] \int d\omega_o F_i(\omega_o) \left[\frac{1}{\omega'+\omega-\omega_o+\varepsilon-i\delta}\right.\right.\right.$$

$$\left.\left.\left. + \frac{1}{\omega'+\omega+\omega_o+\varepsilon-i\delta}\right]\right]^2\right\}$$

APPENDIX II

Amplitude of Van Hove and Phillips Singularities in S_1-I-S_2 Tunneling Characteristics

In the following section the calculation by Scalapino and Anderson[29] of the amplitude of singularities in G'(V) for an S-I-S junction is discussed and extended to the case of S_1-I-S_2 junction.

Starting from Eq. (2) of the previous section and the Eliashberg equations

$$\psi(E) = \int_{\Delta^o}^{\infty} \mathrm{Re}\left\{\frac{\Delta(E')}{[E'^2-\Delta^2(E')]^{1/2}}\right\} [K^+(E,E')-V_c]dE \qquad (1)$$

$$(1-Z(E)E = \int_{\Delta^o}^{\infty} \mathrm{Re}\left\{\frac{E}{[E'^2-\Delta^2(E')]^{1/2}}\right\} [K^-(E,E')]dE \qquad (2)$$

$$K^{\pm}(EE') = \int j\omega_o\alpha^2(\omega_o)F(\omega_o)\left[\frac{1}{E'+E+\omega_o-i\delta} \pm \frac{1}{E'+E-\omega_o-i\delta}\right] \qquad (3)$$

$$\frac{\psi(E)}{Z(E)} = \Delta(E)$$

Scalapino and Anderson consider those singular contributions from the addition of singularities in (a) the resonant phonon denominator $E' + E - \omega_o$ and (b) the square root singularity at the gap edge with ω_o a critical points of $F(\omega_o)$. Singularities in $\psi(E)$ and $Z(E)$ are ignored as a first approximation. This is valid if the singularities first obtained in the integration do not propagate (i.e. yield an

equivalent strength singularity) if they are iterated. $\psi_o(E\ \omega_o)$ is evaluated for the case of an Einstein phonon spectrum $F(\omega_o) = \delta(\omega-\omega_o)$ and the result is subsequently integrated over the actual density of states in the vicinity of a critical point.

$$\psi(E) = \int \psi_o(E,\omega_o)d\omega_o \tag{4}$$

This is just reversing the order of integration in Eq.(3) and is justified if only the most singular contributions are considered. We have

$$\psi_o(E\ \omega_o) = \alpha^2(\omega_c) \int_{\Delta_o}^{\infty} dE' \mathrm{Re}\left[\frac{\Delta(E')}{(E'+\Delta^*(E'))^{1/2}(E'-\Delta(E'))^{1/2}}\right]\left(\frac{1}{E'-E+\omega_o-i\delta}\right) \tag{5}$$

Choosing a contour with a branch cut along the real axis the only contribution is from the pole at $E' = E - \omega_c + i\delta$

$$\psi_o(E) = \alpha^2(\omega_c)\ \mathrm{Re}\left[\frac{\Delta(E-\omega_o)}{[E+\Delta^*(E-\omega_c)+\omega_c]^{1/2}\ [E-\Delta(E-\omega_o)-\omega_o]^{1/2}}\right] \tag{6}$$

Since E is positive in this formulation the only singularity occurs when $E \cong \omega_c + \Delta(\Delta^o)$ as in the previous section we have.

$$\psi_o(E) \cong \frac{\alpha^2(\omega_c)\pi}{(2\Delta^o)^{1/2}}\left[\frac{1}{[E - (\omega_c+\Delta^o)]^{1/2}}\right] \tag{7}$$

Both real and imaginary components are included. When $E < \omega_c + \Delta^\circ$ the -i branch of the square root is taken. In the vicinity of a Van Hove critical point the phonon dispersion of the branch takes the form

$$\omega^{\lambda} = \omega^{\lambda}_{c} + a \sum_{\alpha} \varepsilon_{\alpha}(q_{\alpha} - q_{\alpha c})^{2} \tag{8}$$

Maximum: $\varepsilon_{\alpha} = -1$

Minimum: $\varepsilon_{\alpha} = +1$

$S_1 : = \varepsilon_1 = \varepsilon_2 = -\varepsilon_3$

$S_2 : = \varepsilon_1 = -\varepsilon_2 = -\varepsilon_3$

Since

$$F^{\lambda}(\omega_o) = \int \frac{dS_{\omega_o}}{\nabla_q \omega^{\lambda}} \tag{9}$$

The density of states in the vicinity of a minimum

$$F(\omega_o) \cong A + \frac{2\pi v_o}{3Za^{3/2}} (\omega_o - \omega_c)^{1/2} \quad \omega_o > \omega_c \tag{10}$$

$$\cong A \qquad \omega_o < \omega_c$$

Z = the number atoms per unit cell

v_o = the volume of the unit cell

a = the radius of curvature of the dispersion relation

The general Van Hove critical point is of the form

$$F^{\lambda}(\omega_o) = A + B(-1)^S|\omega_c - \omega_o|^{1/2}\ \Theta(\varepsilon(\omega_c-\omega_o))$$

Max.	S = 0	ε = +1	(11)
Min.	S = 0	ε = -1	
S_1	S = 1	ε = +1	
S_2	S = 1	ε = -1	

The singular portion of $\psi(E)$ and $Z(E)E$ can be written as

$$\psi_S(E) = (Z(E)E)_S = \int \frac{(-1)^S\ |\omega_c-\omega_o|^{1/2}\ \Theta(\varepsilon(\omega_c-\omega_o))d\omega_o}{(E - \omega_o - \Delta^\circ)^{1/2}} \qquad (12)$$

We obtain the result

$$\psi_S(E) = (Z(E)E)_S = (i)^P\ C[\pi|Z|[\Theta(Z)] + i|Z|\ell n|Z|]$$

Max.	P = 0	$Z \equiv \omega_c + \Delta_o - E$	(13)
Min.	P = 1		
S_1	P = 2		
S_2	P = 3		

with

$$C = \frac{\pi^2}{3\sqrt{2}}\ \frac{v_o\sqrt{\Delta^\circ}}{Za^{3/2}}\ \alpha^2$$

The logarithmic singularity alternately becomes attached to the Imaginary then real parts of ψ_S as the type of the maximum is changed.

From Appendix I (6) we can evaluate the current in an S_1-I-S_2 junction as

$$I \cong I_o(V) + \sqrt{\frac{\Delta_L}{2}} \int_o^a \frac{d\varepsilon}{\varepsilon^{1/2}} \left\{1 + \frac{\mathrm{Re}[\Delta_R^2(V'+\Delta_R^o-\varepsilon)]}{(V'+\Delta_R^o-\varepsilon)^2}\right\}$$

$$+\sqrt{\frac{\Delta_R}{2}} \int_o^a \frac{d\varepsilon}{\varepsilon^{1/2}} \left\{1 + \mathrm{Re}\ \frac{[\Delta_L^2(V'+\Delta^o-\varepsilon)]}{(V'+\Delta_L^o-\varepsilon)^2}\right\} \qquad (14)$$

$$\omega_c = V' = V - \Delta_L^o - \Delta_R^o$$

$$\mathrm{Re}\left(\frac{\Delta(E)}{E}\right)^2 \equiv \mathrm{Re}\left(\frac{\psi(E)}{Z(E)E}\right)^2$$

Where $\psi(E)$; $Z(E)E$ are the sum of the analytic and singular terms.

$$\mathrm{Re}\left(\frac{\psi_o(E) + \psi_S(E)}{Z_o(E)E + (Z(E)E)_S}\right)^2$$

expanding and using

$$\psi_S(E) = (Z(E)E)_S \qquad (15)$$

$$\frac{1}{E^2}\ \mathrm{Re}(\Delta_o(E))^2 + \frac{2}{E^2}\ \mathrm{Re}\left[\frac{\Delta_o(E)}{Z_o(E)}\ \psi_S(E)\right]$$

The singular part of the density of states thus can be written

$$N_S(E) = \frac{1}{E^2}\left[\beta\ \mathrm{Re}\ \psi_S + \gamma\ \mathrm{In}\psi_S\right] \qquad (16)$$

with

$$\beta = \mathrm{Re}\ \frac{\Delta_o}{Z_o}\ ; \qquad \gamma = \mathrm{In}\ \frac{\Delta_o}{Z_o}$$

As the singularity changes character the coefficient of the logarithmic singularity will shift from β to γ, I has the form

$$I = F(V) + \frac{\pi^2}{6} \frac{V_o}{Za^{3/2}} \sqrt{\Delta_L \Delta_R}\, \alpha^2 \times$$

$$\int \frac{d\varepsilon}{(\varepsilon)^{1/2}} \left\{ \beta \, \mathrm{Re}\, [i^P |\omega_c - V' + \varepsilon|\ \pi\varepsilon(\omega_c - V' + \varepsilon) + i\ell n|\omega_c - V' + \varepsilon)|] \right. \tag{17}$$

$$\left. + \gamma \mathrm{In}[i^P |\omega_c - V' + \varepsilon| \pi\Theta(\omega_c - V' + \varepsilon) + i\ell n|\omega_c - V' + \varepsilon|] \right\}$$

+ contribution from other superconductor

Defining

$$I_1(V) = \int \frac{d\varepsilon}{\varepsilon^{1/2}} \ |\omega_c - V' + \varepsilon|\ \Theta(\omega_c - V' + \varepsilon) \tag{18}$$

$$I_2(V) = \int \frac{d\varepsilon}{\varepsilon^{1/2}} \ \ell n|\omega_c - V' + \varepsilon|$$

We have

$$\frac{dI_1(V)}{dV} \cong - \int \frac{d\varepsilon}{\varepsilon^{1/2}} \ \Theta(\omega_c - V' + \varepsilon)$$

$$\frac{d^2 I_1(V)}{dV^2} = \frac{1}{|V' - \omega_c|^{1/2}} \tag{19}$$

Similarly

$$\frac{d^2 I_2(V)}{dV^2} = \frac{1}{|V' - \omega_c|^{1/2}}$$

$$V' = V - \Delta_L - \Delta_R$$

Thus though $I_1''(V)$ and $I_2''(V)$ are symmetric the weighting of the square root singularity with β, or γ causes a large assymmetry in the shape of the peak. $(I''(V))$ since in general $\gamma \gg \beta$. The general expression $G'(V) \equiv I'''(V)$ is from (17)

$$G'(V) \cong \frac{\pi^2}{6} \alpha_j^2 \frac{\sqrt{\Delta_L^\circ \Delta_R^\circ}}{(\omega_j + \Delta_{S_j})^2} \begin{pmatrix} \pm \beta_j \\ \pm \gamma_j \end{pmatrix} \frac{V_o}{(a)^{3/2} Z} \left[\frac{1}{|V' - \omega_{c_i}|^{1/2}} \right]$$

$$j = L, R$$

$$\begin{pmatrix} \pm \beta_j \\ \pm \gamma_j \end{pmatrix} = \left\{ \begin{array}{lll} \beta & \gamma & \text{Max.} \\ -\gamma & -\beta & \text{Min.} \\ \beta & -\gamma & S_1 \\ \gamma & \beta & S_2 \end{array} \right\} \qquad (20)$$

$$V' < \omega_c \qquad V' > \omega_c$$

We can distinguish between these singularities by the positive or negative going direction of the singularity and its assymmetry.

For identical superconductor junctions the second term in (20) yields an identical contribution whereas for S_1-I-S_2 the critical points of the two superconductors generally do not coincide. In actual junctions of course the critical point singularities are broadened due to broadening of the gap singularity, finite width of the phonon line and thermal effects. It must be noted that any anisotropy of the energy gap(s) comes twice in the calculation - once in the production of the square

root singularity of the Einstein spectrum order parameter and last in the integration at the square root singularity of the second superconductor.

REFERENCES

1. J. Bardeen, L. N. Cooper, and J. R. Schrieffer, Phys, Rev. 106, 162 (1957).

2. I. Giaever, H. R. Hart Jr., and K. Mergerle, Phys. Rev. 126, 941 (1962).

3. M. H. Cohen, L. M. Falicov, and J. C. Phillips, Phys. Rev. Letters 8, 316 (1962).

4. B. N. Taylor, E. Burstein, and D. N. Langenberg. Bull. Am. Phys. Soc. 7, 190 (1962).

5. J. Nicol, S. Shapiro and P. H. Smith, Phys. Rev. Letters 5, 461 (1960); S. Shapiro, P. H. Smith, J. Nicol, J. L. Miles, and P. F. Strong. IBM J. Res. Develop. 6, 34 (1962).

6. D. J. Scalapino and B. N. Taylor to be published.

7. N. V. Zavaritskii, Soviet Phys. JETP 18, 1260 (1964); JETP 21, 557 (1965).

8. B. L. Blackford, R. H. March, Phys. Rev. 186, 397 (1969).

9. J. C. Keister, L. S. Straus, and W. D. Gregory, J. Appl. Phys. 42, 642 (1971).

10. J. N. Sweet, Thesis: Microwave Photon Assisted Tunneling in Superconducting Tunnel Junctions 1970, UCRL-19653.

11. J. M. Rowell, in Tunneling Phenomena in Solids, edited by E. Burstein and S. Lundquist (Plenum Press, N.Y., 1969) pp. 273-286.

12. An example of an In-I-In junction fabricated by the author is shown in Fig. 4. Gap width is approximately 20%.

13. S. A. Buckner, T. F. Finnegan, and D. N. Langenberg Phys. Rev. Letters, 28, 150 (1972).

14. I. Giaever, in Tunneling Phenomena in Solids, op. cit., pp. 255-271.

15. J. M. Rowell and W. I. Feldmann, Phys. Rev. 172, 393 (1968).

16. J. M. Rowell and W. I. Feldmann, Phys. Rev. 172, 393 (1968).

17. I. Giaever, in Tunneling Phenomena in Solids, op.cit., pp. 255-271.

18. I. Giaever, H. R. Hart Jr., and K. Mergerle, Phys. Rev. 126, 941 (1962).

19. J. R. Schrieffer, D. J. Scalapino and J. W. Wilkins, Phys. Rev. Letters 10, 336 (63).

20. Y. Nambu, Phys. Rev. 117, 648 (60).

21. L. P. Gorkov, Zh. Eksperim. i Teor. Fiz. 34, 735 (58)(English transl.: Soviet Phys. - JETP 7, 505 (58)).

22. G. M. Eliashberg, Zh. Eksperim. i Teor. Fiz. 38, 966 (60)(English transl.: Soviet Phys. - JETP 11, 696 (60)).

23. J. M. Rowell, P. W. Anderson, and D. E. Thomas, Phys. Rev. Letters 10, 334 (63).

24. J. R. Schrieffer, Theory of Superconductivity, (W. A. Benjamin, Inc. 1964) pp. 164-202.

25. D. J. Scalapino, in Superconductivity, vol. 1 Ed. R. D. Parks (Marcel Dekker Inc., New York, 1969).

26. W. L. McMillan and J. M. Rowell, Phys. Rev. Letters 4, 108 (1965).

27. Van Hove, Phys. Rev. 89, 1189 (1953).

28. J. C. Phillips, Phys. Rev. 104, 1263 (1956).

29. D. J. Scalapino, and P. W. Anderson, Phys. Rev. 133, 921 (1964).

30. P. W. Anderson and J. M. Rowell, Phys. Rev. Letters 10, 230 (1963).

31. R. C. Jaklevic and J. Lambe, Phys. Rev. Letters 17, 1139 (1966); J. Lambe and R. C. Jaklevic, Phys. Rev. 165, 821 (1968).

32. D. C. Tsui, R. E. Dietz, and L. R. Walker, Phys. Rev. Letters 27, 1729 (1971).

33. L. Y. L. Shen and J. M. Rowell, Phys. Rev. 165, 566 (1968).

34. I. K. Yanson, B. I. Verkin, L. I. Ostrovskii, A. B. Teplitskii, and O. I. Shklyarevskii, JETP Lett. (USA) 14, #1, 26 (1971).

35. A. Leger, J. Klein, M. Belin and D. Defourneau, Solid State Communications, 11, 1331 (1972).

36. B. D. Josephson, Phys. Letters 1, 251 (1962).

37. B. D. Josephson, in Superconductivity vol. 1, op.cit. pp. 423-447; B. D. Josephson, Advan. Phys. 14, 419 (1965).

38. P. W. Anderson, Lectures on the Many-Body Problem, Vol. 2, (Academic Press, New York, 1964).

39. V. Ambegaokar and A. Baratoff, Phys. Rev. Letters 10, 486 (1963); 11, 104(E) (1963).

40. T. A. Fulton, and D. E. McCumber, Phys. Rev. 175, 585 (1968).

41. N. R. Werthamer, Phys. Rev. 147, 255 (1966).

42. C. S. Owen, and D. J. Scalapino, Phys. Rev. 164, 538 (1967).

43. D. D. Coon and M. D. Fisk, Phys. Rev. 138, A744 (1965).

44. Wide semiconducting barriers composed of Carbon (ref. (c) Table II) Germanium (ref. (d) Table II) and PbTe (ref. (h) Table III) exhibit broadened gap characteristics. For these wide barriers electron interactions in the barrier region may contribute to the observed broadening.

45. I. Giaever and H. R. Zeller, Phys. Rev. Letters 20, 1504 (1968).

46. R. H. Fowler and L. Nordheim, Proc. Roy. Soc. (London) A119, 173 (1928).

47. J. K. Yanson, Soviet Phys. JETP 33, 951 (1971).

48. J. Shroen, J. of Appl. Phys. 39, 2671 (1968).

49. A. M. Toxen, Phys. Rev. 127, 382 (1962).

50. R. Dynes, Bell Telephone Tabulation (to be published), J. M. Rowell and W. L. McMillan, ibid.; R. C. Dynes, Phys. Rev. B2, 664 (1970).

51. J. M. Rowell, private communication.
W. Kohn, Phys. Rev. Lett. 2, 393 (1959); E. J. Woll, Jr. and W. Kohn, Phys. Rev. 126, 1693 (1962).

52. J. G. Adler and J. S. Rogers, Phys. Rev. Letters 10, 217 (1963).

53. J. M. Rowell and L. Kopf, Phys. Rev. 137, 907 (1964).

54. H. G. Smith and W. Reichardt, to be published.

55. M. Born and T. von Karman, Physik. Z. 13, 297 (1912); 14, 15 (1913).

56. J. M. Rowell, P. W. Anderson, and D. E. Thomas, Phys. Rev. Letters 10, 334 (1963).

57. B. N. Brockhouse, T. Arase, G. Caglioti, K. R. Rao, and A. D. B. Woods, Phys. Rev. 128, 1099 (1962); J. M. Rose, B. N. Brockhouse, and E. C. Swensen, Phys. Rev. Letters 14, 544 (1965).

58. R. Stedman, L. Almquist, G. Nilsson, and G. Raunio, Phys. Rev. 162, 545 (1967).

59. C. B. Walker, Phys. Rev. 103, 547 (1956); R. Stedman and G. Nilsson, Phys. Rev. 145, 492 (1966).

60. J. C. Swihart, D. J. Scalapino and Y. Wada, Proceedings of the 9th Int. Low Temperature Physics Conference, 607 (1965).

61. Similarly the ratio of the longitudinal phonon steps in the conductance curves of Al-I-Pb and Pb-I-Pb junctions is predicted to be $2\left(\frac{\Delta^o_{Pb}}{\Delta^o_{Al}}\right)^{1/2} = 5.6$ at T = 0°K with Δ^o_{Al} = .17 mV

Conductance curves for Al-I-Pb at 1.2°K courtesy of D. McBride indicate an experimental ratio of 4.8 ± .5 with the uncertainty stemming from the estimation of the Al gap (.15 - .2 mV) from the position of the logarithmic cusp at the difference in energy gaps.

62. R. T. Mina and M. S. Khaikin, Sov. Phys. JETP 24, 42 (1966).

63. K. D. Sevier, Low Energy Electron Spectroscopy (Wiley, New York, 1972).

64. G. A. Somorjai and F. J. Szalkowski, Auger Spectroscopy on Surfaces, UCRL-20368 (1970).

65. Rolf H. Muller, Principles of Ellipsometry, LBL-187 (1971).

66. D. W. Davis, D. A. Shirley, T. D. Thomas, J. Chem. Phys. 56, 671 (1972).

67. D. T. Clark, D. Kilcast, Nature Physical Science 233, 77 (1971).

68. Private Communication from B. E. Mills via S. Kowalczyk: the F(1s)/C(1s) cross section ratio = 3.39 ± .1

69. C. B. Duke, Tunneling in Solids, Solid State Physics, Suppl. 10 (Academic Press, N. Y. 1969).

70. Duncan McBride, Gene Rochlin and Paul Hansma, Bull. Am. Phys. Soc., Ser. 2, 18 #3, p. 412 (March 1973). Duncan McBride, Gene Rochlin and Paul Hansma: to be published.

71. D. J. Scalapino and S. M. Marcus, Phys. Rev. Letters 18, 459 (1967).

72. J. P. Hurault, Phys. Rev. 155, 592 (1968).

73. A. D. Brailsford and L. C. Davis, Phys. Rev. B2, 1708 (1970).

74. L. C. Davis, Phys. Rev. B2, 1714 (1970).

75. R. Combescot, J. Phys. C: Solid St. Phys. 4, (G.B.), 2611 (1971).

76. W. Schattke and G. K. Birkner, Z. Physik 252, 12 (1972).

77. G. I. Rochlin, "Improved Design Liquid Helium Temperature Regulator Using Operational Amplifier Circuits" UCRL-19024, June 1969.

FIGURE CAPTIONS

Fig. 1. Current-voltage curves of a typical In-I-Pb junction at 0.9°K. The current scale is expanded by factors of 10. The first graph on the right has the current scale as given. Very little excess current is observed.

Fig. 2. Current-voltage curve of the same junction as in Fig. 1 at 1.5°K. The negative resistance region depends on a nonzero thermal population of quasiparticles and is larger at this higher temperature.

Fig. 3. In-I-In current-voltage curve. The step at one-half the energy gap (0.51 meV) is typical of low resistance junctions of In. Higher resistance junctions have been made which do not exhibit this effect and have substantially the same derivative characteristics.

Fig. 4. In-I-In current voltage oscilloscope trace showing the large Josephson current at the origin.

Fig. 5. Amplitude of the Josephson current for an In-I-In junction as a function of magnetic field. The current could be made zero to within the limits of oscilloscope resolution which was 0.3% of the zero field maximum of 780 microamps.

Fig. 6. Self resonant Fisk steps exhibited by an In-I-In junction at 1.2°K in a magnetic field of a few gauss. The field was adjusted to maximize the first steps; others are visible as wiggles at higher voltages.

Fig. 7. In-I-Pb current voltage trace showing Josephson current at the origin. The magnitude of the current is smaller than simple theory would predict because of circuit noise which is comparable to the coupling energy of the junction.

Fig. 8. Second harmonic signal vs voltage for an Al-I-In junction at 0.3°K vs voltage obtained by R. C. Dynes.[50] (b) Second harmonic signal vs voltage for an In-I-In junction at 0.9°K obtained by the author.

Fig. 9. (Lower Curve) The phonon density of states $F(\omega)$ of In obtained by fitting the inelastic neutron scattering data obtained by Smith and Reichardt to the Born von Karmon nearest neighbors forced constants theory. (See Smith and Reichardt to be published.)

(Upper Curve) The tunneling density of states $\alpha^2(\omega)\ F(\omega)$ obtained using the McMillan inversion equations from conductance and second derivative data by R. C. Dynes. (See R. C. Dynes to be published.[50])

Fig. 10. (a) Dynamic resistance of an In-I-Pb junction at 4.2°K and 1.15°K plotted as a function of voltage above Δ_{Pb} (Upper curve) or $2\Delta_{Pb}$ (Lower Curve). (b) Normalized conductance of a Pb-I-Pb junction obtained by McMillan and Rowell.

Fig. 11. Second harmonic structure near the gap edge for an In-I-In junction at 1.2°K. The upper and lower curves correspond to negative and positive bias on the base Indium electrode respectively and are displaced for clarity. The arrows indicate the location of reproducible structure which may correspond to Kohn anomalies.

Fig. 12. (a) Second harmonic signal vs voltage for an In-I-Pb junction at 1.15°K. Arrows indicate location of large structure in the second derivative curve for an In-I-In junction (see Fig. 8b). (b) Second harmonic signal for a Pb-I-Pb junction at 0.9°K from McMillan and Rowell.[50] The structure in both traces is primarily due to the Pb phonon spectrum.

Fig. 13. Auger spectrum obtained from the surface of In films which had (a) been reacted with "flourinert," (b) been subsequently exposed to an ion bombardment to strip away a portion of the surface layer and (c) had merely been exposed to atmosphere.

Fig. 14. The carbon (1S) peak from an X-ray Photoemission Spectrum (XPS) obtained from In film reacted with "flourinert". An In film simply exposed to air was used as a control. The zero shift of the sample and the multiple peaks indicate a variety of potential sites surrounding the carbon atoms of the sample. The carbon in the control is probably atmospheric CO_2 contamination.

Fig. 15. The fluorine (1S) peak obtained from the same XPS curve as Fig. 14.

Fig. 16. Fowler Nordheim plot of I-V characteristic of an In-I-Ag junction. The stochiometry of the insulator has been determined to be $(C_2F_4)_n$. The plot extends to very high fields ($\sim 10^7$ V/cm). The slope of the plot for high voltages gives the barrier heights for both polarities.

Fig. 17. "Tunneling spectrum" of an In-I-In junction at 4.2°K. The peaks correspond to vibrational or rotational energy levels of ionic species in the barrier.

Fig. 18. "Tunneling spectrum" of an In-I-Pb junction at 4.2°K. The structure is similar at low voltages to that shown in Fig. 17; high voltage characteristics indicate hydrocarbon species. The arrows represent prominent peaks in the infrared spectrum of $(CF_2)_n$, poly-tetrafluoroethylene, and (CF_4), tetrafluoromethane.

Fig. 19. Current-voltage and dynamic resistance curves of an Au-I-In junction at 1.2°K. The fluorocarbon insulating layer was grown on the Au!

Fig. 20. Second harmonic structure for an Au-I-In junction at 1.2°K indicating low energy structure possibly due to Au or In phonons.

Fig. 21. Scanning electron micrograph of In surface with (upper picture) and without (lower picture) a fluorocarbon insulating layer.

Fig. 22. Reaction chamber and pumping system for plasma discharge.

Fig. 23. Helium 6 in. double dewar used for low temperature sample evaluation and associated electronics.

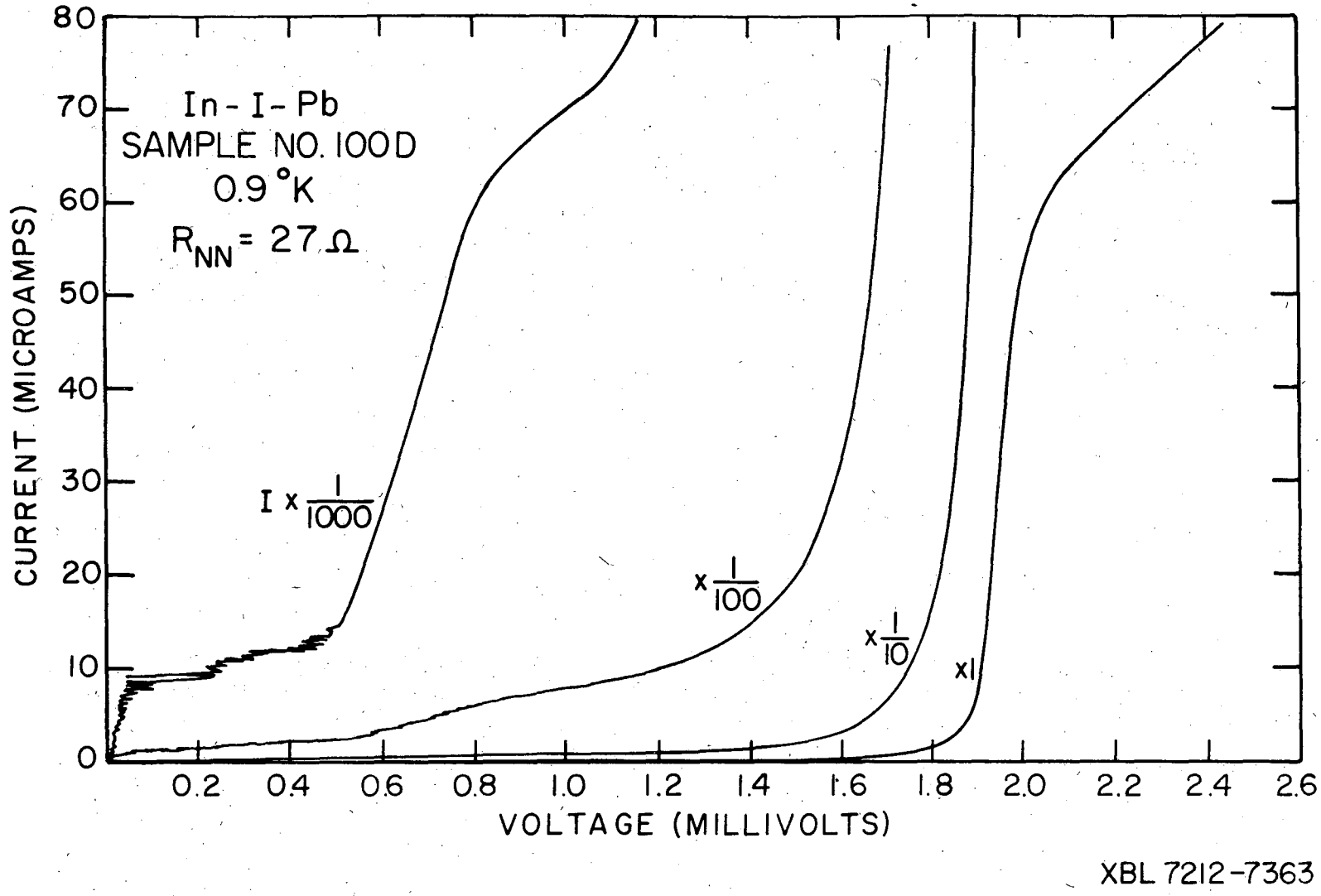
In - I - Pb
SAMPLE NO. 100D
0.9 °K
R_{NN} = 27 Ω
I x 1/1000
x 1/100
x 1/10
x1
CURRENT (MICROAMPS)
VOLTAGE (MILLIVOLTS)
0
10
20
30
40
50
60
70
80
0.2
0.4
0.6
0.8
1.0
1.2
1.4
1.6
1.8
2.0
2.2
2.4
2.6
XBL 7212-7363

Fig. 1.

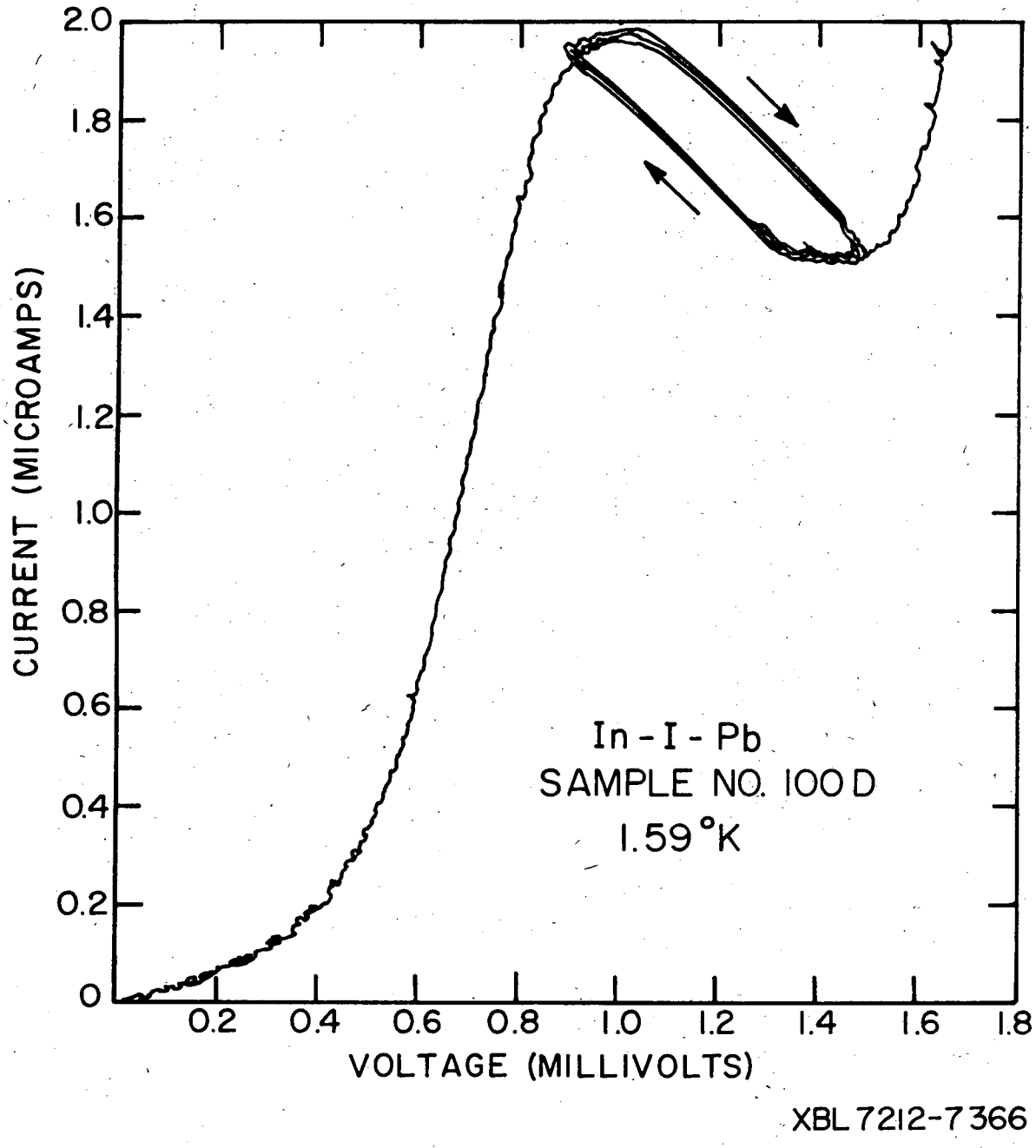
2.0
1.8
1.6
1.4
1.2
1.0
0.8
0.6
0.4
0.2
0
CURRENT (MICROAMPS)
0.2
0.4
0.6
0.8
1.0
1.2
1.4
1.6
1.8
VOLTAGE (MILLIVOLTS)
In - I - Pb
SAMPLE NO. 100 D
1.59 °K
XBL 7212-7366

Fig. 2.

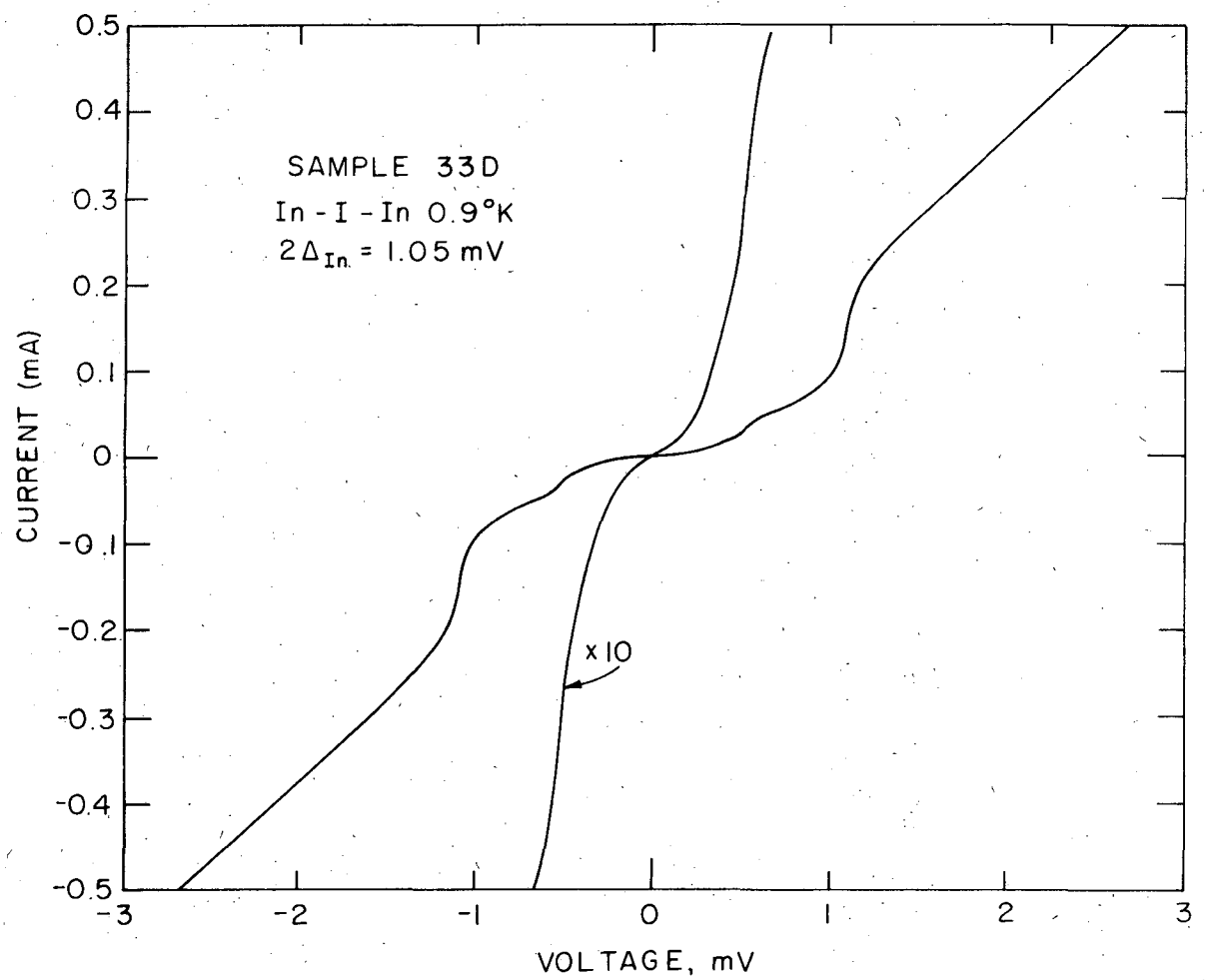

XBL728-6759

Fig. 3.

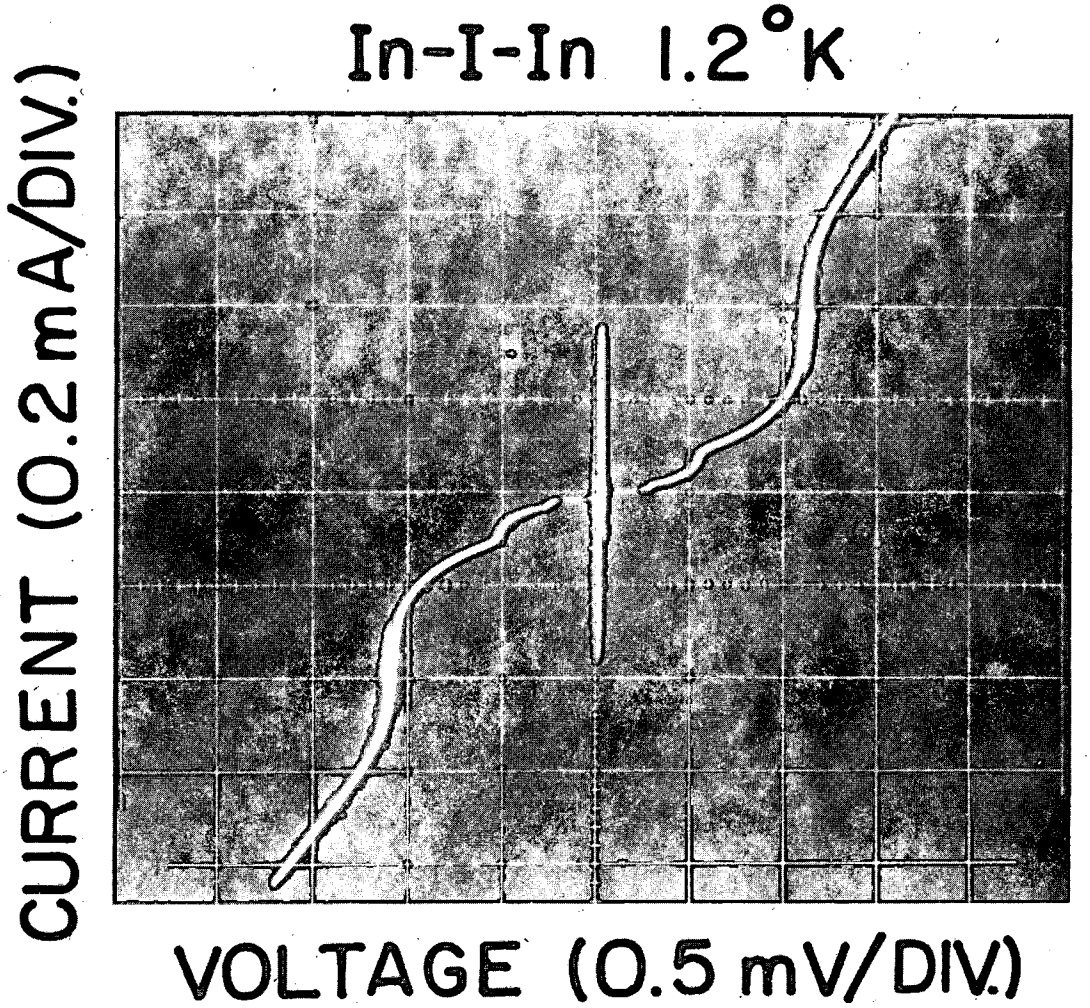

XBB 7212-6220

Fig. 4.

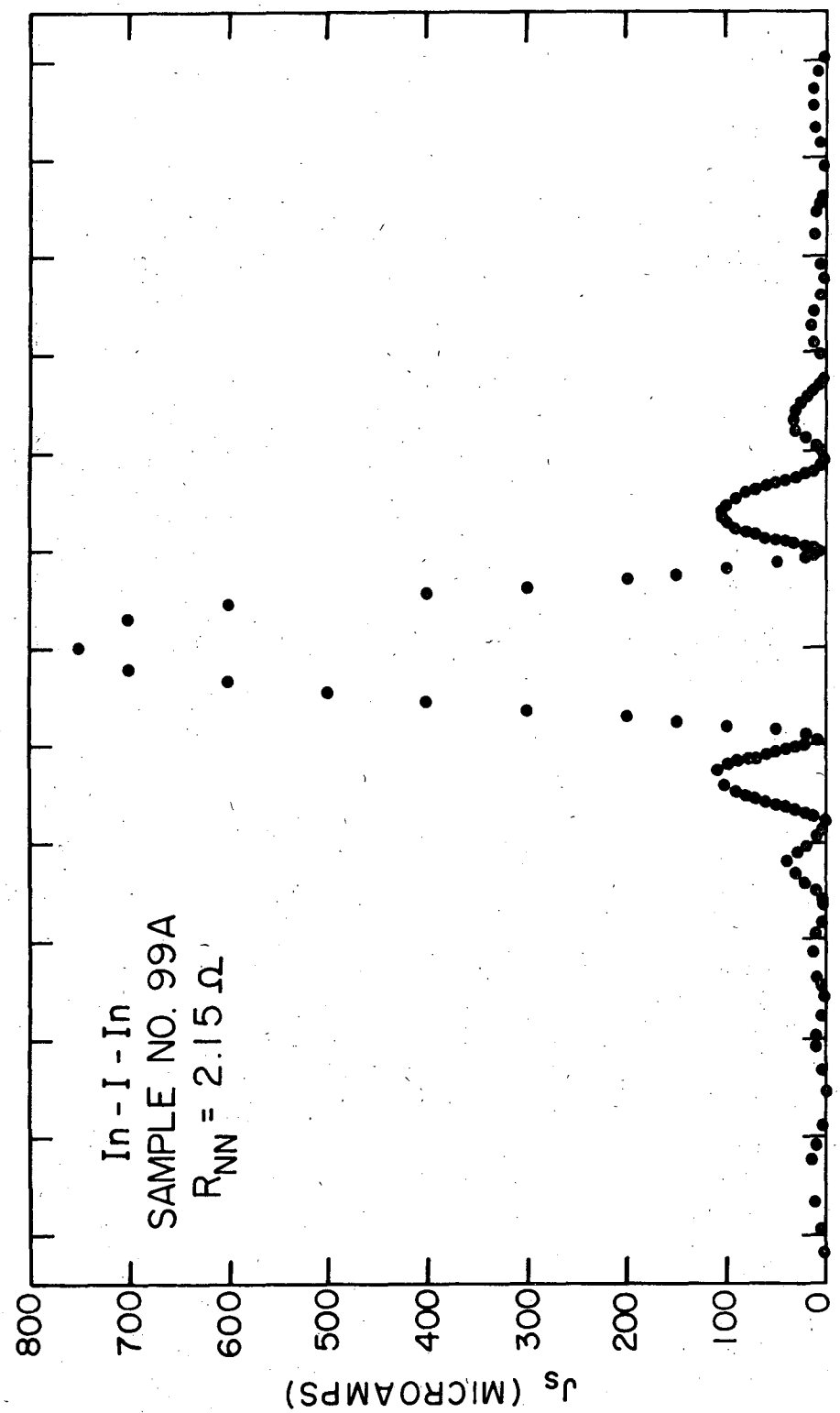

XBL 7212-7365

Fig. 5.

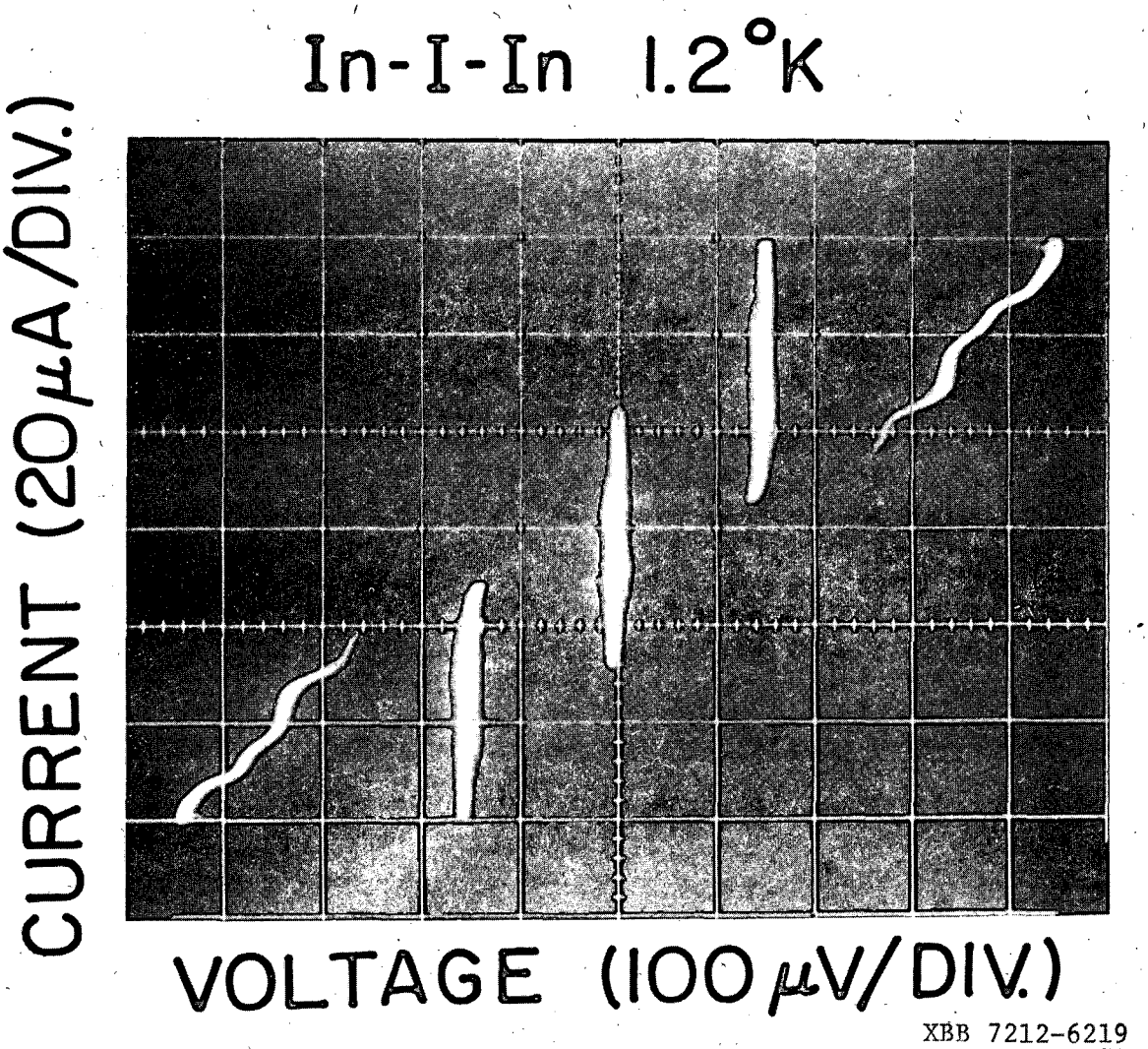

Fig. 6.

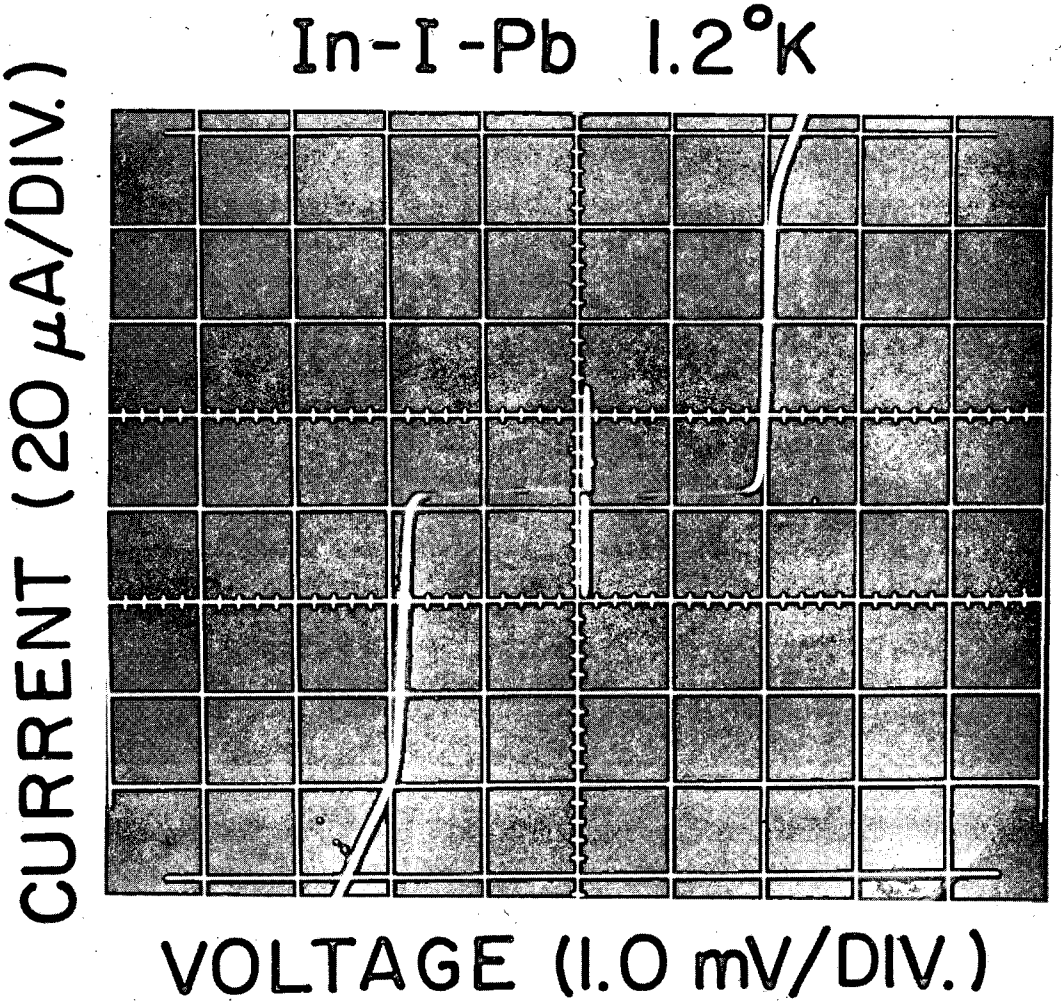

XBB 7212-6222

Fig. 7.

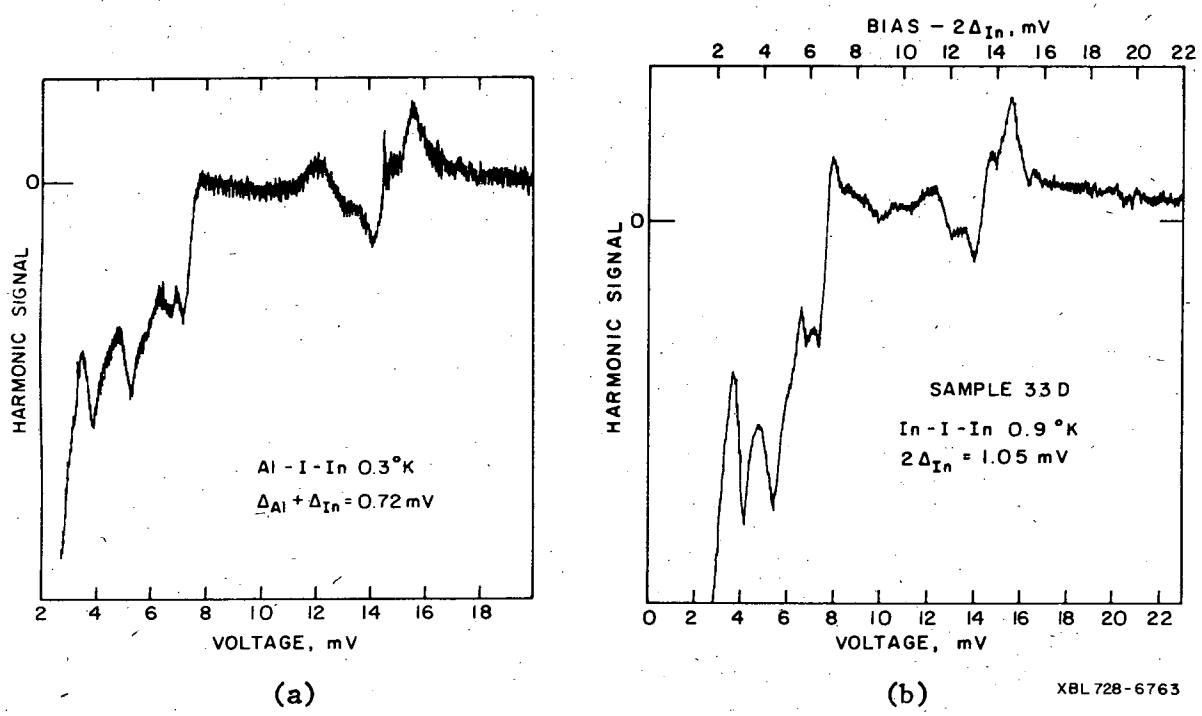
HARMONIC SIGNAL
0
Al - I - In 0.3°K
$\Delta_{Al} + \Delta_{In}$ = 0.72 mV
2 4 6 8 10 12 14 16 18
VOLTAGE, mV
(a)
BIAS − $2\Delta_{In}$, mV
2 4 6 8 10 12 14 16 18 20 22
HARMONIC SIGNAL
0
SAMPLE 33 D
In - I - In 0.9 °K
$2\Delta_{In}$ = 1.05 mV
0 2 4 6 8 10 12 14 16 18 20 22
VOLTAGE, mV
(b)
XBL 728-6763

Fig. 8.

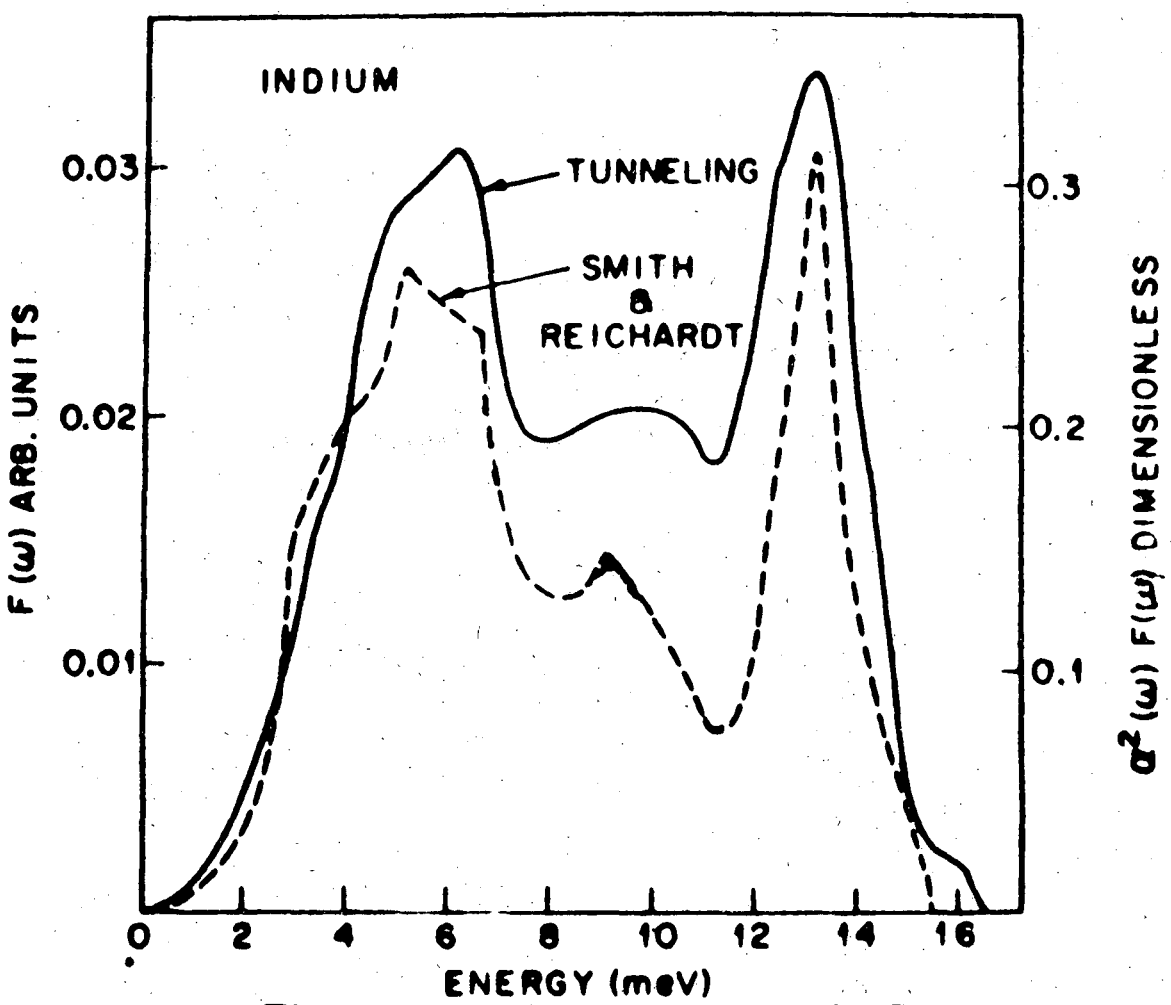

Phonon spectrum of In.

XBL 732-144

Fig. 9.

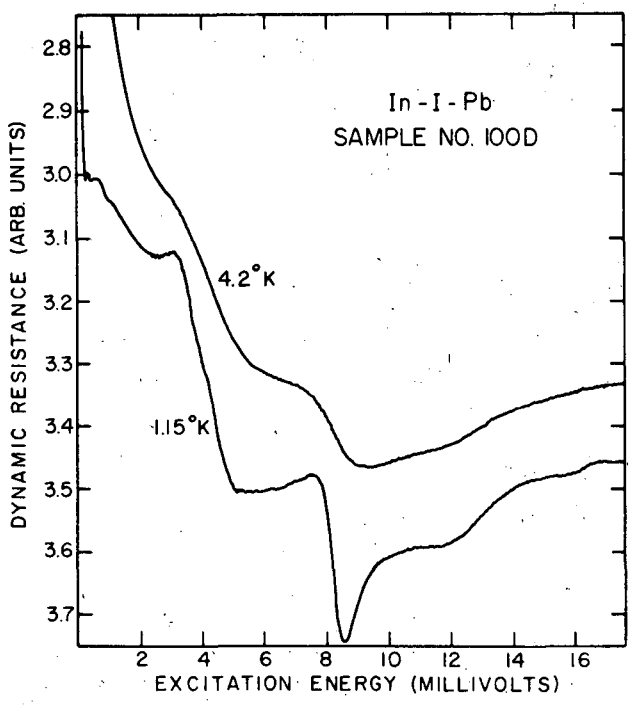

(a)

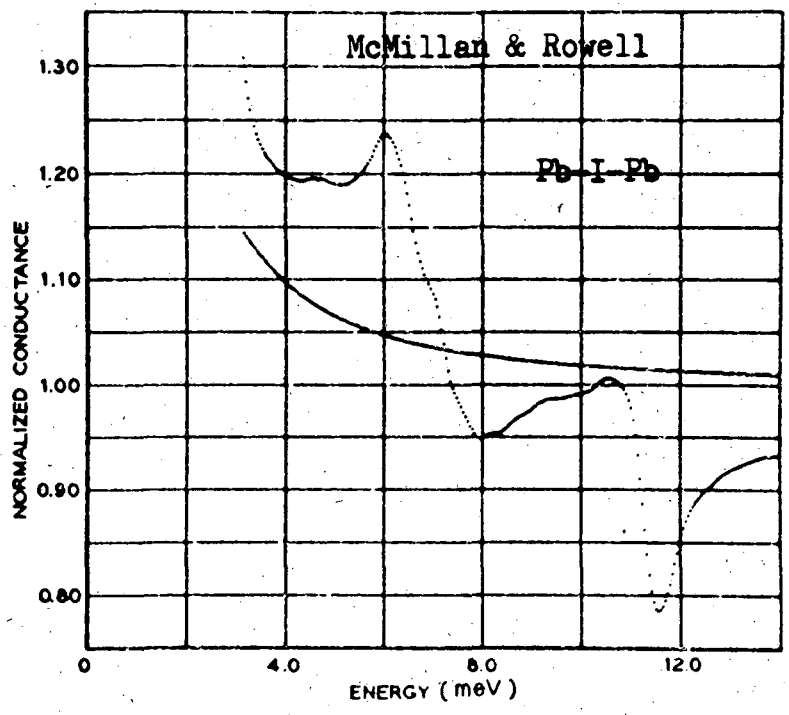

(b)

XBL 7212-7491

Fig. 10.

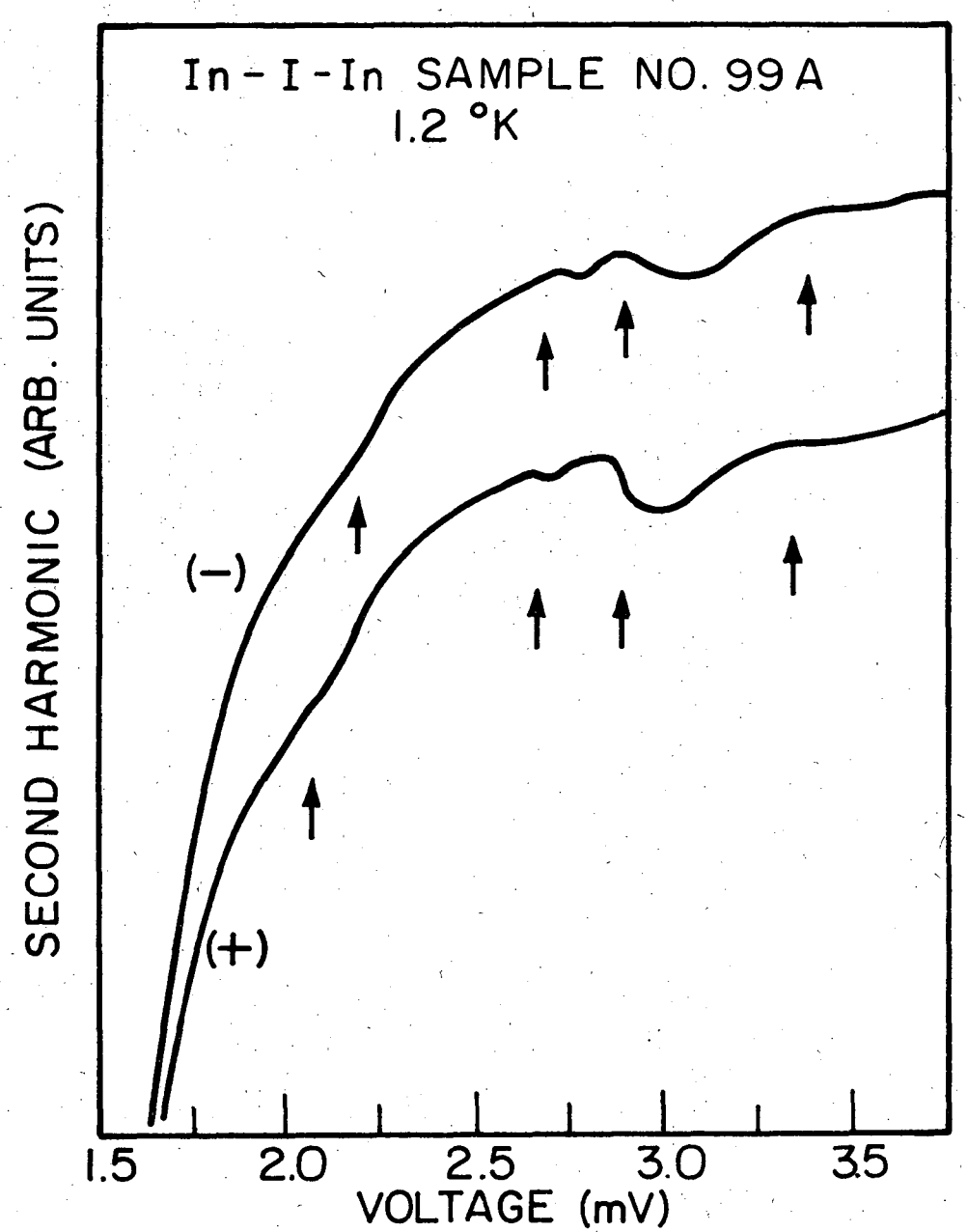

XBL 732-5747

Fig. 11.

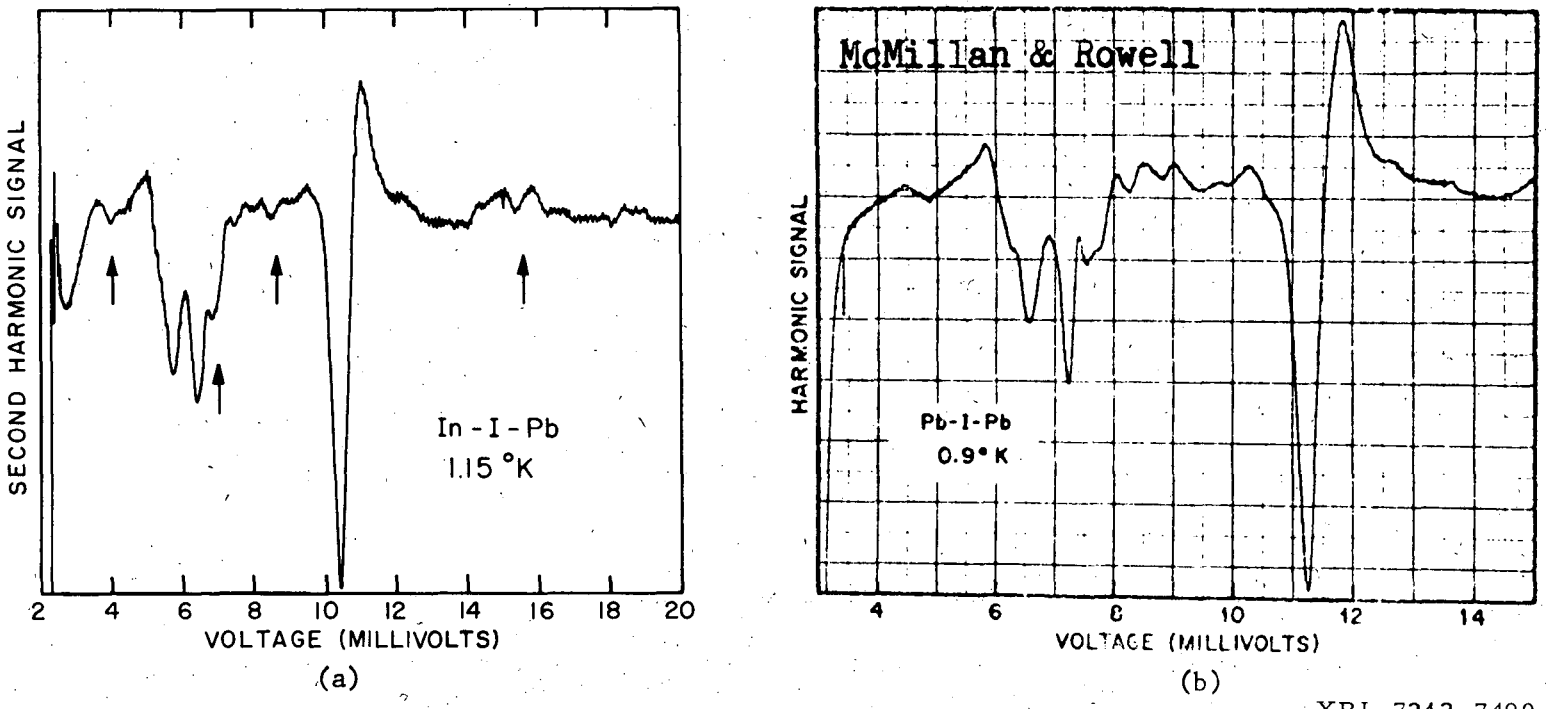

XBL 7212-7490

Fig. 12.

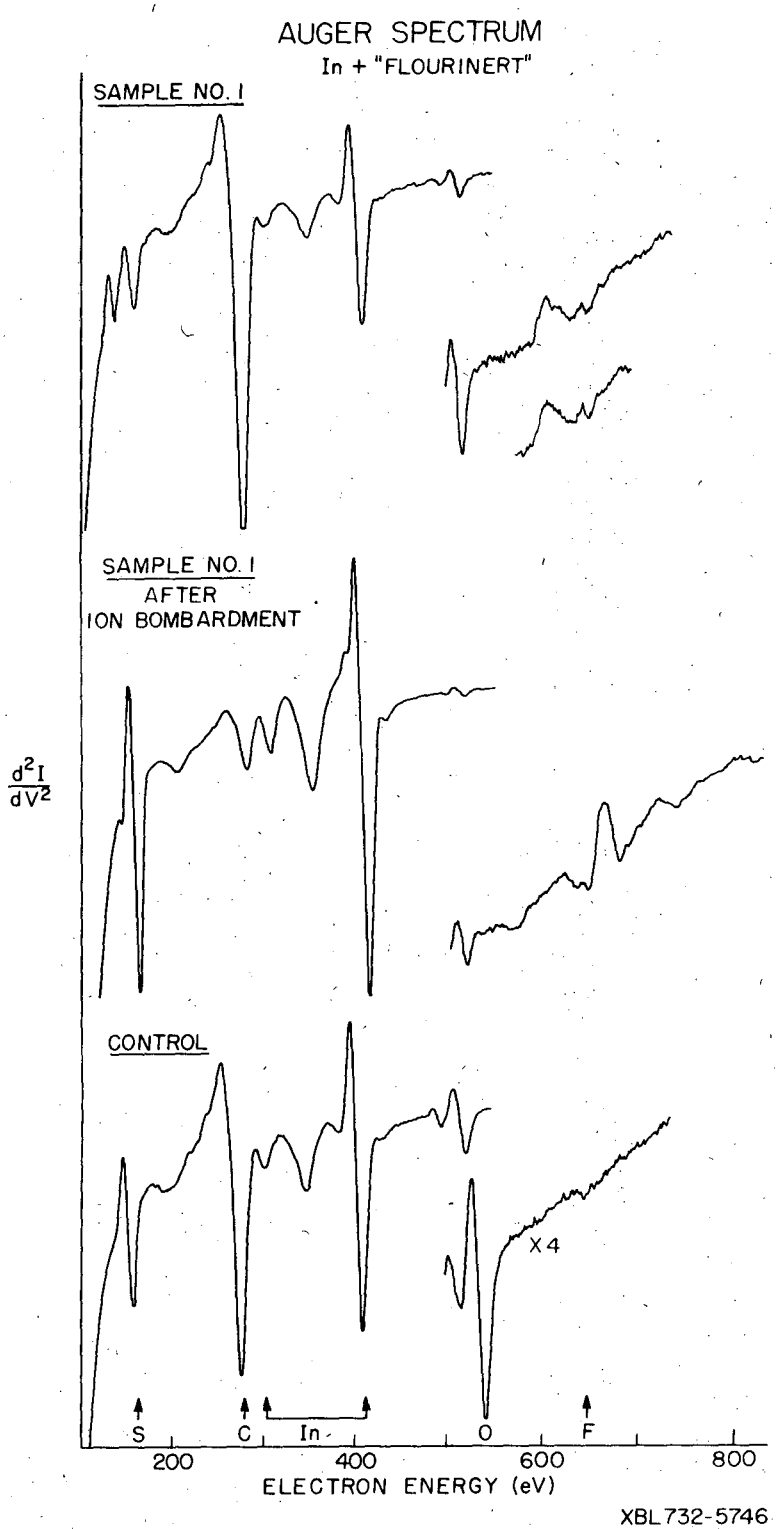

Fig. 13.

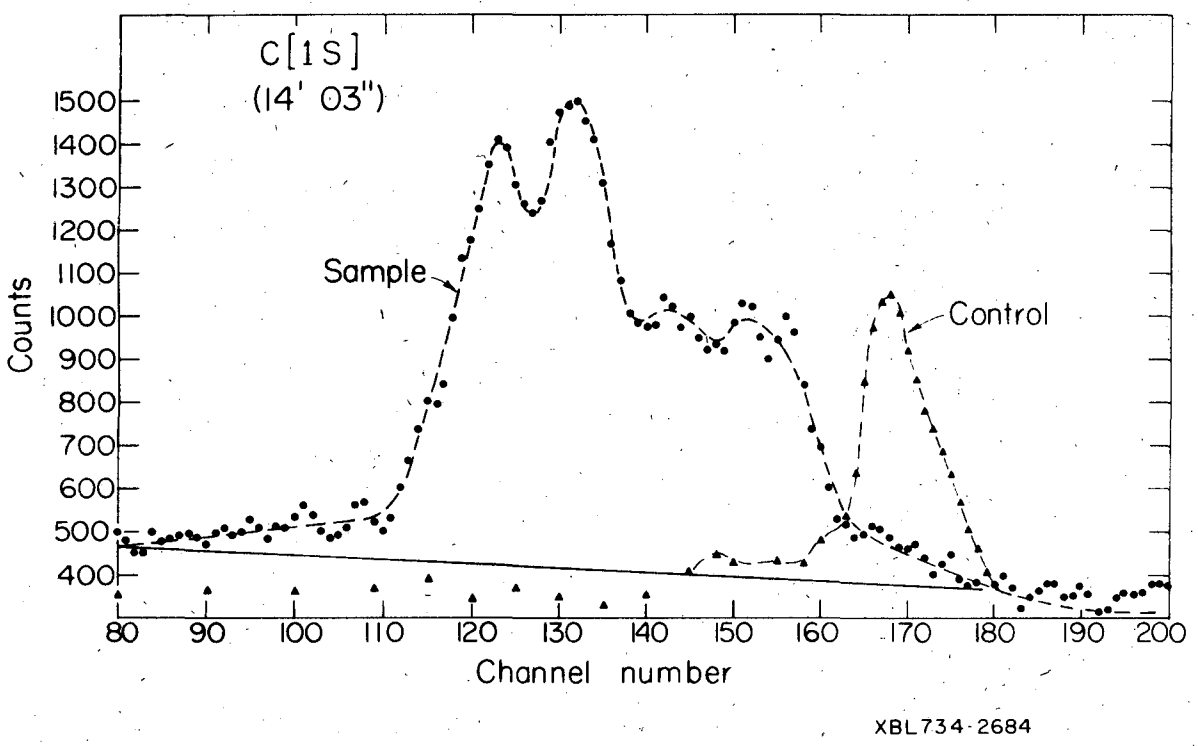
C[1S]
(14' 03")
Sample
Control
Counts
1500
1400
1300
1200
1100
1000
900
800
700
600
500
400
80
90
100
110
120
130
140
150
160
170
180
190
200
Channel number
XBL734-2684

Fig. 14.

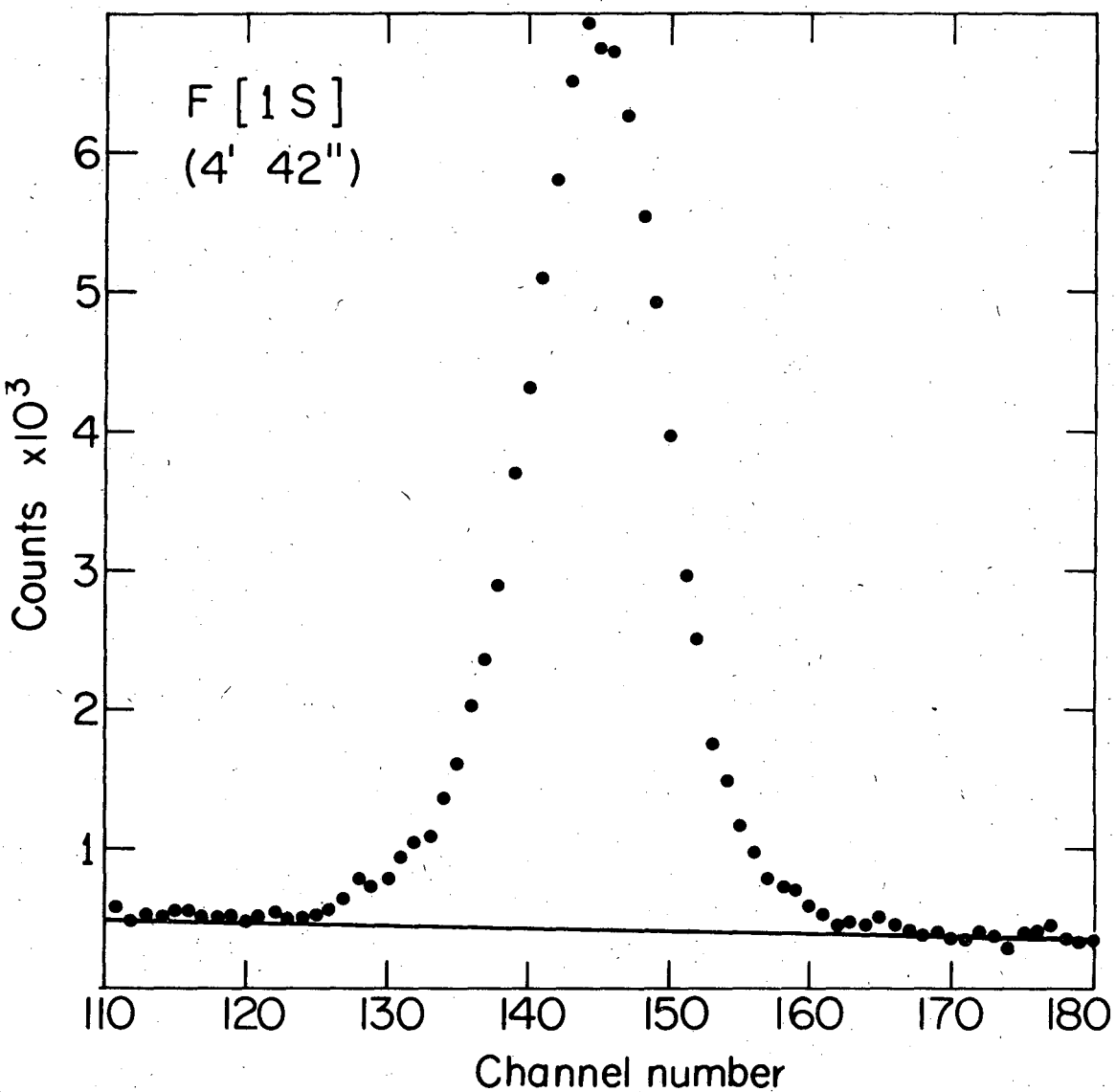
F [1S]
(4' 42")
Counts x10^3
1
2
3
4
5
6
110
120
130
140
150
160
170
180
Channel number
XBL734-2683

Fig. 15.

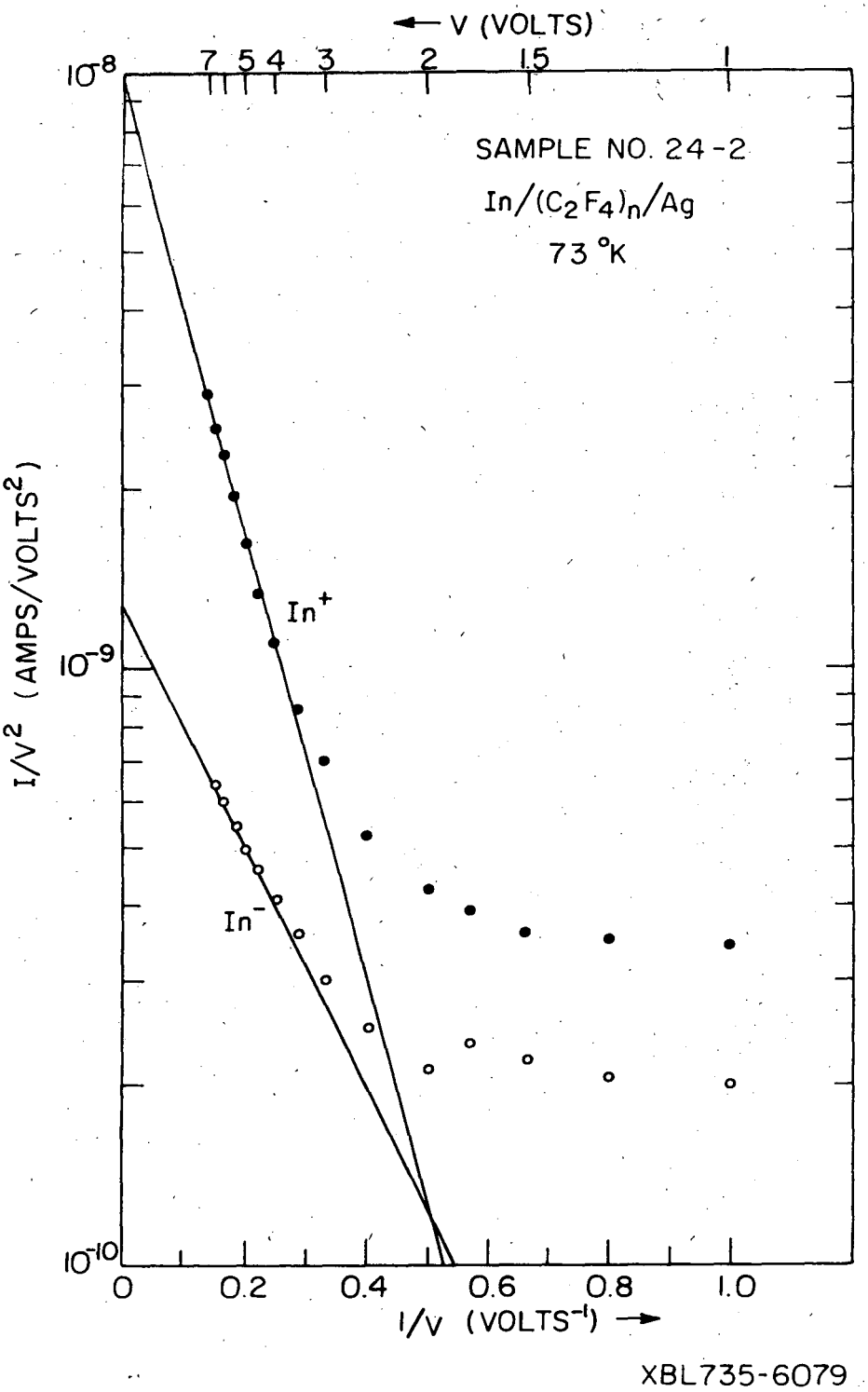
V (VOLTS)
7 5 4 3 2 1.5 1
SAMPLE NO. 24-2
In/(C2F4)n/Ag
73 °K
In+
In−
I/V2 (AMPS/VOLTS2)
10-8
10-9
10-10
0 0.2 0.4 0.6 0.8 1.0
I/V (VOLTS-1)
XBL735-6079

Fig. 16.

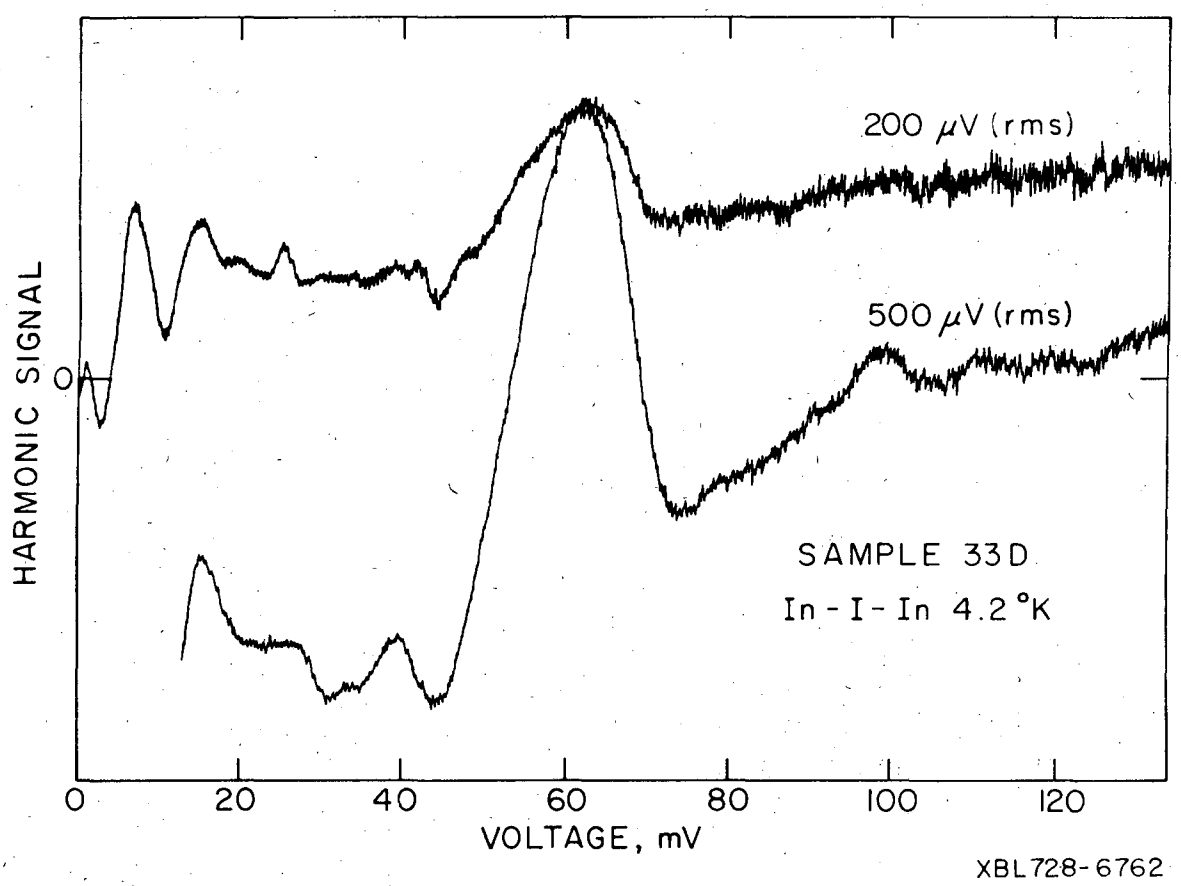

Fig. 17.

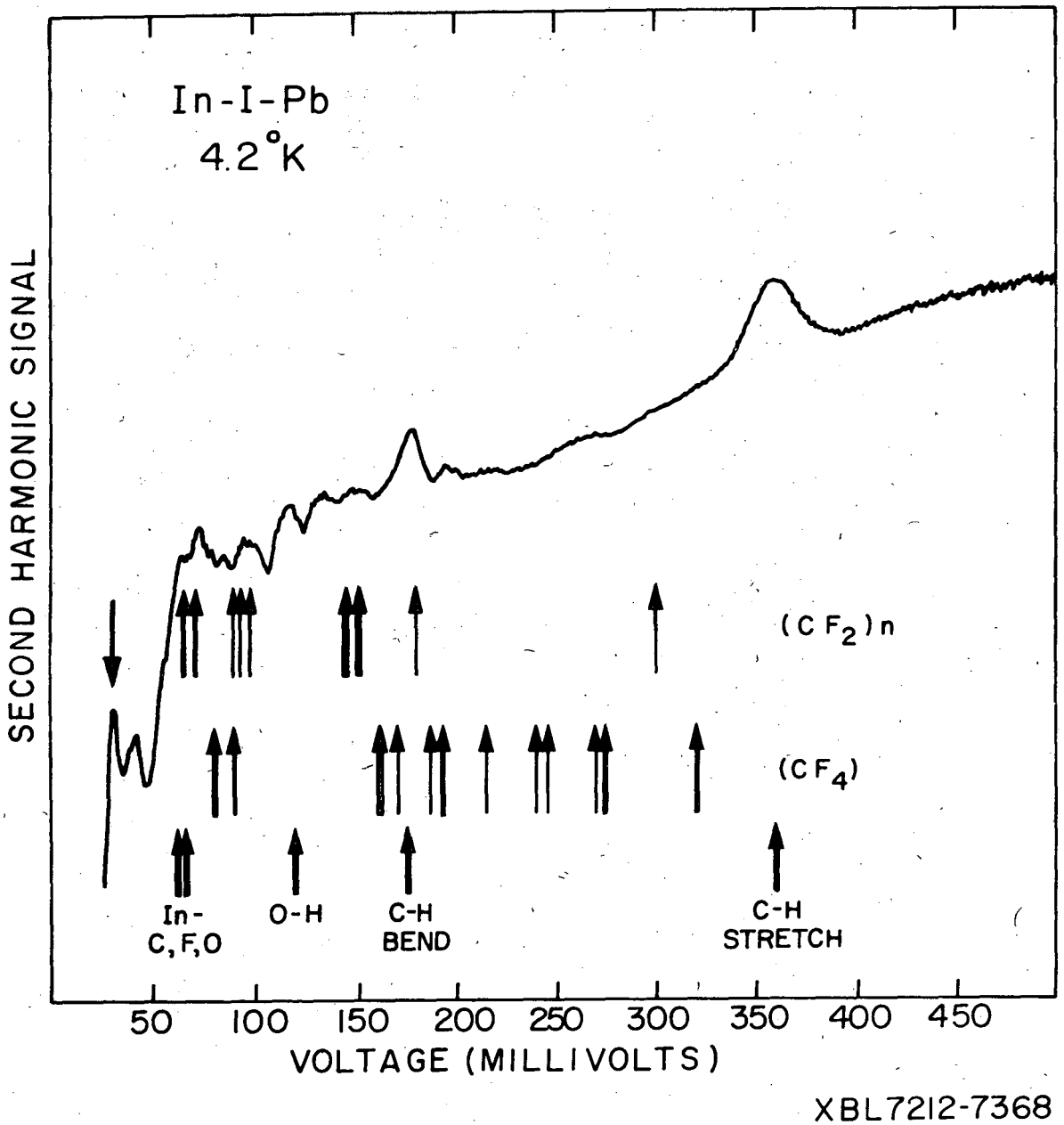
In-I-Pb
4.2°K
SECOND HARMONIC SIGNAL
(CF2)n
(CF4)
In-
C,F,O
O-H
C-H
BEND
C-H
STRETCH
50
100
150
200
250
300
350
400
450
VOLTAGE (MILLIVOLTS)
XBL7212-7368

Fig. 18.

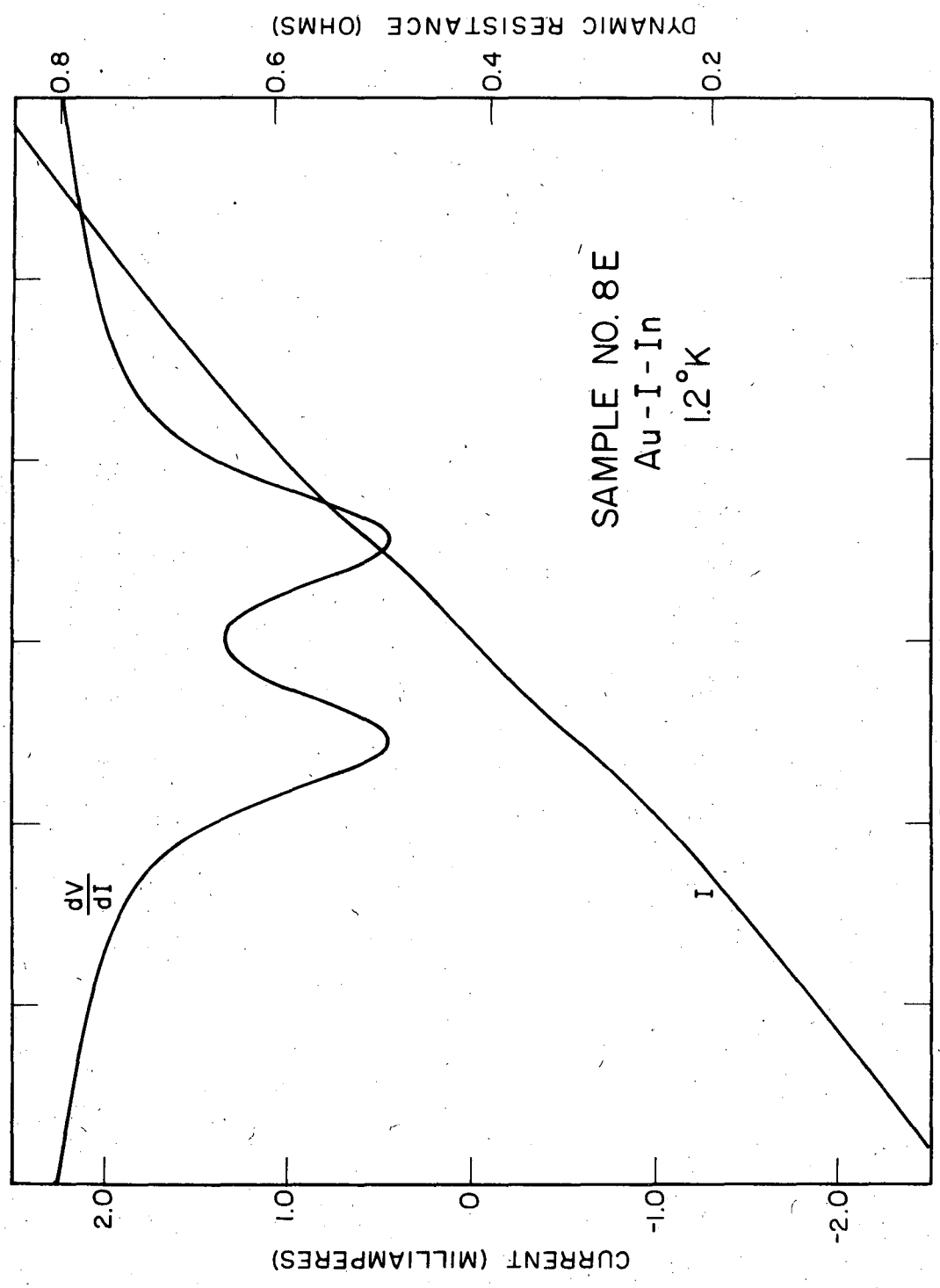

XBL731-5667

Fig. 19.

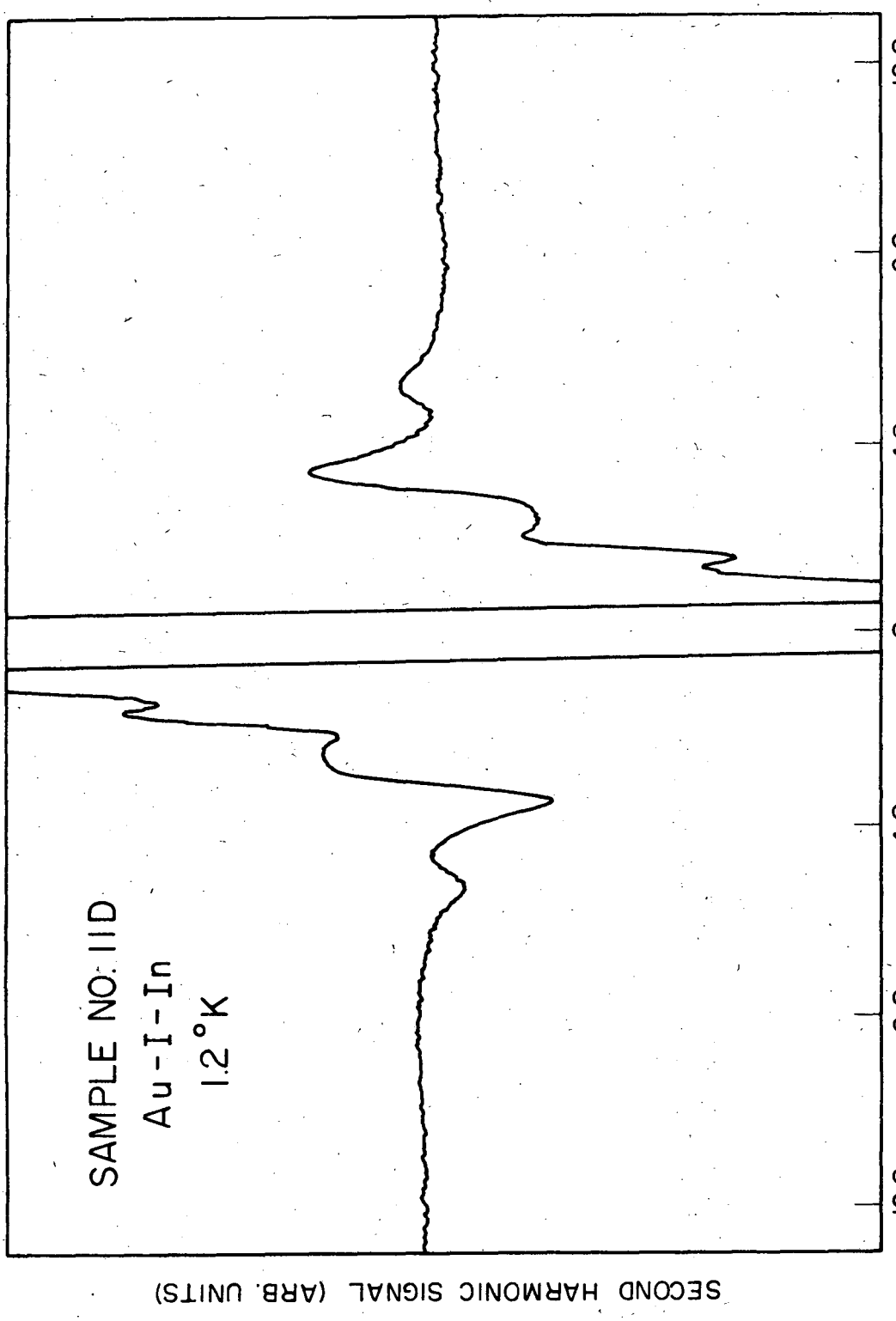

XBL731-5668

Fig. 20.

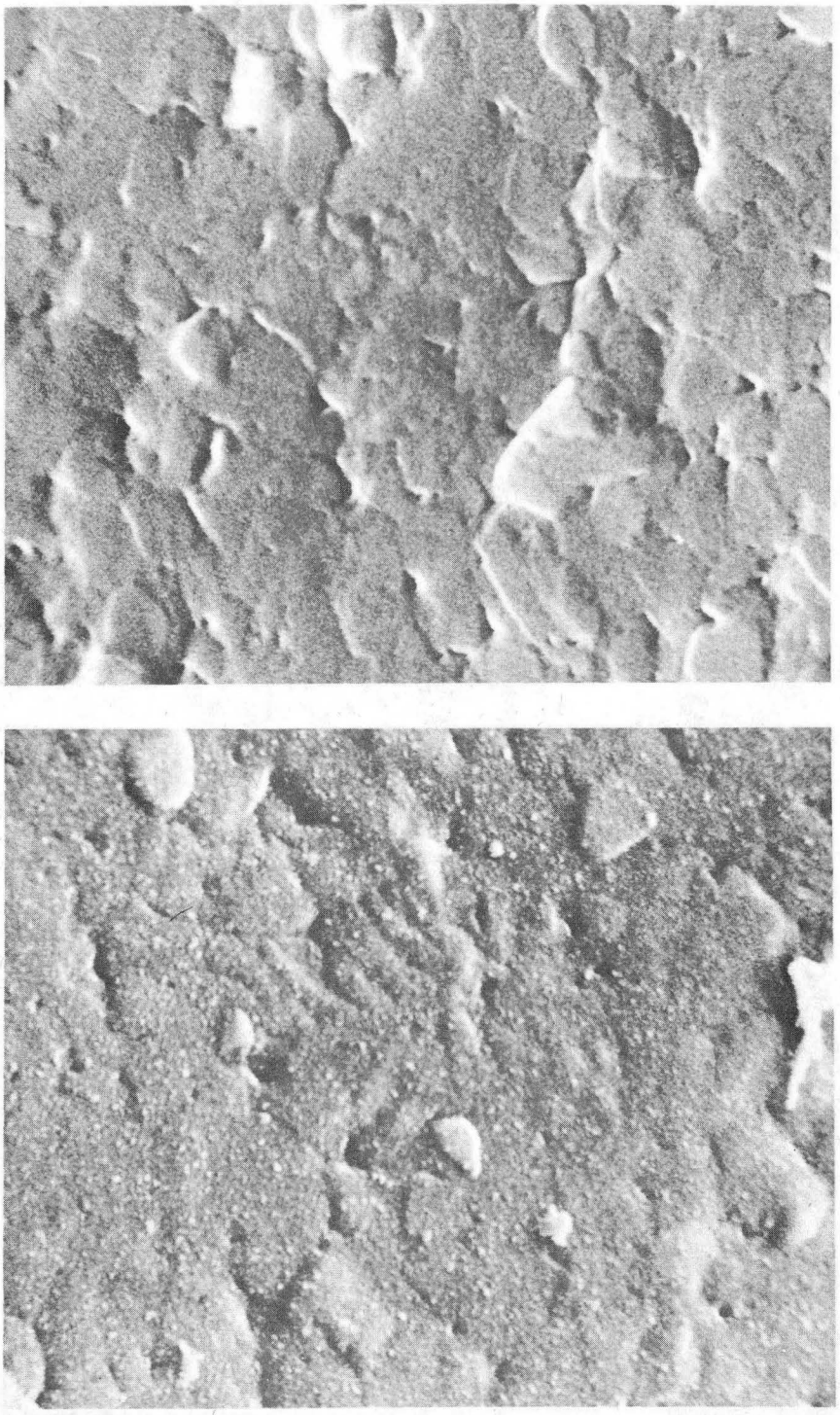

XBB 735-3022

Fig. 21.

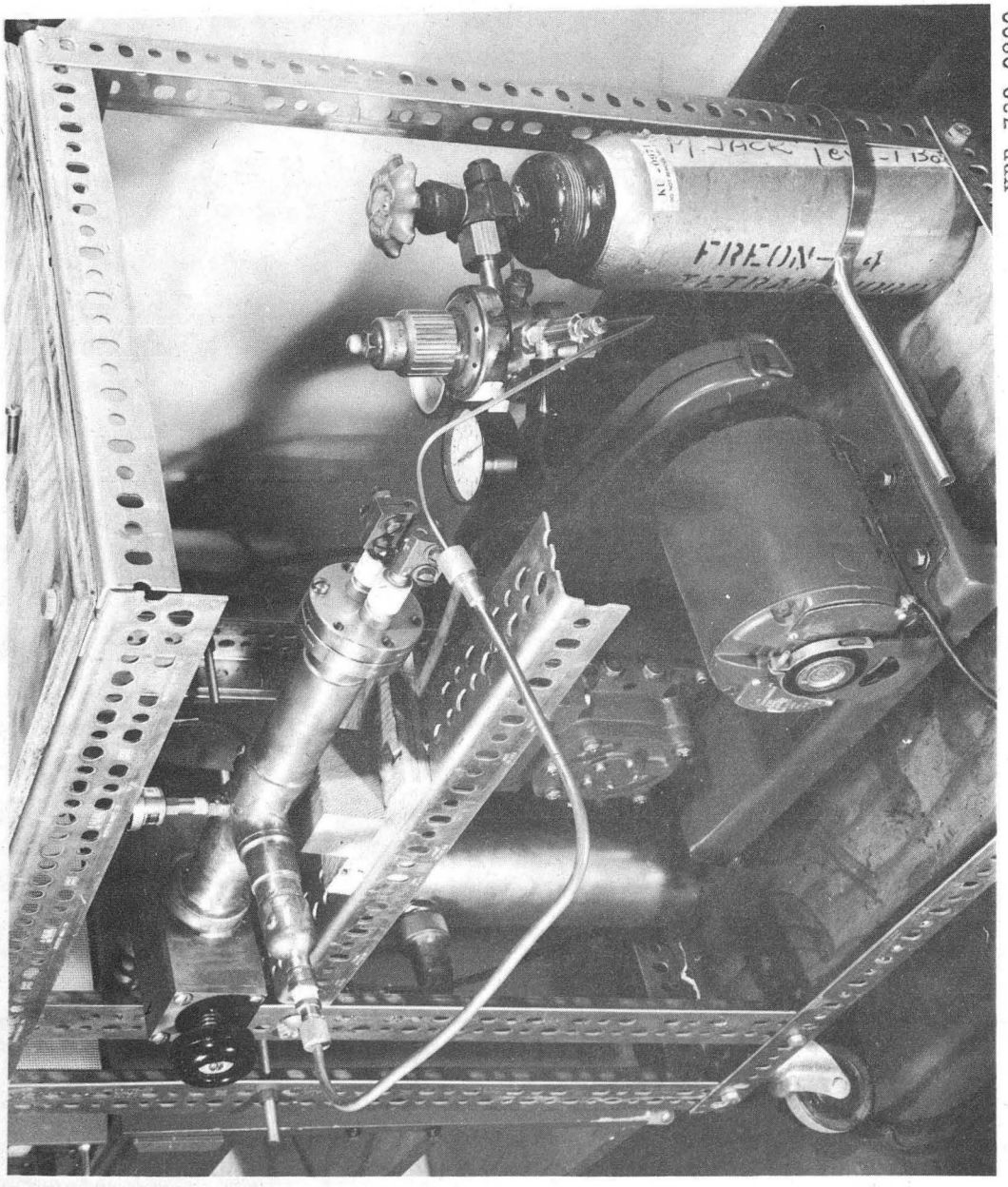

XBB 732-0800

Fig. 22.

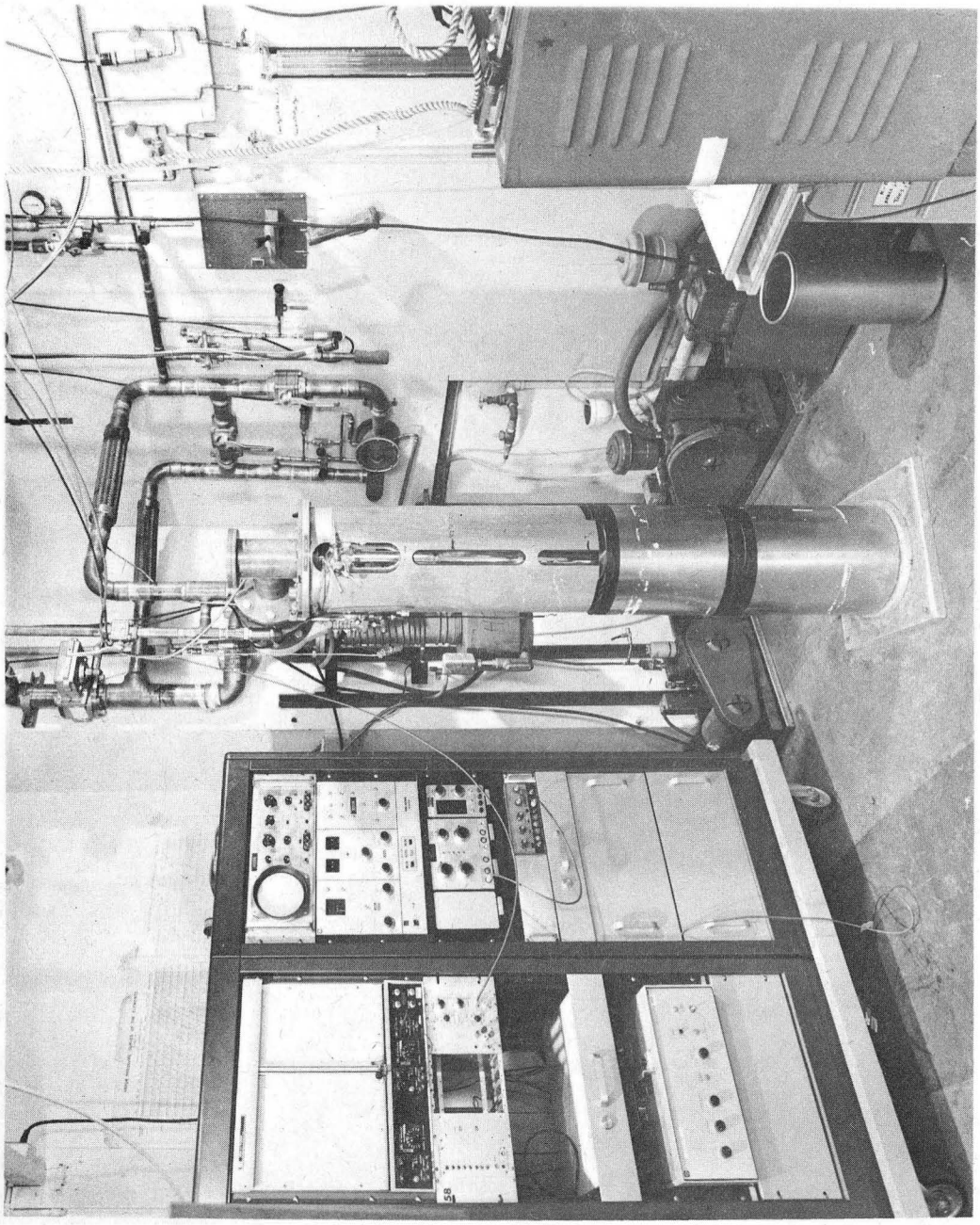

XBB 732-0801

Fig. 23.

TECHNICAL INFORMATION DIVISION
LAWRENCE BERKELEY LABORATORY
UNIVERSITY OF CALIFORNIA
BERKELEY, CALIFORNIA 94720